Synthesis of bifunctional poly(ethylene oxides) and their use as ligands to nanoparticles

Dissertation

Submitted to the Faculty of Chemistry, University of Hamburg

for the degree of Doctor of Natural Sciences

by

Charlotta Olsson

from Malmö (Sweden)

Hamburg 2009

The work described in this thesis was carried out at the Institute of Physical Chemistry, University of Hamburg in the group of Prof. Dr. Stephan Förster.

1. Referee: Prof. Dr. Stephan Förster
2. Referee: Prof. Dr. Horst Weller

To my family

Table of content

1 Introduction

Nanoparticles have during the last couple of decades been widely investigated due to the possible applications within the field of biomedicine, optics and electronics. In this thesis special interest is given to nanoparticles within biomedicine, hence to water-soluble nanoparticles.

Semiconductor nanoparticles offer the advantage of having size tunable luminescence, which make them suitable for studies of interactions between biomolecules on a cellular level, whereas magnetic nanoparticles offer the possibility for magnetic drug targeting. These nanoparticles have dimensions that are smaller or comparable to those of cells, viruses and genes and can therefore be directed close to a biological entity of interest with a localized magnetic field. In addition, the particles can be held at the site until completion of the therapy and then be removed. Another interesting application for magnetic nanoparticles is hyperthermia treatment, which is seen as a supplementary treatment to chemotherapy, radiotherapy, and surgery in cancer therapy. In order to use nanoparticles within biomedicine they have to remain in the circulation long enough to reach the intended target tissue. Upon entry into the organism, nanoparticles are recognized as foreign and removed from the circulation within seconds to minutes via non-specific phagocytosis. In order to create nanoparticles with longer circulation times, the particle surface needs to be modified to prevent recognition by the host immune system, e.g. limiting phagocytosis, and thereby increase the circulation time of the particles from minutes to hours or even days[1]. Surface modification with poly(ethylene oxide) (PEO) has emerged as a common strategy to extend the circulation time. Due to the uncharged and highly hydrophilic character of the PEO in combination with low toxicity and immunogenicity, particles covered by PEO adopt stealth character which makes them attractive for biomedical applications. Special attention has been given to bifunctional PEOs due to the possibility to attach one end of the PEO to the nanoparticle and the other to a biologically active substance.

Generating nanoparticles with PEO as ligands is not possible via a direct synthesis of the nanoparticles. With the knowledge of today, synthesis of high quality nanoparticles can only be obtained with hydrophobic ligands. However the ligands are only loosely bonded to the nanoparticle core which means that the shell can be manipulated and replaced. Replacement of the shell, i.e. ligand exchange, is a frequently employed method to obtain a phase transfer of nanoparticles in an organic solvent to an aqueous one. There is a wide range of ligands

which can stabilize nanoparticles. The two important criteria for a ligand are that it has a functionality through which a connection with the nanoparticle can be achieved, and that it has a suitable water-soluble part.

PEO is highly water-soluble but lacks a functionality to bind to nanoparticles which means that it has to be functionalized before it can be used as a stabilizing ligand. The overall aim of this study was to synthezise bifunctional PEOs with one group that attaches to the nanoparticle and one which could be coupled to a biological active substance. Within the frame of this thesis different PEO-based ligands were synthesized for stabilization of aqueous colloidal solutions of nanoparticles. Once the polymers were synthesized a method for ligand exchange to CdSe/CdS and Fe_3O_4 nanoparticles was optimized.

The possibility to encapsulate the water-soluble nanoparticles in vesicles was also investigated, and an experiment to couple nanoparticles with a shell of bifunctional PEOs to hydroxy groups on vesicles was performed. All vesicle solutions were analyzed by fluorescence microscopy and confocal laser scanning microscopy.

The polymer-nanoparticle conjugate can also be described as an amphiphilic molecule, consisting of a hydrophobic inorganic core with a layer of hydrophilic polymers. The conjugate can be compared with amphiphilic blockcopolymers which are prone to spontaneous organization (self-assembly) in aqueous solutions. The structures that take form by self-assembly can be predicted and controlled by changing the balance of the constituents of the molecule. Based on this, the possibility to form these superstructures with the polymer-nanoparticle conjugates was also explored.

2 Background

2.1 Nanoparticles

Nanoparticles are small crystals that consist of a few hundred to over thousand atoms. Due to their small size, in nanometer scale, they experience properties that differ from those of the corresponding bulk crystals[2].

2.1.1 Semiconductor nanoparticles

Semiconductor nanoparticles (NP) or quantum dots (QD) are of great interest due to their unique photoluminescence characteristics. Their potential applications are being investigated within the field of light emitting diodes and lasers[3], solar cells[4, 5] and biological labeling[6, 7]. These applications are mainly based on their photoluminescence characteristic, which derives from the electronic structure that is influenced by their small size (size quantization effect). Semiconductor nanoparticles show the most illustrative example of this effect. The band gap, E_g is a material constant that defines the energy level between the highest occupied and the lowest unoccupied electron energy state (conduction and valence band, respectively). When excited to the valence band an electron forms a bound state with the positive hole through Coulomb interactions, a so-called Wannier exciton. When looked upon as a hydrogen atom the exciton can be described by the Bohr radius. The Bohr radius for semiconductors such as CdSe is in the range of 1-10 nm. When the size of the particle approaches the Bohr radius of the exciton, the energy of the exciton is increased due to the confinement of the electron and the hole. Therefore, with decreasing size of the nanoparticle the band gap is increased. This phenomenon is known as the quantum confinement or size quantization effect. An analytical expression of the effect of the particle size on the band gap energy is presented in the form of the widely used Brus equation.[8]

$$E = E_g + \frac{h^2}{8r^2}\left(\frac{1}{m_e^*} + \frac{1}{m_h^*}\right) - \frac{1.8e^2}{4\pi\varepsilon\varepsilon_0 r} \qquad (2.1)$$

The first term on the right hand side represents the band gap of the bulk material. The second term describes the positive contribution of the confinement energy with a $1/r^2$ dependence, where h is the Planck constant , m_e^* and m_h^* the effective mass of the electron and the hole, respectively. The third term, varies as a function of 1/r, takes into account the Coulomb-interaction effects on the electrons and holes, where ε is the dielectric constant of the semiconductor and ε_0 the dielectric constant of vacuum. Small values of r means that the confinement term is dominant , making E greater than E_g. For large values of r, tha value of E approaches that of E_g.

The size quantization effect can be explained by the linear combination of atomic orbitals (LCAO) theory. By combining atomic orbitals (AO), an equal number of molecular orbitals (MO) are formed. When increasing the number of atoms, the number of MO increases and for an infinite number of atoms (bulk) the MO merges into bands (figure 2.1)

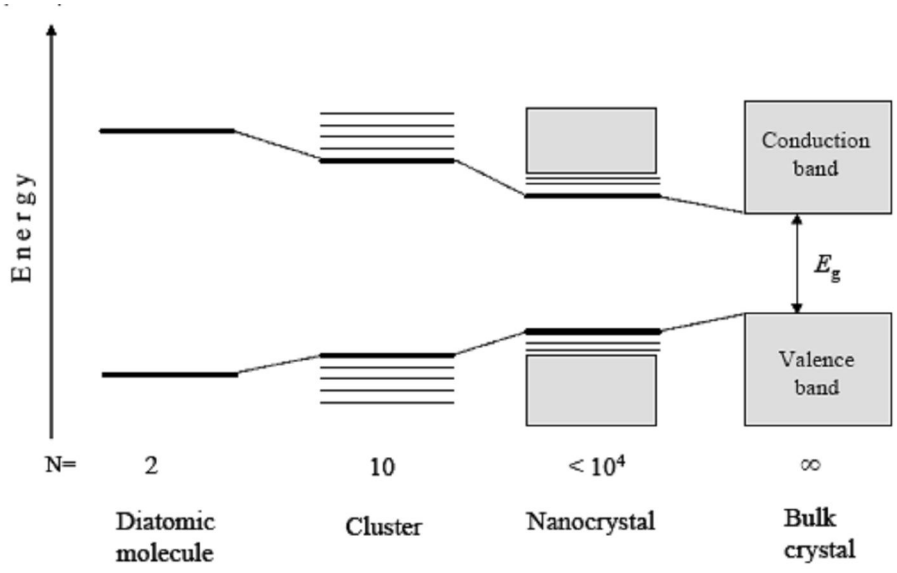

Figure 2.1: Evolution of molecular orbitals into bands.

The size of nanoparticles lies between molecules and bulk, and with a decreasing number of atoms the distance between the highest occupied and the lowest unoccupied molecular orbital increases. Changes of the band gap causes visible shifts in absorption onset and the position of the luminescence peak. Thus, by changing the size of the crystal different spectral colors of emission can be obtained. Such properties offer great possibilities for multicoloring of biological samples[9, 10].

2.1.2 Magnetic particles

A material's response on a magnetic field depends on its inner structure of the material. Depending on the properties of the material, magnetism can be divided into three main groups; diamagnetism, paramagnetism and ferro- ferri- and antiferro-magnetism[11].

Each material with atoms, ions or molecules, which do not have any unpaired electrons are diamagnetic. These materials have no magnetic moment since the single moments of each electron cancel each other out. However, if a magnetic field is applied on such a material a weak magnetic moment will be induced, which disappears when the external field is removed.

In contrast, paramagnetic substances are materials with atoms, ions or molecules that have unpaired electrons, which results in a permanent magnetic moment. Without an external magnetic field, the magnetic moments are randomly distributed due to thermal movement.

Ferromagnetic characteristics are only observed below a critical temperature, called the Curie temperature. A spontaneous magnetization arises from an internal field where the magnetic moments arrange parallel to each other. The arrangement of the electron spin is disrupted due to thermal movement when the temperature is above the Curie temperature. The interaction of the atoms can be described with quantum mechanic exchange energies. Two electrons can be either parallel or antiparallel to each other. By positive exchange energies the spins will take a parallel configuration leading to ferromagnetism. To minimize the energy of a ferromagnetic material magnetic domains are formed which are also called Weiss domains. Within the domain the spins are parallel to each other, however the domains are not parallel to one another. To lower the exchange energy between the domains, domain walls are formed called Bloch walls (figure 2.2). Within a Bloch wall the magnetization turns 180°.

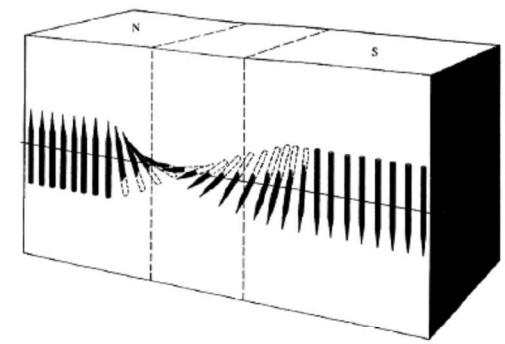

Figure 2.2: Bloch wall[12].

Because of the random distribution of the domains the magnetic moment is very small. In order for a ferromagnetic material to reach the magnetic saturation a homogeneous magnetic field needs to be added.

The relationship between magnetic flux density, B and the field strength, H of a ferromagnetic material is not linear, instead a hysteresis is observed (figure 2.3). The magnetic moment is directed parallel to an applied magnetic field which gives the dotted curve in figure 2.3. The magnetization rises until it reaches its magnetic saturation. When the field strength is reduced to zero the flux density no longer follow the original curve. To bring the magnetization to zero the coercivity field strength H_c is necessary. Based on the coercivity, materials can be divided into two groups; soft- and hard magnets. Soft magnets can be demagnetized in a weak magnetic field and have a small coercivity (H_c < 10 Oe). In opposite thereto hard magnets have a high coercivity (H_c > 100 Oe) and can also be named permanent magnets.

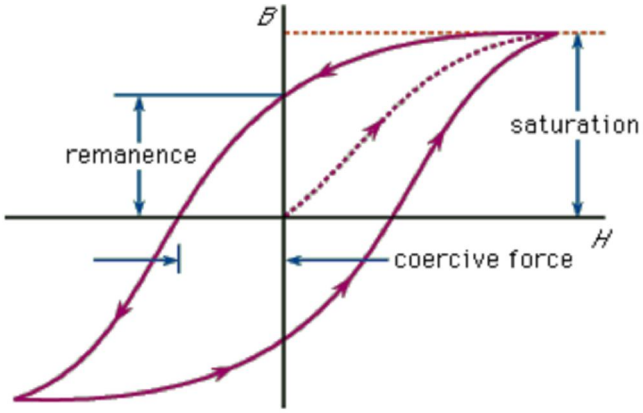

Figure 2.3: Hysteresis[13].

If all exchange energies are negative, neighbouring atoms will be aligned antiparallel to each other. The energies neutralize each other and the material seems non-magnetic, so called antiferromagnetism. If an external field is applied on such a material a weak magnetic moment arises, having the same magnitude as paramagnetic substances.

A substance containing two different ions, like magnetite (Fe_3O_4), with negative exchange energies will be aligned like antiferromagnetic substances. By such compounds the energies will not be able to neutralize each other and the same sort of spontaneous magnetism as for the ferromagnetic materials arises, called ferrimagnetism.

As described for ferromagnetism and ferrimagnetism, the material domains are separated by Bloch walls. The walls have a characteristic width and when the size of the investigated particles gets smaller, the existence of domain boundaries will be energetically unfavourable. When the particles size drops below a critical value, there is only one domain per particle. Very small particles do not show any specific magnetic direction since the system rotates due to thermal fluctuation. In such a case, the particles are called superparamagnetic and they behave paramagnetically but with a much higher magnetic moment. In order for the magnetism of a particle to rotate it has to overcome an energy barrier. The energy barrier gets smaller with a smaller particle size and when the particle is small enough, the thermal energy is sufficient to rotate the magnetism. For superparamagnetic particles the thermal fluctuation prevents stable magnetism. By cooling the particles the movements of the magnetism can be prevented and the particles will behave ferromagnetically.

2.2 Anionic polymerization

Different mechanisms are used for the synthesis of polymers, and the most important and most frequently used are the radical, cationic, anionic and the radical atom transfer polymerization. They all include the same steps, of which the first is the initiation step followed by the growth of the chain and finalized by the termination of the reaction.

The anionic polymerization, which has been used in this thesis, was first described in 1956 by Szwarc[14]. The unique feature of living anionic polymerization is that it leads to polymers with a low polydispersity (PD) without any side reactions. The polymerization is called “living” because the anion is active during the whole polymerization and more monomer can be added instead of terminating the polymerization. To maintain the living characteristic it is important that no humidity or oxygen is present, which could lead to an early termination through a deactivation of the anion. To avoid humidity and oxygen the reaction is performed in a special glass aparatus under nitrogen or argon atmosphere. A schematic picture of the glass aparatus is shown in figure 2.4.

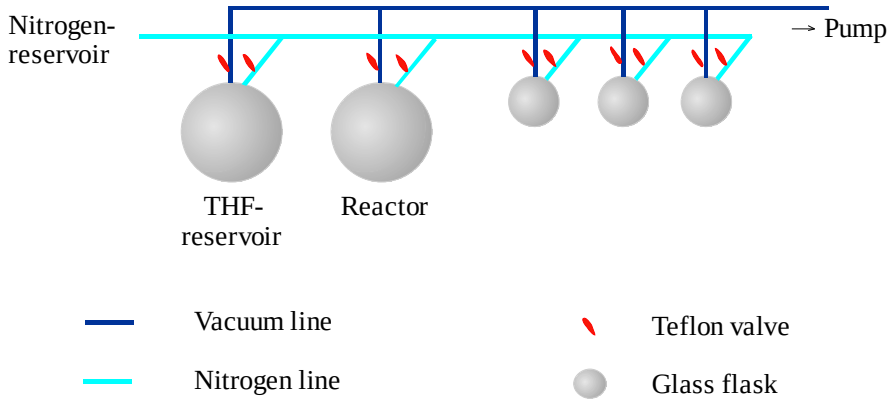

Figure 2.4: A schematic picture of the anionic setup.

With anionic polymerization it is possible to synthesize polymers with a very narrow polydispersity. Each initiator molecule starts a chain of polymer and with each added monomer the degree of polymerization is increased by one. This means that the degree of polymerization N_p is proportional to the yield Y and the molecular ratio of the initial concentration of the monomer M and the initiator I.

$$N_p = \left(\frac{[M]_0}{[I]_0} \right) Y \qquad (2.2)$$

By using the equation 2.1 the molecular mass of a polymer can be calculated over the ratio of monomer to initiator, which makes it possible to synthesize a polymer of desired molecular mass.

The dispersity of the polymer depends heavily on the rate of the initiation. If it is fast, that is faster than the growth of the polymer, the result is a small polydispersity (PD<1.1). To produce a small PD the initiation should be performed at a low temperature. As initiator for the polymerization, metal organic compounds that easily can leave the metal as a cation are used (scheme 2.1). The general rule states that the more instable the formed anion is, the more reactive is the initiator.

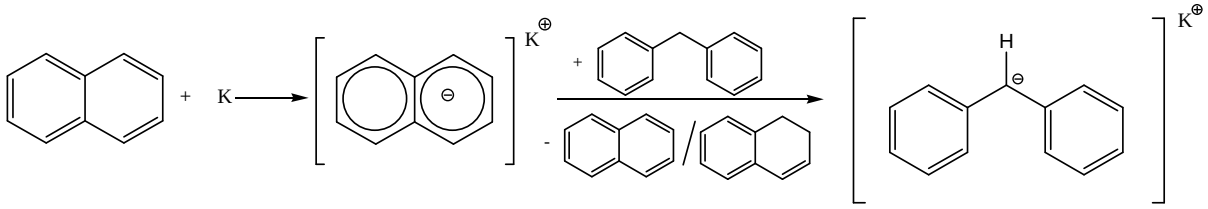

Scheme 2.1. Reaction route for the initiator diphenylmethyl sodium.

In an anionic polymerization a suitable monomer is a substance which is able to stabilize an anionic charge. This may be done with electronegative groups as substituents or in cyclic compounds. In this thesis ethylene oxide was used as monomer and a ring opening anionic polymerization was performed to get polyethylene oxide.

2.2.1 α-ω-functionalized poly(ethyleneoxide)

Poly(ethylene oxide) (PEO), also called poly(ethylene glycol) (PEG) in the literature, is widely used as a covalent modifier of biological molecules and surfaces due to its excellent physical and biological properties.

PEO is usually synthesized via anionic ring-opening polymerization of ethylene oxide. Compared to many other polymers, PEO has a relatively narrow molecular weight distribution (M_w/M_n), which is normally less than 1.1[15]. PEO has been investigated for several years and a few PEO-conjugates, which are used within the field of drug delivery, are already on the market (Adagen®, Oncospar® and PEG-Intron®)[16]. The ability of PEO to improve the pharmacological and biological properties of a therapeutically useful substance makes it very attractive for drug delivery. PEO is an amphiphilic polymer, which dissolves in organic solvents as well as in water. When bound to a water insoluble compound, the conjugate usually shows increased water solubility or dispersibility. In addition, PEO is non-toxic and has the lowest level of protein or cellular absorption of any known polymer[17]. The latter feature contributes to the prevention of bacterial surface growth and makes it difficult for the immune system to recognize the PEO-conjugate. To summarize, PEO-conjugates can increase the solubility of a therapeutical substance in aqueous media and yield improved circulation times *in vivo*.

Since PEO consists of repeating ether units that are essentially non-reactive, it has to be reacted with or adsorbed onto other compounds through terminal functional groups. This

makes the synthesis of heterobifunctional PEO very interesting. Two methods for the synthesis exist (scheme 2.2) of which the most direct procedure is to start the anionic synthesis with a functional group followed by termination with another functional moiety. The other method is based on end group modification of PEO diols, followed by separation of the resultant statistical mixture of the three end products (scheme 2.2 B). The statistical distribution leads to a low yield for this method. These approaches are often complicated with several reaction steps and the separation of chemically similar polymers that only differs in the end group structure[18, 19] .

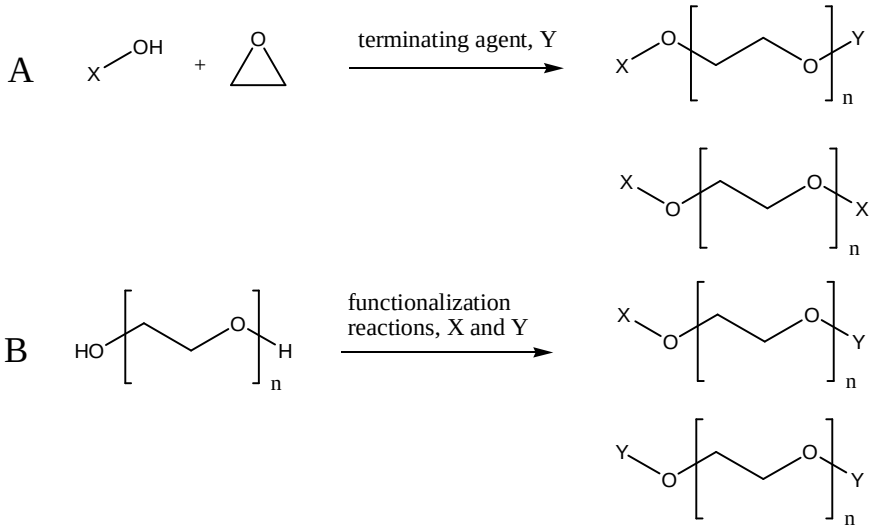

Scheme 2.2 Synthetic routes to synthesize heterobifunctional PEOs: A shows the direct synthesis of heterobifunctional PEO and B show end group modification of PEO diols.

In this thesis, the first described method (method A in scheme 2.2) has been used to achieve the desired heterobifunctional PEO. An array of literature linked to this topic exists[20, 21, 22]

2.3 Water soluble nanoparticles

Both magnetic nanoparticles and quantum dots have a very promising application within the field of biomedicine. The magnetic particles could be used as drug carriers, so called "magnetic drug delivery" first proposed by Widder et al.[23]. The concept of magnetic drug targeting is to inject magnetic nanoparticles to which drug molecules are attached. The particles are then guided to a specific site with a localized magnetic field. The particles are

held at the site until the therapy is complete and then removed. Another interesting application for magnetic nanoparticles is in hyperthermia treatment which is considered as a supplementary treatment to chemotherapy, radiotherapy, and surgery in cancer therapy[24, 25, 26]. The method is based on the fact that when magnetic nanoparticles are exposed to a varying magnetic field, heat is generated by the magnetic hysteresis loss, due to Néel-relaxation and Brown relaxation[27, 28]. These heat sources destroy the tumor cells, which are more sensitive to temperatures above 41°C than their normal counterpart.

The quantum dots have been found to be useful within the field of biolabelling. When investigating cells and cellular processes it is important to visualize the structures and compartments within the cell. Since cells are almost transparent to visible light, no direct observation is possible. Therefore structures and molecules of interest must be labeled with a marker that can be observed directly. One of the most common techniques used is fluorescence labeling. However, traditional fluorophores have their limitations since they are very sensitive to the local environment (thermal fluctuations of the solvent)[29]. As a consequence of conformational fluctuations the fluorophores can be reversibly transferred in states where they cannot fluoresce anymore and the fluorescence goes “on” and “off”, which is called blinking[30]. Upon optical excitation fluorophores can loose their fluorescent properties in irreversible light-induced reactions such as photo-oxidation, a phenomenon called photobleaching. In contrast to fluorescence labeling, the quantum dots show more stable photoluminescence, thus allowing for more long-term experiments. Another advantage of the quantum dots is their narrow emission and broad adsorption spectra in comparison to the very broad emission peak and narrow excitation window of organic fluorophores (figure 2.5).

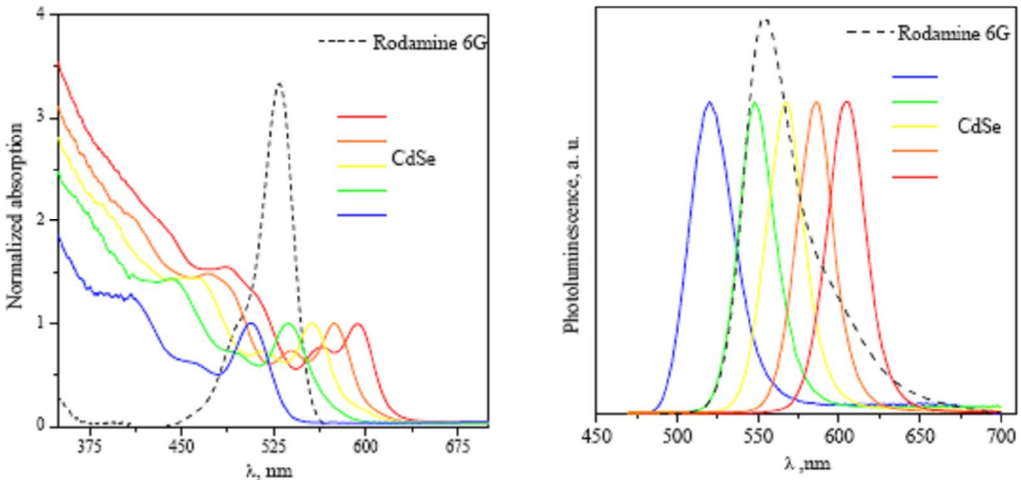

Figure 2.5 Comparison of the absorpton and emission spectra of CdSe nanoparticles of different size and the organic fluorophore Rhodamin 6G.

The emission color of the quantum dots can be determined only by changing the size of the particle. The particles can be excited with the same wavelength light since the absorption characteristics do not differ significantly in the low wavelength region. To observe multiple colors with organic dyes (traditional fluorophores), chemically different species must be used and the most suitable experimental conditions for each dye must be chosen.

To be able to use the nanoparticles in biomedicine the first step is to make them water soluble. One method to get water soluble nanoparticles is to perform the synthesis directly in water in the presence of hydrophilic ligands. However it is generally not possible to synthesize high-quality nanoparticles (NP) with a low dispersity directly in water. The best way to prepare high-quality NP is to use an organometallic synthesis at high temperature in the presence of organic ligands. That makes them insoluble in water and they must be further processed to become water soluble. There are two basic strategies to achieve this; ligand exchange reaction and encapsulation in micelle-like structures (figure 2.6). In this thesis the ligand exchange reaction is used to make the NP water soluble.

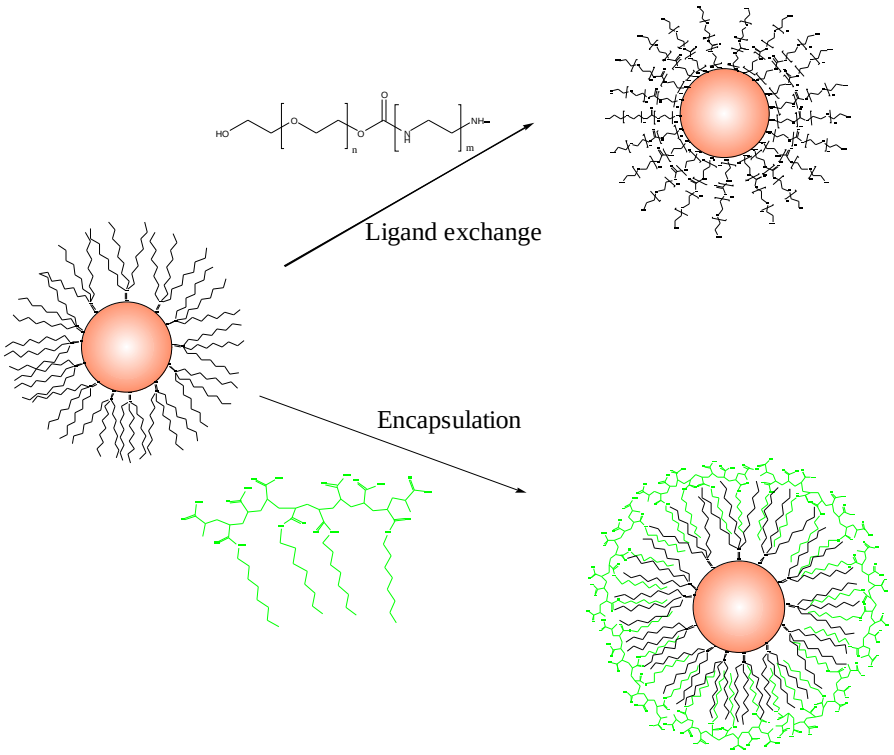

Figure 2.6 A schematic picture of the two strategies used to make nanoparticles soluble.

2.3.1 Ligand exchange

The purpose of a ligand exchange reaction on a nanoparticle is to replace the original hydrophobic ligands. A functionality that is reactive towards the surface atoms of the nanoparticle is necessary for the change to take place. Functionalities that are known to interact with the metal surface are amines[31, 32], carboxylic acids[33], thiols[34, 35], phophines[36] and phosphine oxides[37].

The first described ligand exchange reaction was performed with mercaptoacetic acid[38]. The mercaptoacetic acid possesses one SH group which can bind to the metal site and a carboxylic acid which provides the water solubility through the repulsive electrostatic interactions of the charged COO^- groups.

Thiols are strong bonding groups to CdSe/CdS core shell nanoparticles and they can replace the original weak ligands, such as amines and carboxylates. However, thiol groups significantly quench the photoluminescence of the NP. Although the NP-thiol conjugates are simple to synthesize they are not very stable (<1 week) due to dynamic thiol-metal

interactions, which means that the thiol ligand bind and unbind in a dynamic equilibrium. Enhanced stability can be achieved by using mercaptocarbonic acids with two instead of one thiol group[39]. However, the water solubility is achieved through the carboxylic acids and almost all carboxy-terminated ligands are unstable in basic pHs and in high ionic strength.

A more laborious but more stable method of making the nanoparticles water soluble is surface silanization where a glass shell is grown around the particle. The first step of this method is to bind a priming layer of mercaptopropyltrimethoxysilane to the nanoparticle surface via the mercapto group. The methoxysilane groups can be crosslinked, which greatly improves the stability. Following this, hydrophilic methoxysilanes are added to generate a hydrophilic silica shell. By cross-linking the methoxysilane groups through the formation of siloxane bonds, a multi-layer shell is formed. If hydrophilic methoxysilanes with phosphonate or ammonium head groups are used in the second step the particles will repel each other electrostatically. If PEO is used instead as the hydrophilic part of the methoxysilanes the particles are stabilized by steric repulsion[40]. The main advantage of surface silanization is the yield of extremely stable nanoparticles, but the silanization process is laborious and the resulting shell is often inhomogeneous.

Another approach is ligand exchange where the nanoparticles are stabilized through steric repulsion, which is to compare with mercaptoacetic acid were the electrostatic interactions stabilize the nanoparticles. As already mentioned in chapter 2.2.1, PEO has gained a lot of interest within the field of biomedicine due to its great properties. The fact that the properties of a nanoparticle are based on the properties of the ligand makes PEO interesting as a ligand.

An interesting anchor group to semiconductor nanoparticles (quantum dots) is the amine group. Amines are known to passivate the surface of CdSe and to block the trapping of electrons at defect sites, leading to an enhancement in the luminescence of the CdSe nanocrystals[41].

2.4 Self assembly

Self assembly is a molecule's spontaneous arrangement to higher ordered structures such as micelles, vesicles or liquid crystals. The molecular requirements for this to take place are the existence of long range repulsive forces and short range attractive forces.

Between A and B (figure 2.7) long range repulsive interaction exists and because of the bond (short range attractive force) they are forced to stay together. When numerous A/B-pairs are gathered in a region with preferably as few A-B contacts as possible, they order themselves in A- and B-domains.

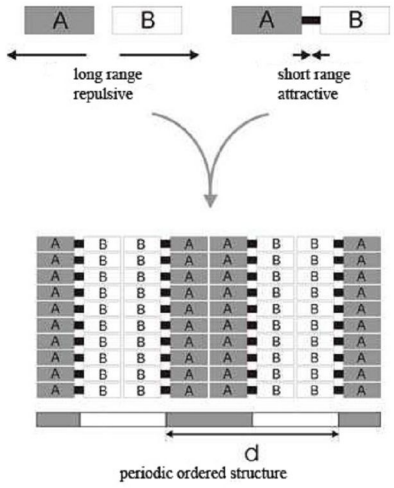

Figure 2.7 Schematic overview of self assembly of A/B-structures[42].

An amphiphilic block copolymer is an example of an A/B pair molecule. Such a molecule contains one lipophilic and one hydrophilic part. The simplest structure is the micelle but depending on solvent and ratio between the two parts many different aggregates may be formed (figure 2.8).

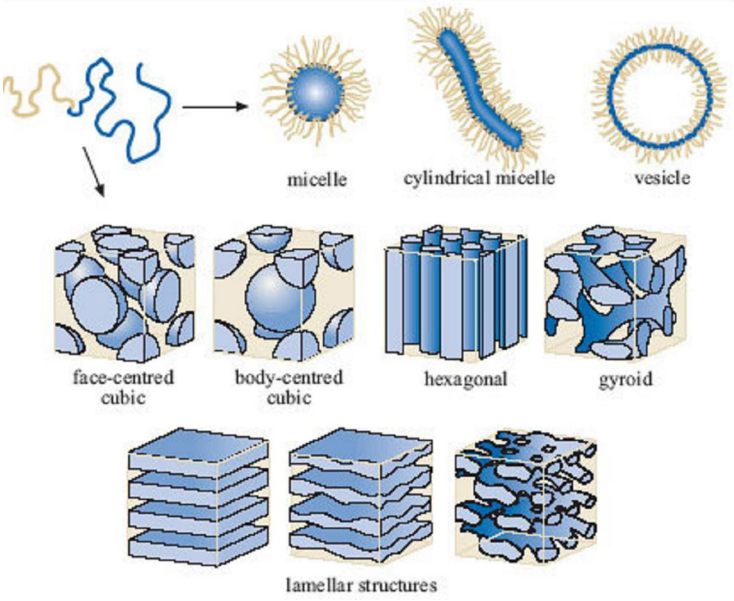

Figure 2.8 Examples of the different aggregates established by block copolymers with hydrophobic and hydrophilic elements[43].

The driving force for these structures to form is minimization of energetic unfavorable interaction. The possible structures are restricted by an amphiphile's need to keep its nonpolar and polar parts surrounded in a favorable way. To predict the size and shape of amphiphilic aggregates the surfactant parameter N_s may be calculated (equation 2.3)[44]. It makes a prediction on the form giving the minimum free energy for the conditions and determines the optimal aggregate shape.

$$N_S = \frac{v}{la_0} \qquad (2.3)$$

The surfactant parameter gives a relation between the volume of the hydrophobic portion of the molecules v, the length of the hydrocarbon chains l and the effective area of the head group a_0. The surfactant number relates the properties of the molecule to the preferred curvature properties of the aggregates.[22]

The surfactant number can be described with the help of the mean curvature H and the gaussian curvature K of the hydrophobic-hydrophilic interface. H and K are given by the two radii of the curvatures (figure 2.9) as shown in equation 2.4 and 2.5.

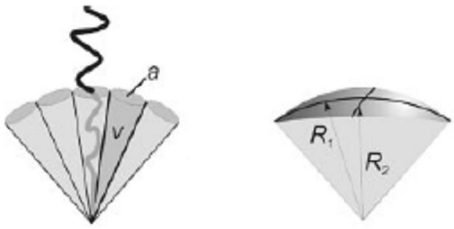

Figure 2.9 Description of the shape of an amphiphile.

$$H = \frac{1}{2}\left(\frac{1}{R_1} + \frac{1}{R_2}\right) \tag{2.4}$$

$$K = \frac{1}{R_1 R_2} \tag{2.5}$$

Small values of N_s imply a highly curved aggregate whereas when N_s is close to unity, planar bilayers usually forms. Spheres, cylinders and bilayers are characterized by certain values of surfactant number and curvature as shown in table 1.1.

Table 1.1

Shape	N_s	H	K
Sphere	1/3	1/R	$1/R^2$
Cylinder	1/2	1/(2R)	0
Bilayer	1	0	0

Several different structures can form when the N_s value lies between 1/3 and 1/2 or 1/2 and 1. The molecules may assemble in a symmetrical aggregate that is slightly off optimal condition or into aggregates of lower symmetry or they may undergo phase separation. Obviously, surfactant numbers only represent an approximate model of the nature of self assembly. However, it offers valuable insight into how changes in solution conditions and molecular structures affect the aggregate shape.

2.5 Methods for characterization

2.5.1 Size exclusion chromatography (SEC)

The size exclusion chromatography, also called gel permeation chromatography, is one of the most important methods for determining the molecular mass and the distribution of the molecular weight of polymers.

GPC differs from other chromatographic methods by the fact that there is no interaction between the mobile phase and the stationary phase. The separation only depends on the hydrodynamic volume of the polymer (figure 2.10).

The analyte is dissolved in an appropriate solvent and then injected into a continually flowing stream of solvent (mobile phase). The mobile phase flows through millions of highly porous rigid particles (normally crosslinked polymers, the stationary phase) which are tightly packed in a column. The pore sizes of these particles are controlled and available in many different sizes.

Molecules with a large hydrodynamic volume can not permeate into the pores and will therefore go straight through the column with the mobile phase without any delay. Very small molecules will permeate in to every pore. The two extremes will not experience any selective separation. This means that the size of the pores in the columns defines the working area. Smaller molecules will stay longer on the column since they diffuse in the pores and will therefore be detected at last.

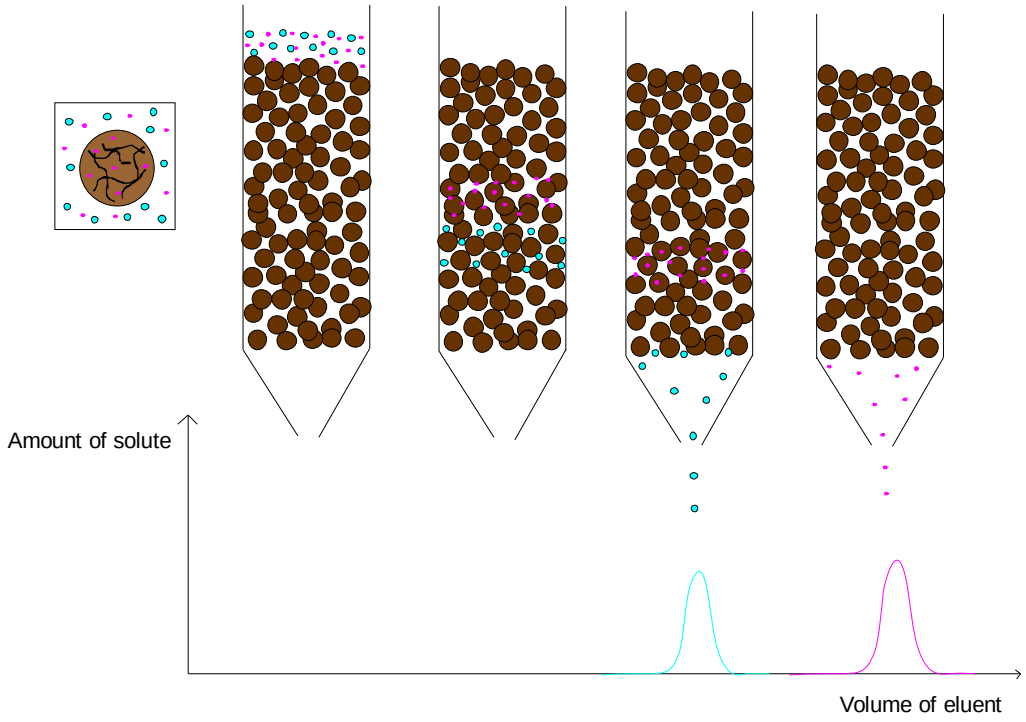

Figure 2.10 Schematic illustration of the separation of molecules with a GPC.

The detection of the polymer is usually done with a differential refractometer, but can also be performed with an UV-detector or a viscosity and light scattering detector.
Since the differential refractometer and the UV-detector only give an elution time and not a definite molecular mass, a calibration is necessary. This is done with a number of polymer standards, where the molecular mass has been determined with other methods such as the mass spectrometry. For an accurate result a calibration for each polymer is necessary since the GPC separates with regard to the hydrodynamic volume. To avoid small differences due to fluctuations in temperature and pressure a substance (internal standard, e.g. toluol) is always measured with the analyte. The relative elution time between the analyte and the internal standard stays constant and fluctuations can be avoided.

2.5.2 Mass spectrometry (MALDI-TOF)

Traditional mass spectroscopy (MS) methods use thermal energy to vaporize non-volatile samples. This makes it unsuitable for measurements of macromolecules, like polymers, since they get decomposed by thermal energy. A fragmentation of the sample results in a loss of the full chemical structure.

It was first in 1987 that Michael Karas and Franz Hillenkamp[45] showed that, with the use of a matrix (a small organic molecule) they were able to measure macromolecules with MS. Koichi Tanaka[46] developed this strategy further and showed later that MALDI (matrix assisted laser desorption and ionization) could be applied to a whole range of biological macromolecules.

MALDI has now developed into the most important mass spectroscopy method for the analysis of polymer samples. MALDI is a special type of MS where a laser is used to volatize the matrix rather than degrading the sample and is thereby able to determine the exact molecular mass.

The matrix is normally a crystalline substance with a conjugated double binding system, for example dithranol (1,8,9-trihydroxyanthracen) which shows a strong absorption in the UV-area (figure 2.11).

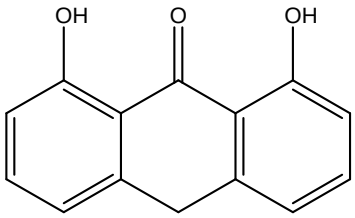

Figure 2.11 Dithranol

In the sample preparation for MALDI it is very important to have an appropriate solvent for the polymer to minimize the interaction between the polymer molecules.

A large excess of the matrix is mixed with the macromolecule and an inorganic salt and then crystallized on a target plate. The target plate is excited with a laser in high vacuum, the matrix absorbs the energy from the laser and then desorbs the polymer. With the addition of the salt the analyte is ionized and is able to accelerate in an electric field. Often every molecule has one charge and the time to reach the detector is determined by the molecular mass of the polymer (figure 2.12).

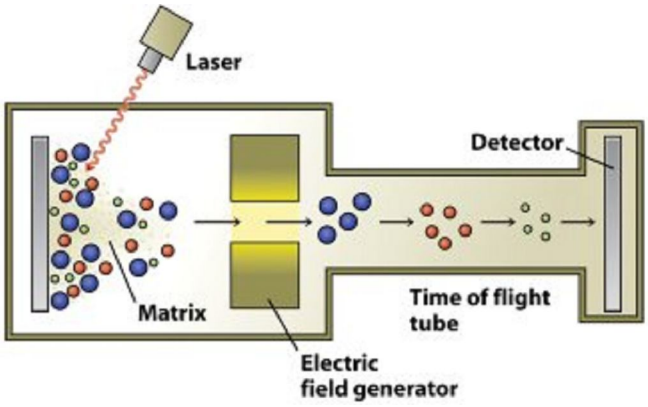

Figure 2.12 Schematic illustration for a linear MALDI-TOF[47].

Calibration of the instrument is done with peptides of a known molecular mass. Peptides have the advantage of being monodisperse and are therefore appropriate to use as calibration substances. Another advantage of peptides is that they are commercially available with every desired molecular mass.

An advantage of MALDI-TOF is the very low amount of analyte needed. For homopolymers the resolution of the separated peaks is very good, making the method suitable for determination of the terminal groups.

When measuring polymers with a high polydispersity or a mixture of polymers it is important to be aware of that higher masses could be discriminated due to a difference in the probability to ionize. A statement about the polydispersity of the polymer is therefore to be made with caution.

2.5.3 Dynamic light scattering (DLS)

Dynamic light scattering is a technique used for measuring the size of a particle within the range of a few nanometers to a few microns. This technique is based on the idea that small particles in a suspension move randomly, called Brownian motion, and that the size of the particle can be related to its motion[48]. This is done by illumination of the sample with a laser beam. The light is scattered and the intensity fluctuations can be detected. The scattered light waves can either arrive at the detector with the same phase and a light spot appears or the phase additions are destructive, canceling each other out. This gives rise to a speckle pattern which consists of areas of bright light and dark areas where no light is detected. Since the

particles are constantly moving due to the Brownian motion the speckle pattern will fluctuate. The DLS measures the rate of intensity fluctuation which is used to calculate the particle size. This measurement is done with a digital correlator, which measures the similarity between two pictures over a period of time. This is expressed with a scale from 0-1 where 1 is perfect correlation and 0 is no correlation. It is well known that small particles move more quickly than larger particles (figure 2.13), this relation is what the DLS uses to calculate the size.

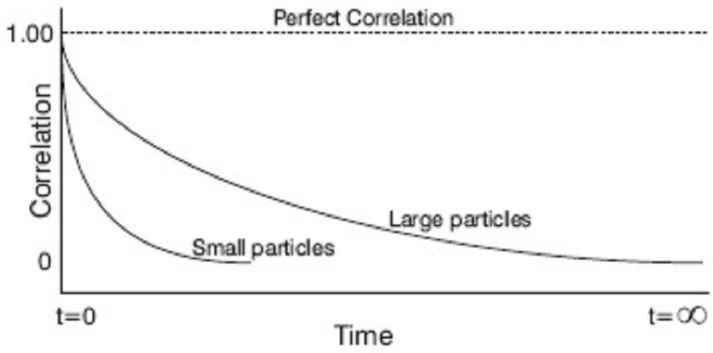

Figure2.13 The correlation as a function of time.

For monodispersed particles in solution the correlation function, *g* decays exponentially with the time *t*[49]

$$g^{(1)}(t) = \exp(-\Gamma t) \qquad (2.6)$$

where the decay rate is

$$\Gamma = Dq^2 \qquad (2.7)$$

where *D* is the diffusion coefficient of the particles and *q* is the magnitude of the scattering wave vector (figure 2.14).

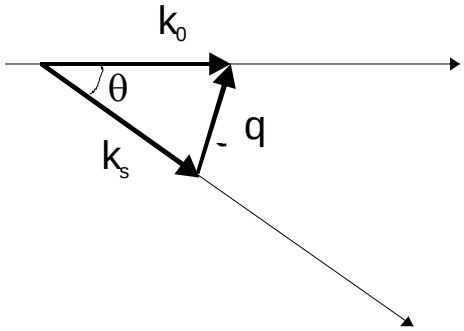

Figure 2.14 Scattering wave vector.

Whereby

$$\vec{q} = \vec{k}_0 - \vec{k}_s \tag{2.8}$$

where the wave vector k_0 is the incident light and k_s is the scattered light. The scattering vectors magnitude is given by

$$q = \frac{4\pi n}{\lambda_0}\sin\left(\frac{\theta}{2}\right) \tag{2.9}$$

where n is the refractive index of the solvent, λ_0 the wavelength of the laser in vacuum and θ is the scattering angle.

The relationship between the hydrodynamic radius, R_h of a particle and its diffusion coefficient, D is defined in the Stokes-Einstein equation

$$D = \frac{k_B T}{6\pi\eta R_h} \tag{2.10}$$

where k_B is the Boltzmann's constant, T is the temperature and η is the dynamic viscosity.

For a polydispersed sample, $g^{(1)}(\tau)$ can not be described as a single exponential, it must be described as a sum or an integral over a distribution of decay rates $G(\Gamma)$ by

$$g^{(1)}(\tau) = \int_0^\infty G(\Gamma)\exp(-\Gamma t)d\Gamma \tag{2.11}$$

where $G(\Gamma)$ is normalized so that

$$\int_0^\infty G(\Gamma)d\Gamma = 1 \qquad (2.12)$$

2.5.4 Light microscopy

When a picture on the retina of the eye is very small it is hard to see details of the object. There are two different possibilities to make the picture on the retina larger, the first is to simply move the object closer to the eye (figure 2.15) and the other is to use an optical instrument.

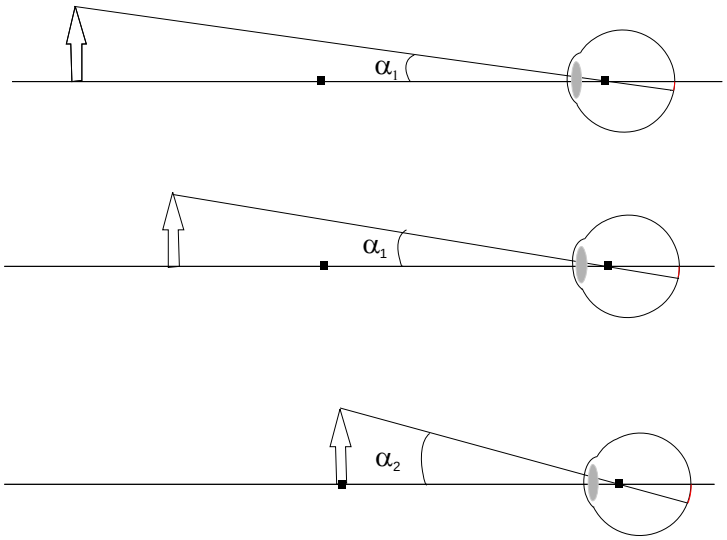

Figure 2.15 The angle of vision α rises when an object is moved closer to the eye.

An object takes up an angle of vision α when looked at without optical instrument and the angle of vision β with the help of an optical instrument. The angular magnification G of the instrument is then given from[50]

$$G = \frac{\beta}{\alpha} \qquad (2.13)$$

The angle vision α is defined as

$$\alpha \approx \tan\alpha = \frac{h}{d_0} \qquad (2.14)$$

where d_0 is the distance for the sharpest vision without optical help (defined as d_0=25 cm).
With a microscope the angle of vision of close by objects can be so much enlarged that details that are invisible for the eye can be studied. The principle of a simple microscope can be viewed in figure 2.16. To reach the enhancement of the object two convex lenses are used, the objective L_1 and the ocular L_2. The objective generates an inverted picture, which is further studied with the ocular. The ocular act like a magnifier and creates an enlarged virtual picture. If the distance between the objective and the ocular is adjusted so that the picture of the objective is situated in the focal point of the ocular, G may be calculated.

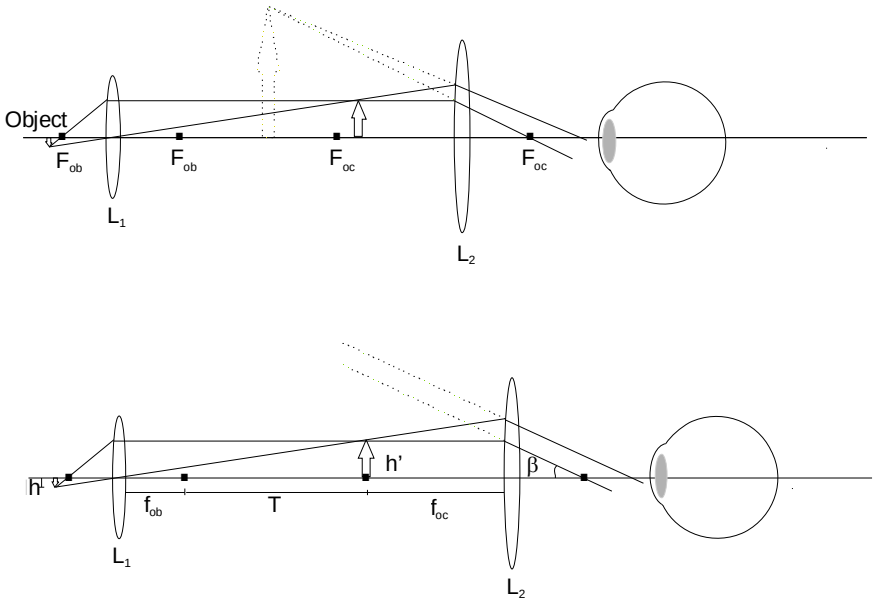

Figure 2.16 The principle of a simple microscope.

The angle of vision β can be defined as

$$\beta \approx \tan\beta = \frac{h'}{f_{oc}} \qquad (2.15)$$

where f_{oc} is the focal distance of the ocular. The pictures height h' is related to the height of the object as

$$\frac{h'}{h} = \frac{T}{f_{ob}} \tag{2.16}$$

The distance T that gives the distance between the objectives focal point and the focal point of the ocular is called the tube length. The angular magnification can now be written as

$$G = \frac{\beta}{\alpha} \approx \frac{d_0}{h} * \frac{h'}{f_{oc}} \tag{2.17}$$

$$G = \frac{T}{f_{ob}} * \frac{d_0}{f_{oc}} \tag{2.18}$$

Modern microscopes have objectives and oculars that are built of several lenses to achieve a larger enlargement and to correct for different aberrations.

The refractive index, *n* of the light is an important variable in optical microscopy for the calculation of the numerical aperature *NA*, which is a measure of the light-gathering and resolving power of microscope objectives and condensers[51]. It was originally defined by Abbe and is given by the expression

$$NA = n * \sin\alpha \tag{2.19}$$

The refractive index is calculated from the ratio of the speed of light in vacuum to that in a second medium of greater intensity. When a light wave incident upon a plane surface separating two media, with different refractive indices, it is refracted when it enters the second medium. The incident angle θ_1 is related to the refraction angle θ_2 by the equation 2.20 known as Snell's law

$$n_1 * \sin(\theta_1) = n_2 * \sin(\theta_2) \tag{2.20}$$

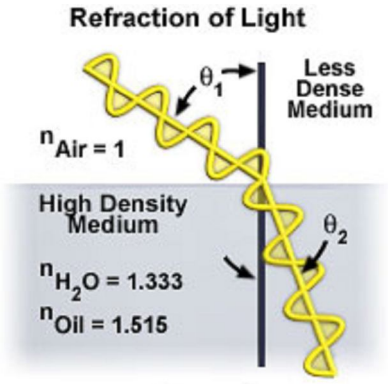

Figure 2.17 The refraction of light when entering a second medium.

As can be seen in fig. 2.17 the angle of refraction is always smaller than the angle of incidence when n_1 is greater than n_2. Alternatively when n_2 is greater than n_1 the angle of refraction is always greater than the angle of incidence. When two refractive indices are equal ($n_1=n_2$) the light passes without refraction.

From equation 2.19 it can be seen that the numerical aperture depends heavily on the refractive index and the one-half angular aperture α. The image forming light waves that pass through the sample and enter the objective as an inverted cone reveal the angular aperture as shown in figure 2.18. This value is determined by the focal length of the objective.

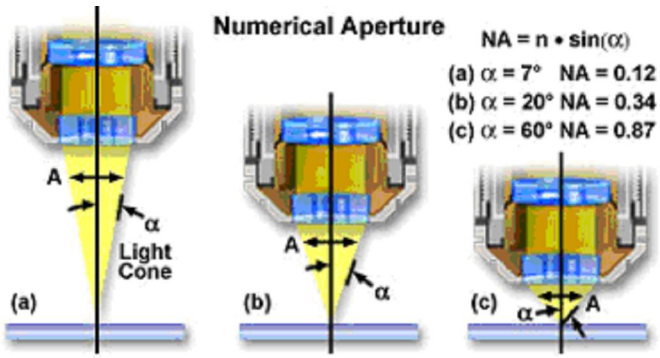

Figure 2.18 Numerical aperature.

It is very difficult to achieve NA values above 0.95 with dry objectives. However, higher NA values can be obtained by increasing the medium refractive index between the sample and the objective resulting in a larger angular aperture α. With the help of immersion oil NA values of 1.42 can be obtained.

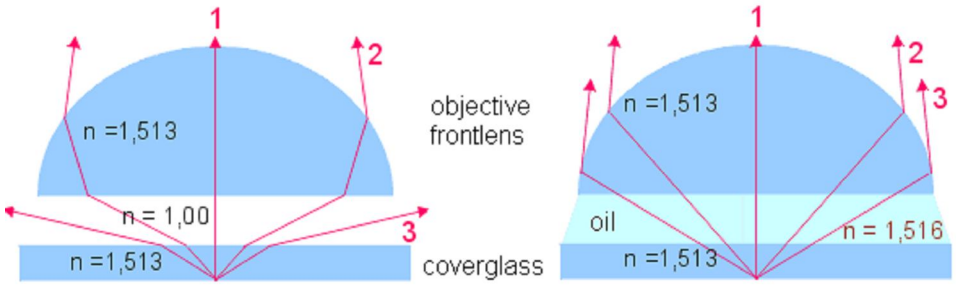

Figure 2.19 Coverglass and objective lens without (left) and with (right) immersion oil[52].

The ability of the objective to resolve two neighboring details depends on the wavelength of the light and the NA of the microscope as follows

$$\Delta x = 1.22 \frac{\lambda}{NA} \qquad (2.21)$$

In equation 2.21, Δx is the resolution and may be defined as the distance between two structures.

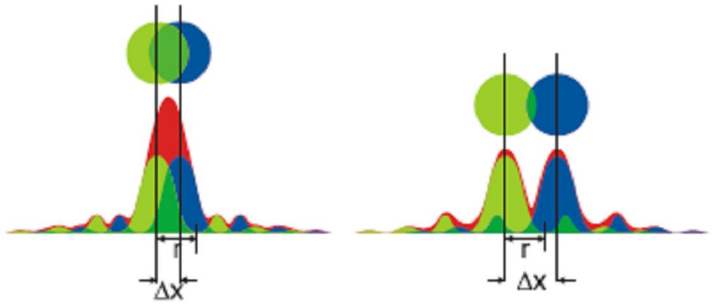

Figure 2.20 Conditions of the separation for the diffraction image[53].

For a microscope with immersion oil with the values of NA (0.95-1.42) and the wavelength λ (400-800), Δx is between 0.4 and 0.7 µm.

Dark and nontransparent samples can be enlarged and studied with a normal microscope. However, to study transparent samples a slightly different setup is needed. When the light

waves go through particles with different refractive indices it is delayed and a phase shift δ arises.

$$\delta = \frac{2\pi}{\lambda} d\left[n_p - n_m\right] \qquad (2.22)$$

The phase shift may be calculated from the thickness *d* of the particle, the wavelength of the light λ and the difference in the refractive indices from the particle and the medium n_p and n_m. Since the difference in light intensity is very weak and the phase shift is not to be seen with the naked eye these objects are displayed with a really poor contrast. With a special setup consisting of a condenser annulus, different lenses and a phase plate, the phase shift can be transferred in amplitude shifts and thereby made visible.

2.5.5 Fluorescence microscopy

In fluorescence microscopy it is the sample itself that emits light. The technique is used to study specimens that are made to fluoresce. It is based on the fact that certain material emits energy as visible light when irradiated with light of a specific wavelength. A mercury-vapor lamp is often used as excitation source. When the radiation from the lamp collides with the atoms in the specimen the electrons are excited to a higher level. The electrons emit light when they relax to a lower level again. For the light to become visible a filter that removes the excited light from the emitted light is used. The filter is based on the fact that the emitted light has a lower energy and a longer wavelength. The fluorescing area is then observed against a dark background.

2.5.6 Confocal laser scanning microscopy (CLSM)

Confocal laser scanning microscopy offers advantages over the conventional optical microscopy like the elimination of out-of-focus light and the ability to collect serial optical sections and to create 3-D pictures of the specimen. When fluorescent specimens are observed with a conventional optical microscope, secondary fluorescence from the specimen that are

not in the region of interest, often interferes with those features in focus. With thicker specimens above 2 micrometers this problem becomes especially obvious.

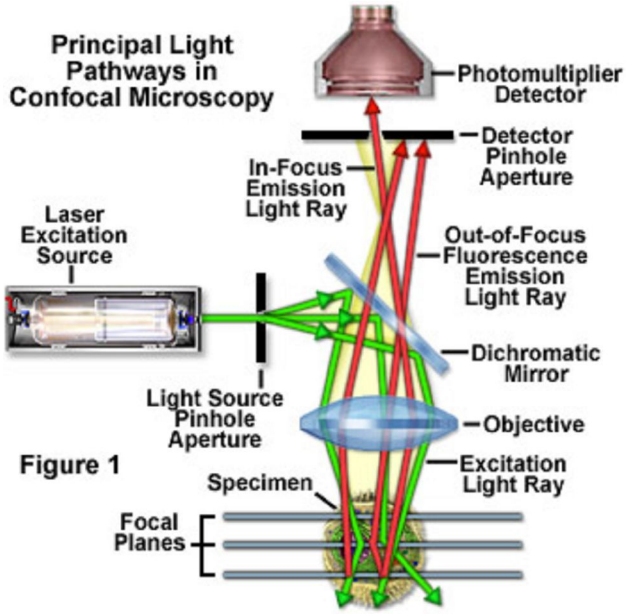

Figure 2.21 The light path in a confocal microscope[54].

The principal light pathways in a basic confocal microscope can be seen in figure 2.21. Coherent light emitted by a laser system passes through a pinhole aperture that is situated in a conjugate plane (confocal) with a scanning point on the specimen and a second pinhole aperture positioned in front of a photomultiplier detector. The laser is reflected by a dichromatic mirror and scanned over the specimen on a defined focal plane. Light emitted as fluorescence of the specimen from points in the same focal plane passes back through the dichromatic mirror and is focused as a confocal point at the detector pinhole aperture. The fluorescence emission that occurs at points above and below the focal plane is not confocal with the pinhole and will only contribute to the resulting image to a very small extent. Refocusing the objective in a confocal microscope gives another focal plane in the specimen and by looking at different focal planes a three-dimensional image of the specimen can be produced.

2.5.7 Transmission electron microscopy (TEM)

The principle of the electron microscope is very similar to that of the light microscope. The most important difference is that in an electron microscope electrons are accelerated and passed through magnetic lenses which focus them in the same way as the glass lenses focus light in a light microscope.

The ray of electrons is produced by a cathode heated up by a current and then accelerated to the anode. The accelerated electrons pass through a hole at the bottom of the anode and are focused by condenser lenses. The specimen, through which the focused beam passes, must be thin to minimize the absorption of the sample. When passing through the specimen the electrons interact with the atoms of the sample. Different amounts of electrons will pass through the specimen depending on its density. A map of density variation can be formed.

After passing through the specimen the scattered electrons are collected by an objective and an image is formed that is subsequently enlarged by an additional lens system called projective. The formed image is made visible on a fluorescent screen or on photographic material.

The resolution of an optical microscope is limited by the wavelength of the light according to equation 2.21 and similarly, the resolution of EM is determined by the wavelength of the electrons. The wavelength of particles can be calculated with the de Broglie's equation

$$\lambda = \frac{h}{p} = \frac{h}{m\upsilon} \qquad (2.23)$$

With λ as the wavelength, h as Planks constant, m the mass of the electron and υ the velocity. It can be seen that with a higher velocity the wavelength can be diminished which leads to a higher resolution according to equation 2.23.

A special sample preparation is needed when liquid samples are studied. The sample is applied on a grid with a pipette. The specimen grid is blotted with a filter paper to remove excess fluid and then rapidly plunged in liquid ethane. To prevent the formation of ice crystals, ethane must be cooled to the temperature of liquid nitrogen.

2.5.8 Isothermal titration microcalorimetry (ITC)

Calorimetry is the science of measuring the heat of chemical reactions or physical changes. Based on heat changes different thermodynamic quantities can be calculated such as enthalpy H, entropy S and the binding constant K_b.

The degree of stability of a complex can be described by the association-, binding-, equilibration-, or stability-constant K_b. Since the nanoparticle-ligand-complex (NL) and the free ligands (L) are in a dynamic equilibrium to each other (figure 2.22) K_b can be calculated from the law of mass action (equation 2.24).

Figure 2.22 Equilibrium reaction between nanoparticle (N) and ligand (L).

$$K_b = \frac{[NL]}{[N][L]} \tag{2.24}$$

From the value of K_b the standard reaction Gibbs energy $\Delta G°$ at equilibration ($\Delta G=0$) can be calculated (equation 2.26)

$$\Delta G = \Delta G° + RT \ln K_B = 0 \tag{2.25}$$

$$\Delta G° = -RT \ln K_B \tag{2.26}$$

By using the fist law of thermodynamic and the assumption that only expansion work is being performed the following is obtained for isotherm and isobar experimental conditions

$$dH = dq \tag{2.27}$$

The change in enthalpy is directly associated with the measured heat from the calorimeter.

From the values of the standard reaction, Gibbs energy $\Delta G°$, the standard reaction enthalpy $\Delta H°$ and the standard reaction entropy $\Delta S°$ can be obtained.

$$\Delta G° = \Delta H° - T * \Delta S° \tag{2.28}$$

A TAM III microcalorimeter from Thermometric was used for these measurements. It is a so called twin calorimeter, which means that it consists of two single calorimeters, one holds the sample and the other one holds a reference. The signal that is reported is the differential signal, i.e. the difference in the heat flow between the sample and the reference side. If the reference calorimeter is inert the signal will directly measure the heat exchange of the sample. A twin calorimeter has proven to be independent of the fluctuations of the thermostat and has therefore an improved sensitivity.

The ligand is titrated with a syringe over a capillary to the sample calorimeter, which results in a heat flow with every injection. An exothermic reaction shows a positive signal and an endothermic reaction show a negative signal (for TAMIII). By integrating the area of a signal the heat quantity per titration can be obtained. When the heat quantity is plotted against the molar concentration of the added ligand the binding enthalpy and the binding constant may be determined. It is important to remember that different effects could influence the result, such as solvent effects and dilution. It is therefore important that both substrates are soluble in the solvent and a dilution experiment should be done to subtract this from the real measurement.

As a result after a measurement a time dependent heat flow curve is to be seen (Figure 2.23). Every peak represents one injection of ligands. By integration of each peak a binding isotherm can be established, where the enthalpy (kJ/mol) against the molar ratio (ligand/substrate) is shown. The binding constant K_b can be received through fitting of the binding isotherm. Modern calorimeters have evaluation software where fitting of the binding isotherm is automatically executed.

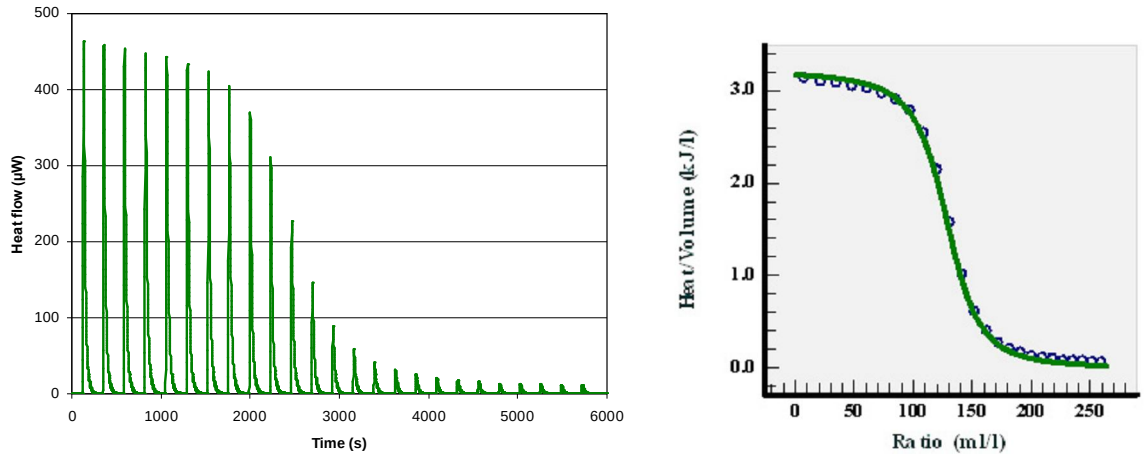

Figure 2.23 A test titration of Ba^{2+} ions to 18-crown-6 ether.

3 Synthesis and characterization

In this thesis bifunctionalized poly(ethylene oxides) (PEOs) were synthesized to act as ligands on nanoparticles to make them water soluble. The polymers were synthesized by anionic polymerization, which is explained in chapter 2.2. Different initiators and terminating agents were used to obtain a bifunctional polymer. The functionalities were chosen in order to obtain an anchor group to a nanocrystal on one end of the PEO and to enable the attachment of a biological molecule on the other end.

3.1 α- and α-ω-functionalized poly(ethylene oxides) by anionic polymerization

The synthesis of PEO was performed via anionic polymerization. A functionality in the α-position can be obtained via the initiator in anionic polymerization. It is important that the initiator is nucleophilic enough to start the polymerization and that the counterion and the growing polymer form a complex which is reactive and able to continue the polymerization. For example, small hard metal ions (e.g. lithium cation) form an intimate ion pair with the living end of the PEO, leading to a stable complex in which no polymerization can take place. Instead larger and softer counterions such as potassium cations were chosen to obtain a solvent-separated ion pair.

The initiators in this thesis were deprotonated with potassium naphthalene and the reaction route for the synthesis of potassium naphthalene is presented in scheme 3.1.

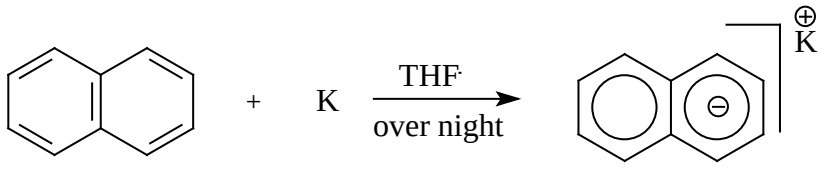

Scheme 3.1 Illustration of the formation of potassium naphthalene.

To obtain a functionality on the ω-position of the PEO, different termination agents for the polymerization can be used. The most common terminating agent is an acid which gives a hydroxylic group on the PEO.

3.1.1 Diphenylmethyl- and methoxy-PEO

To introduce a diphenylmethyl group to PEO, diphenylmethyl potassium can be used as initiator. Similarly methoxy-groups can be introduced to PEO using 2-methoxyethanyl potassium as initiator. To obtain the initiators diphenylmethane or methoxyethanol, respectively, are added to a solution of potassium naphthalene and stirred at room temperature under an inert atmosphere for 3 days. The base (potassium naphthalene) deprotonates the diphenylmethane or the 2-methoxyethanol and the negatively formed compound can be used as initiator for the polymerization. The reaction route for the formation of the initiator is illustrated in scheme 3.2.

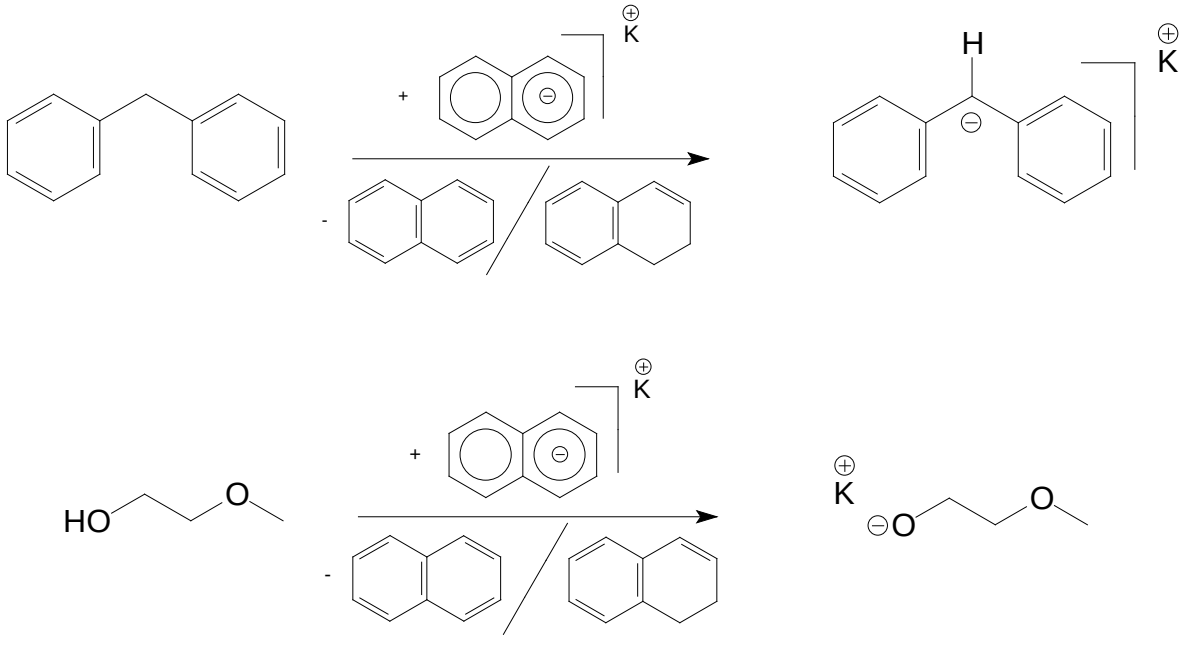

Scheme 3.2 The reaction route of the formation of the initiators, diphenylmethyl potassium and 2-methoxyethanyl potassium.

During the anionic polymerization it is important to exclude humidity because it terminates the chain reaction. Therefore the reaction is performed under an argon or nitrogen

atmosphere. The EO is dried with several steps, first over calciumhydrid, then over a sodium mirror and finally over butyllitium. The dried EO is subsequently condensed over to the reaction flask were it is dissolved in dry tetrahydrofuran (THF). To obtain a low PD, the initiator must quickly be added at the melting point of THF. Following the addition of the initiator the polymerization starts. Normally, the polymerization is quenched by adding acid, which results in a hydroxyl group on the other end of the PEO. The reaction route for PEO synthesis is displayed in scheme 3.3.

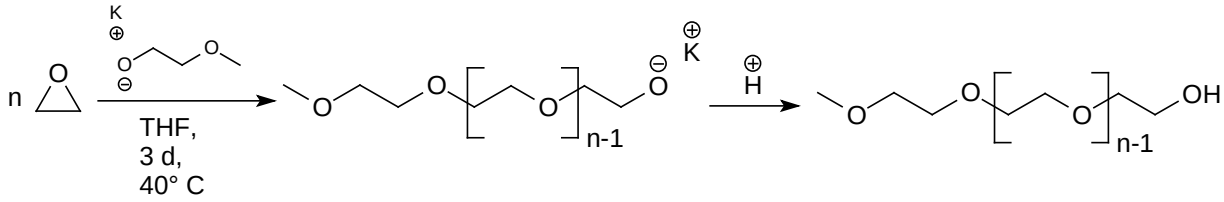

Scheme 3.3 Polymerization of PEO.

For the determination of the molecular mass and the PD, GPC and MALDI-TOF were employed. The methoxy initiator is widely used in the literature for synthesis of PEO[55, 56] and the initiator as well as the PEO is commercially available. The PEOs from both diphenylmethyl potassium and 2-methoxyethanyl potassium can be synthesized with a low PD. The GPC spectrum for an m-PEG (PEO-47) together with the PD is presented in figure 3.1.

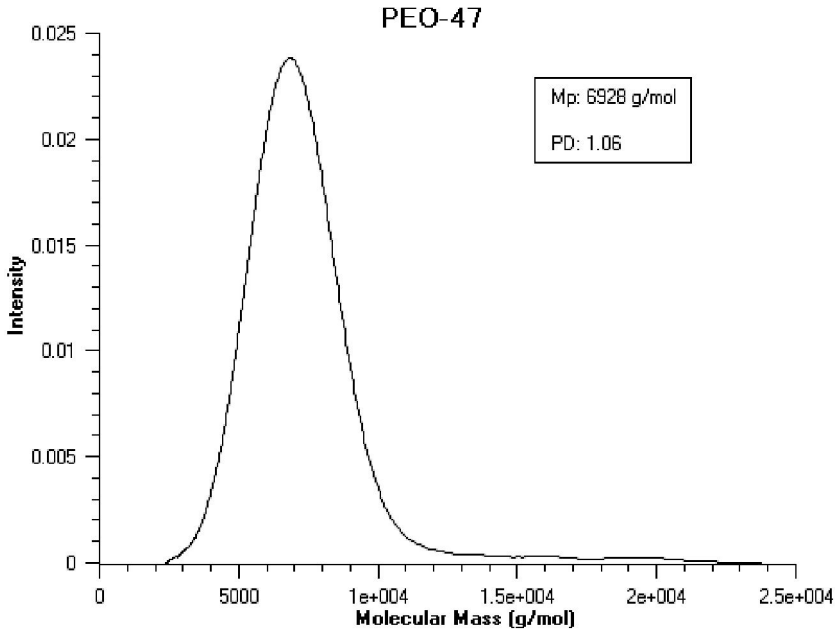

Figure 3.1 Molecular mass curves from the GPC of PEO-47 obtained in DMF at 70°C.

Both initiators are inert to further reactions and were used as a first step to investigate the possibilities of reactions on the ω-position of the polymer.

3.1.2 Acetal-PEO

An acetal group can be introduced to the PEO through the initiator 3,3-diethoxy-1-propanol. 3,3-diethoxy-1-propanol can be deprotonated in the same way as previously described in chapter 3.1.1. An acetal can easily be hydrolyzed to an aldehyde, which would enable further coupling reactions. The reaction route can be seen in scheme 3.4.

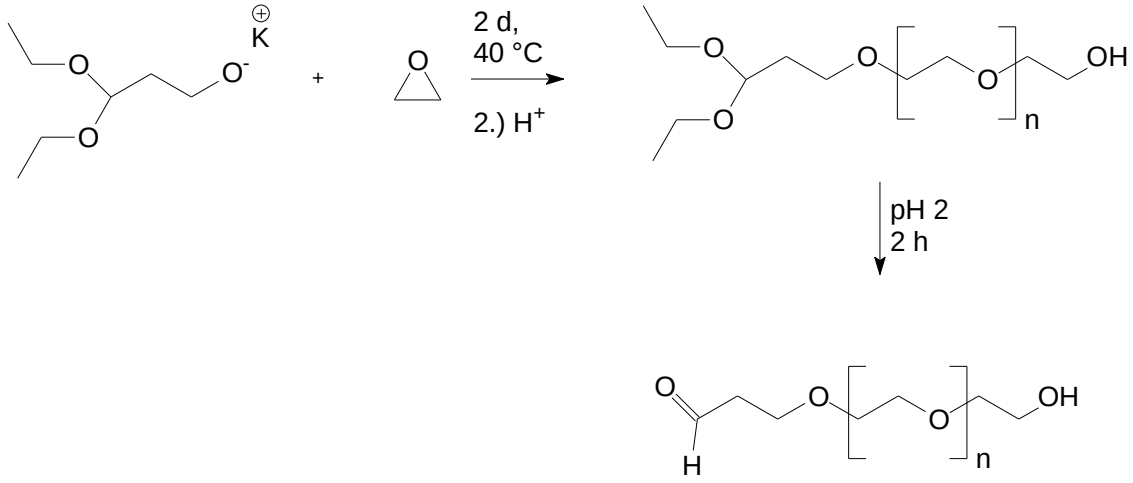

Scheme 3.4 The reaction route of aldehyde-PEO via anionic polymerization.

The polymer was characterized with GPC, MALDI and ^{1}H-NMR. The GPC and MALDI showed a low PD of the polymer. The ^{1}H-NMR spectrums of PEO with the acetal and the aldehyde, respectively, are presented in figure 3.2.

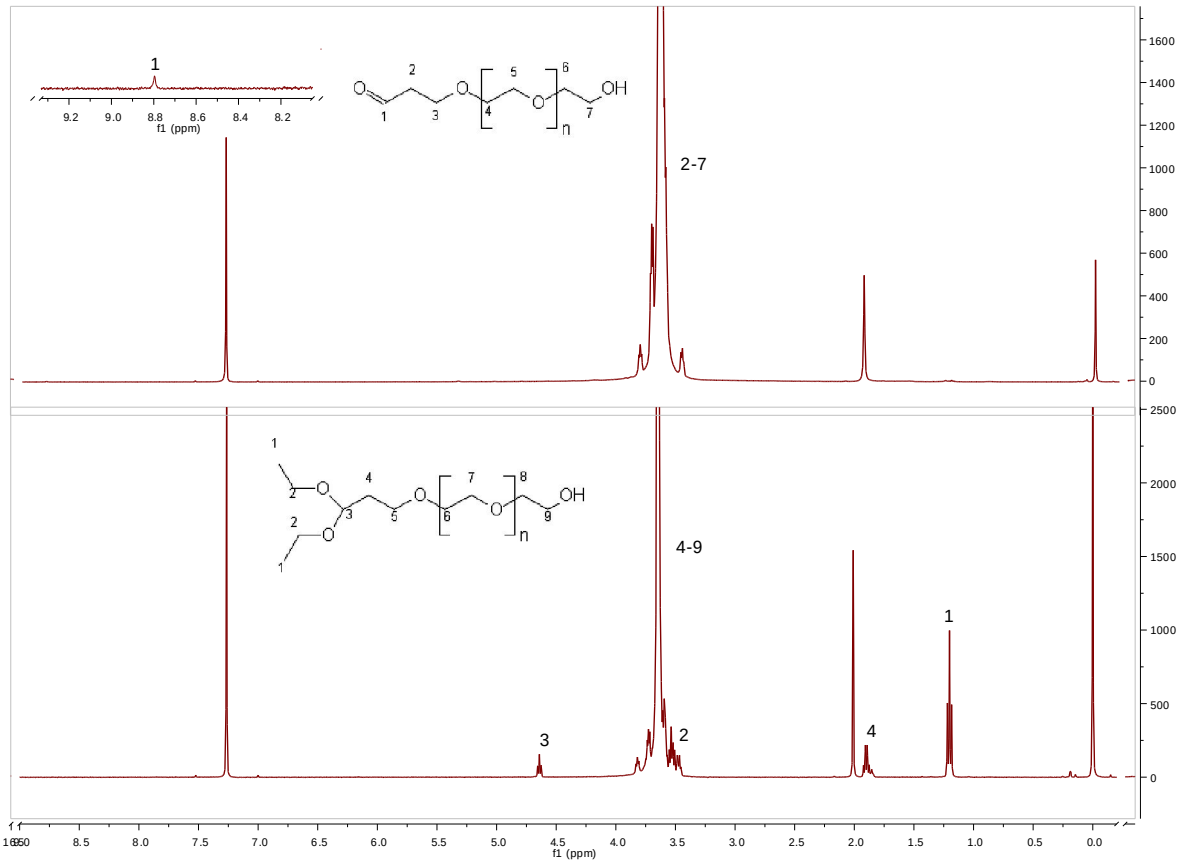

Figure 3.2 ^{1}H-NMR spectrum of PEO-44 with an aldehyde (top) and with the acetal group (bottom) obtained in $CDCl_3$.

The signals from the acetal are clearly visible at 4.64, 1.91 and 1.20 ppm, marked with 3, 4, and 1 respectively. The ratio of the integrals of the acetal signals to the signal of the PEO by 3.64 ppm can be used to calculate the molecular mass of the polymer. The calculated value was in good agreement with the measured molecular mass from the MALDI and the GPC. After hydrolysis of the polymer, the signals of the acetal disappear and a small signal at 8.8 ppm from the aldehyde is observed (figure 3.2). The signal from the aldehyde is not always detectable, which can be explained after observing a tail in the GPC spectra. The tail suggests that the aldehyde group reacts with the hydroxyl group on the other end of the PEO creating a PEO of double molecular mass. The GPC spectrum of the PEO-aldehyde obtained a couple of minutes after the hydrolysis, can be seen in figure 3.3.

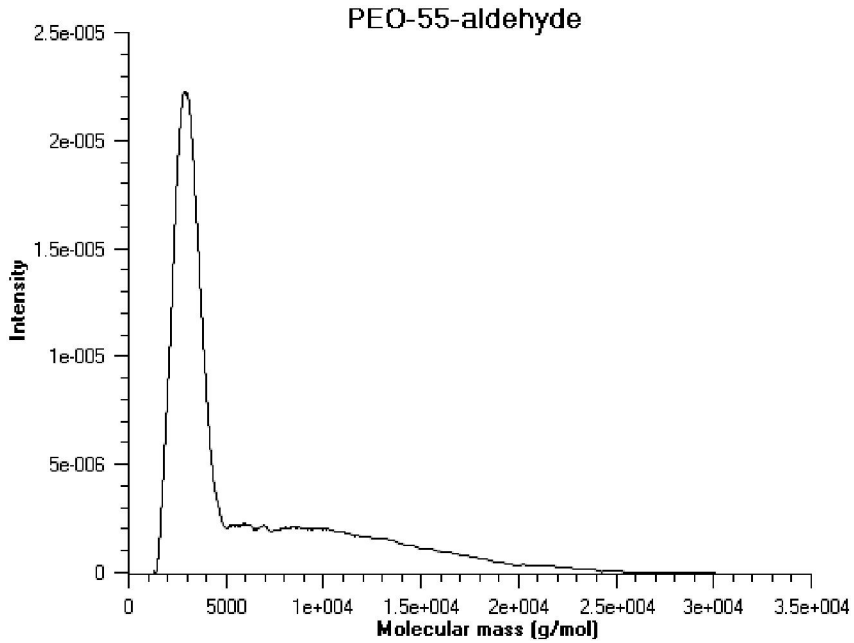

Figure 3.3 A GPC spectrum of hydrolysed PEO-55, a clear tail after the signal is observed.

3.1.3 Acrylate-PEO

2-hydroxy acrylate was used as initiator to obtain an acrylate functionality on the PEO. According to the data from GPC and MALDI a polymer of the desired molecular mass was obtained, however the signals from the acrylate could not be detected in the ^{1}H-NMR.

3.1.4 Carboxylic acid-PEO

For the introduction of a carboxylic acid on the PEO, ethyl bromoacetate was used as a termination agent. Hydrolysis of the ester transforms it into a carboxylic acid. The synthesis of the PEO was performed with anionic polymerization, which could be initiated with an arbitrary initiator. The reaction route with a methoxy initiator is shown in scheme 3.5.

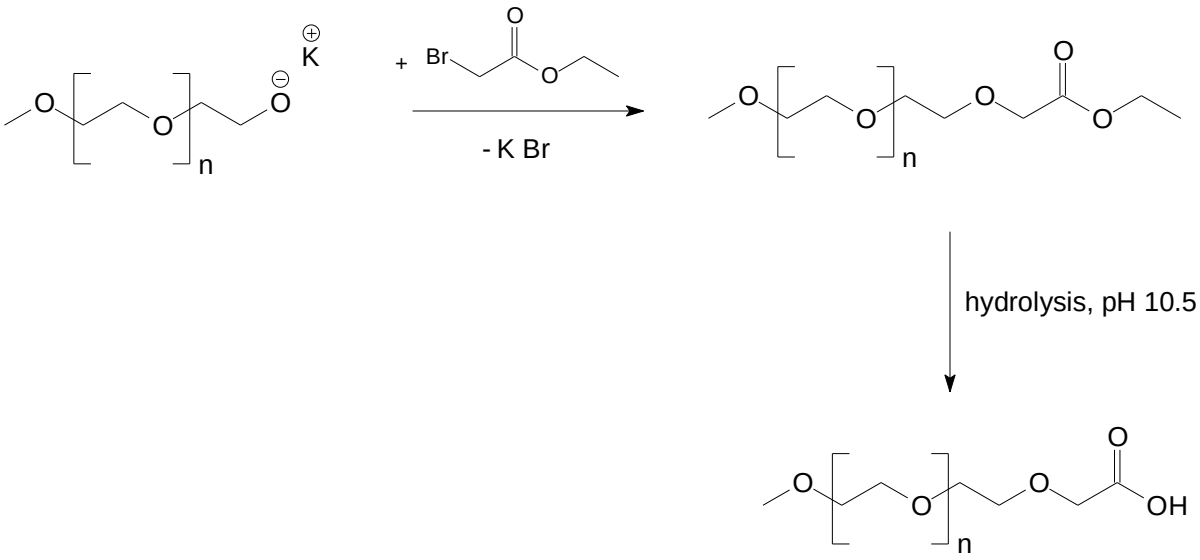

Scheme 3.5 The reaction route for a PEO with a carboxylic acid.

The ^{13}C-NMR of α-methoxy-ω-carboxylic acid-PEO is presented in figure 3.4.

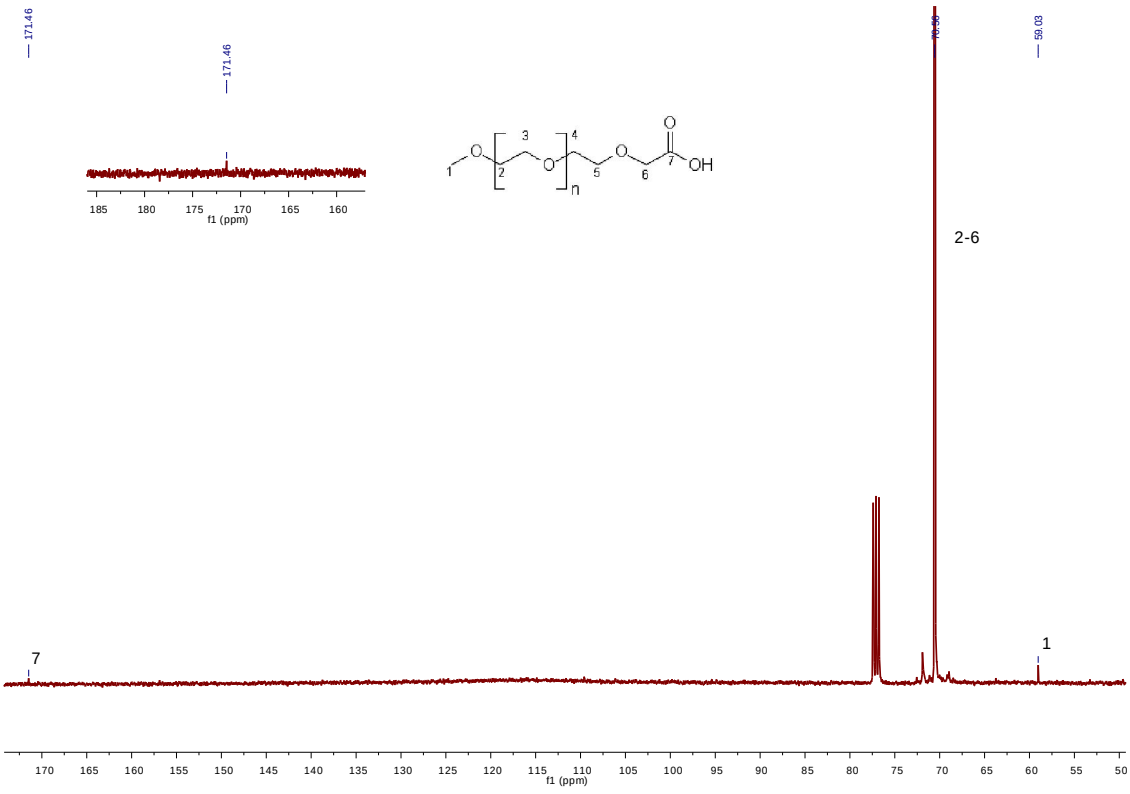

Figure 3.4 ^{13}C-NMR spectrum of PEO-39 obtained in $CDCl_3$.

The small signal observed at 171.46 ppm is the signal from the carboxylic acid and at 59 ppm the signal from the methoxy group can be observed. A titration with NaOH was performed to detect the conversion of the ester to carboxylic acid, showing a conversion of 92%.
The different PEOs synthezised in this thesis and their main characteristics are summarized in table 3.1.

Table 3.1. Main characteristics of synthesized PEOs.

Name	**Molecular mass MALDI (g/mol)**	**Molecular mass GPC (g/mol)**	**Polydispersity**	**α- position**	**ω-position**
PEO-36		2031	1.01.	diphenyl	carboxylic acid
PEO-37	3112	3000/6000		methoxy	carboxylic acid
PEO-38		2400	1.06	methoxy	carboxylic acid
PEO-39	2490	2450	1.05	methoxy	carboxylic acid
PEO-44	2050	2400	1.05	protected aldehyde	hydroxy
PEO-47	5600	6900	1.06	diphenyl	hydroxy
PEO-48		28000	1.05	diphenyl	hydroxy
PEO-49	2130	2200	1.05	methoxy	hydroxy
PEO-50		7500	1.15	acrylate	hydroxy
PEO-51	3450	3500	1.04	methoxy	hydroxy
PEO-52		7900		methoxy	hydroxy
PEO-53		1150	1.05	acrylate	hydroxy
PEO-54	1781	2550	1.03	aldehyde	carboxylic acid
PEO-55	2300	2996	1.08	protected aldehyde	hydroxy
PEO-56	3800	5575	1.08	methoxy	hydroxy
PEO-58		19424	1.14	methoxy	hydroxy

3.2 Functionalization reactions on poly(ethylene oxide)

3.2.1 Amine

It is well known that amines are good anchor groups to CdS, thus it is desirable to have amine groups on one end of the PEO. To introduce an amine on the PEO, the hydroxyl or carboxyl group had to be activated. An m-PEG was used to avoid the disturbance of a reactive group on the α-position. Several different activation groups were tested; 1) N-hydroxysuccinimide (NHS)[57], 2) 4-nitrophenyl chloroformate (NPCF)[58, 59], 3) triflouroethanesulphonyl chloride (TRES)[60] 4) N, N'-disuccinimidyl carbonate (DSC)[61] and 5) carbonyldiimidazole (CDI)[62].
NHS can be used to activate carboxy-capped PEO. The reaction was performed in DCM in the presence of DCC at 0°C for 1 hour and then another 24 hours at room temperature (scheme 3.6). The obtained yield after the purification process was low, and therefore alternative approaches for activation of PEO were tested.

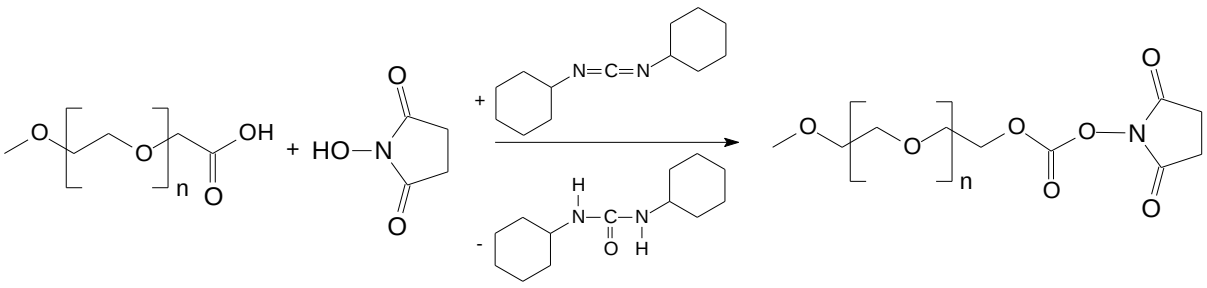

Scheme 3.6 The reaction route of the activation of PEO with NHS.

The activation with NPCF was performed on the hydroxyl group of the PEO, and two different methods were tested (scheme 3.7). The first approach was performed in THF in the presence of DMAP for 2 hours at room temperature. The second approach was performed in DCM in the presence of TEA and then stirred at room temperature for 16 hours. The products from both of the reaction mixtures were very difficult to purify and it was not possible to completely separate the product from the by-products and the reactants. Another drawback was that a definite double peak was detected by the GPC, showing the double molecular mass. This suggests that NPCF activates a PEO for further coupling to another PEO via the hydroxyl group, making it non-reactive for further coupling with amines.

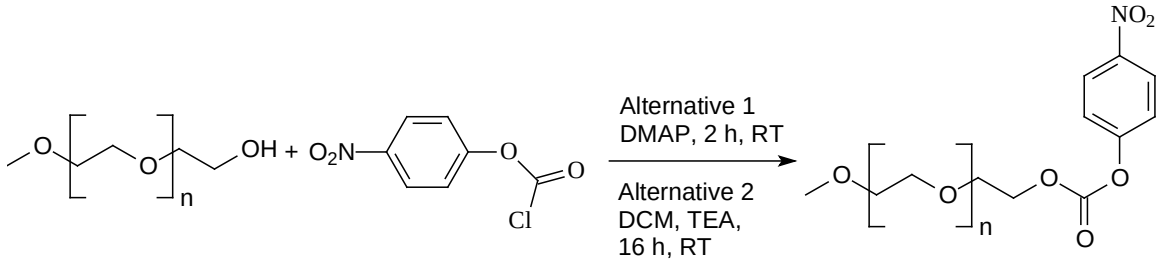

Scheme 3.7 Reaction routes of the activation of PEO with NPCF.

The activation with TRES was performed in THF under a nitrogen atmosphere and in the presence of TEA at 0°C for 4 hours (scheme 3.8). The obtained yield was low and other approaches were tested.

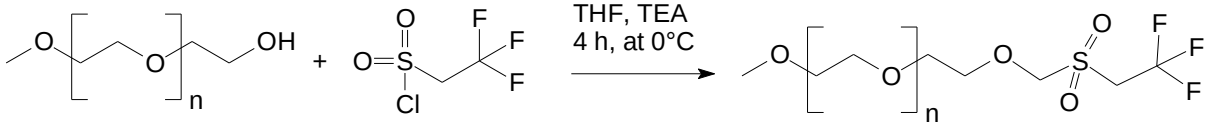

Scheme 3.8 Reaction route of the activation of PEO with TRES.

In the GPC a strong double coupling was observed, which made it non-reactive for further coupling reactions.

The activation of PEO with DSC was performed according to scheme 3.9. No product could be detected, which could be due to the fact that the DSC had a very low solubility in the solvent. The reaction was also performed at a higher temperature but the problem remained. Other different solvents were tested (for example THF, $CHCl_3$) but no improvement in solubility was observed.

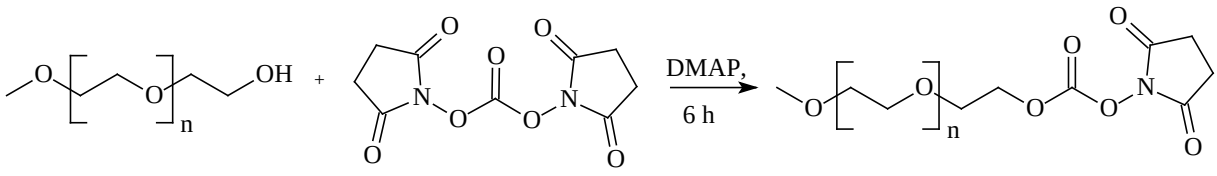

Scheme 3.9 Reaction route of the activation of PEO with DSC.

CDI can be used to activate a hydroxyl group. The reaction scheme for m-PEO with CDI is presented in scheme 3.10.

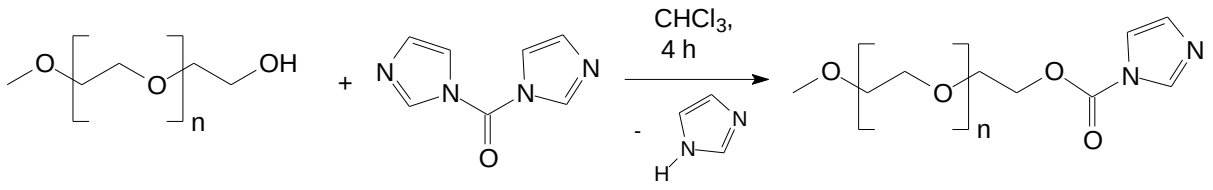

Scheme 3.10 Reaction route of the activation of PEO wit CDI.

The reaction was performed in chloroform, which was previously washed with water and dried over Na_2SO_4 to remove alcohols. During the activation with CDI problems with double coupling arised which were eliminated by adding excess of CDI. After 4 hours of stirring at room temperature the reaction mixture was washed with water. The unreacted CDI was hydrolyzed in water to imidazole and stayed in the water phase. The chloroform phase was dried over Na_2SO_4 and precipitated in cold diethyl ether to obtain the product imidazole-PEO.
In a MALDI spectrum of PEO-49 mixed with PEO-49-imidazole two curves can be seen where one is shifted to a higher molecular mass (figure 3.5). The shift is in good agreement with the molecular mass of the imidazole group.

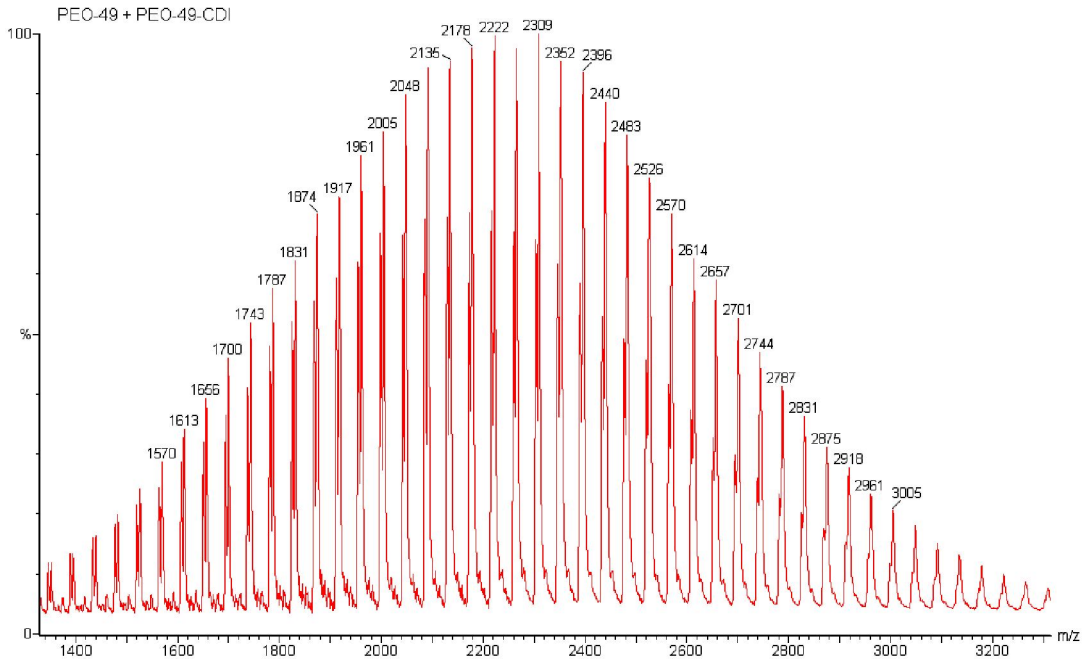

Figure 3.5 A MALDI spectrum of a mixture of PEO-49 and PEO-49-imidazole.

The ^{1}H-NMR of the PEO-imidazole is presented in figure 3.6. The three signals from the protons on the imidazole are clearly visible at 8.16, 7.45 and 7.07 ppm. The integral of the

signals from the imidazole in comparison with the signal from the PEO, shows a conversion of nearly 100%.

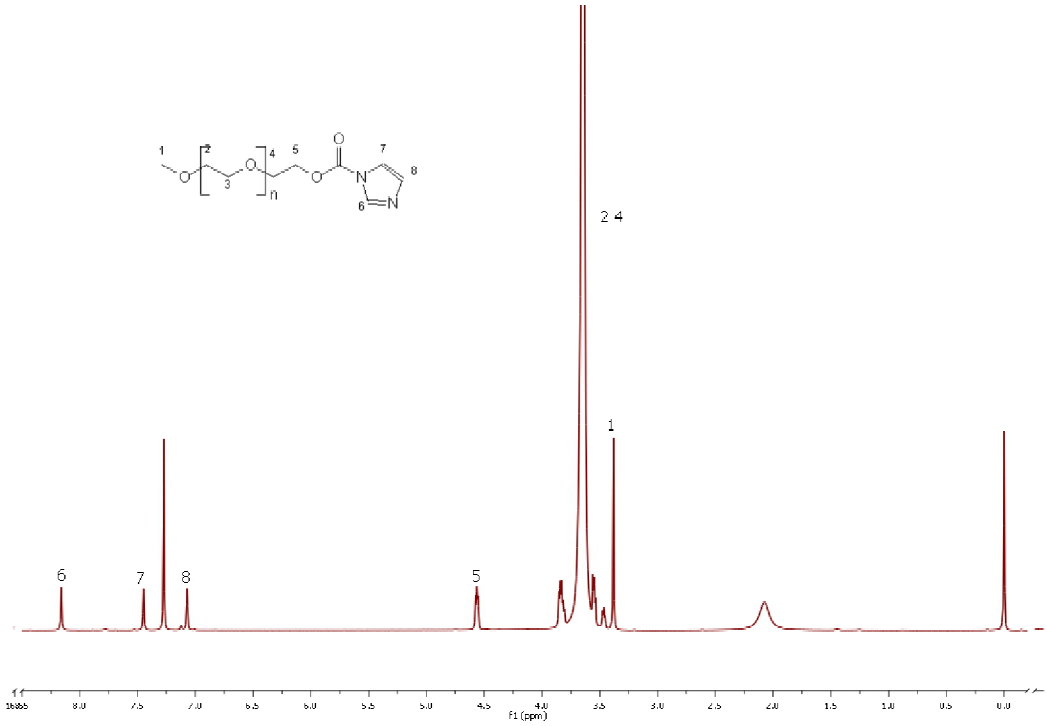

Figure 3.6 ^{1}H-NMR spectrum obtained in $CDCl_3$ of PEO-49-imidazole.

The activated PEO was further reacted with an amine group, where different lengths were tested to compare their ability to act as ligands to nanoparticles. The different amines used were; diethylenetriamine (DETA), triethylenetetramine (TETA), tetraethylenepentamine (TEPA), pentaethylenehexamine (PEHA) and a branched poly (ethyleneimine) (PEI). The synthetic route can be seen in scheme 3.11.

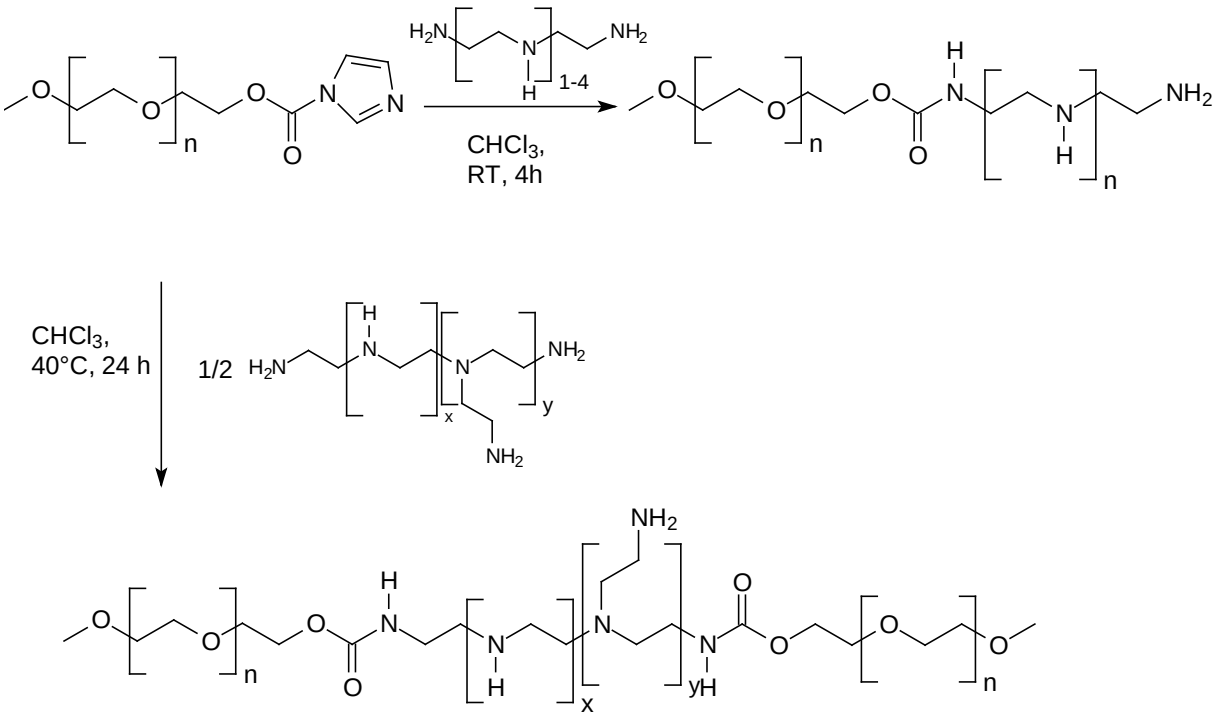

Scheme 3.11 Synthetic route of the aminofunctionalized PEO from the CDI activated PEO.

In order to avoid that one amine molecule reacts with several polymers resulting in double or triple molecular mass, a large excess of the amine was necessary. GPC was used to ascertain that the desired molecular mass was obtained.

The GPC curves of PEO with different amines can be seen in figure 3.7. It is noticeable that an expected shift to higher molecular mass with the longer amines cannot be observed, which is due to the fact that amines strongly bind to the column filling of the GPC[63]. A small amount of by-product is detected with the GPC, which corresponds to the signal of low intensity at higher molecular mass in the spectrum. This signal has twice the molecular mass of the strong signal, which indicates that a small amount of the amines has reacted with two PEO chains.

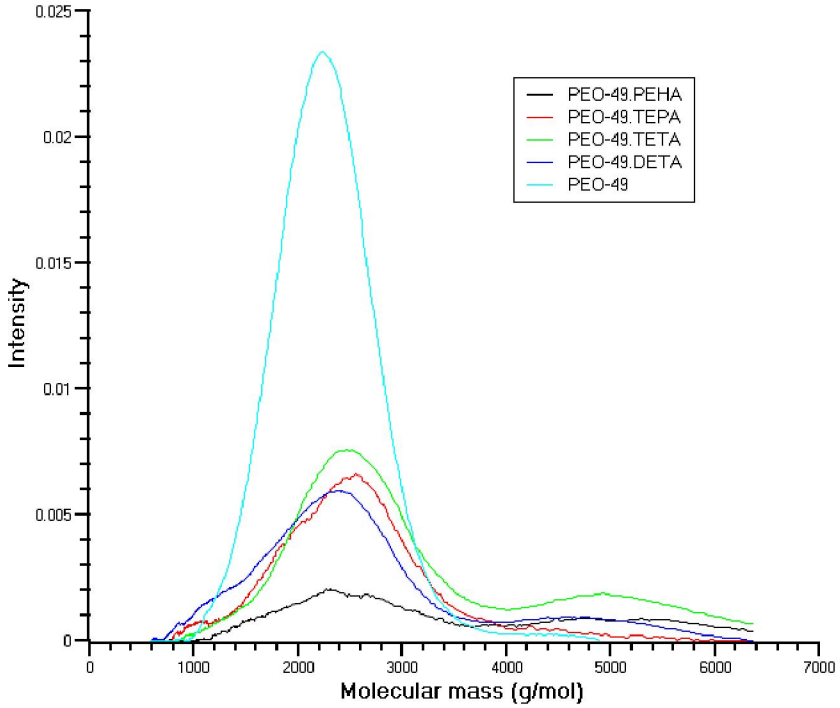

Figure 3.7 GPC spectrum of PEO-49 with amines of different lengths obtained in DMF at 70 °C.

The unreacted amine was removed from the product in multiple precipitation steps in diethylether. It is crucial that the diethylether is not too cold (about 8-10 °C) to prevent that the free amine precipitates together with the PEO. After each precipitation step a ^{1}H-NMR spectrum was made to control that all unreacted amines were removed. In figure 3.8 the number of protons from the amine in relationship to one PEO-chain is presented. It is apparent that 3-4 precipitations are necessary to remove the excess of unreacted amines.

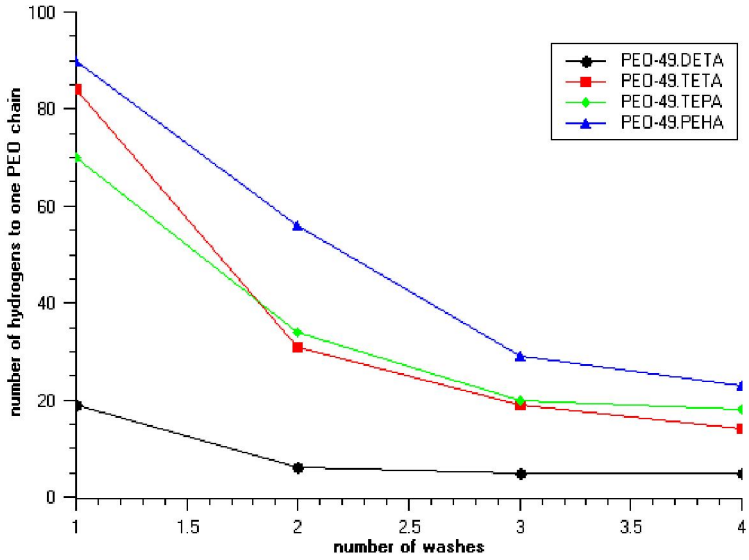

Figure 3.8 Relation between the number of precipitations and the number of protons of the amine.

A ^{1}H-NMR spectrum of PEO-49-DETA after three precipitations is presented in figure 3.9.

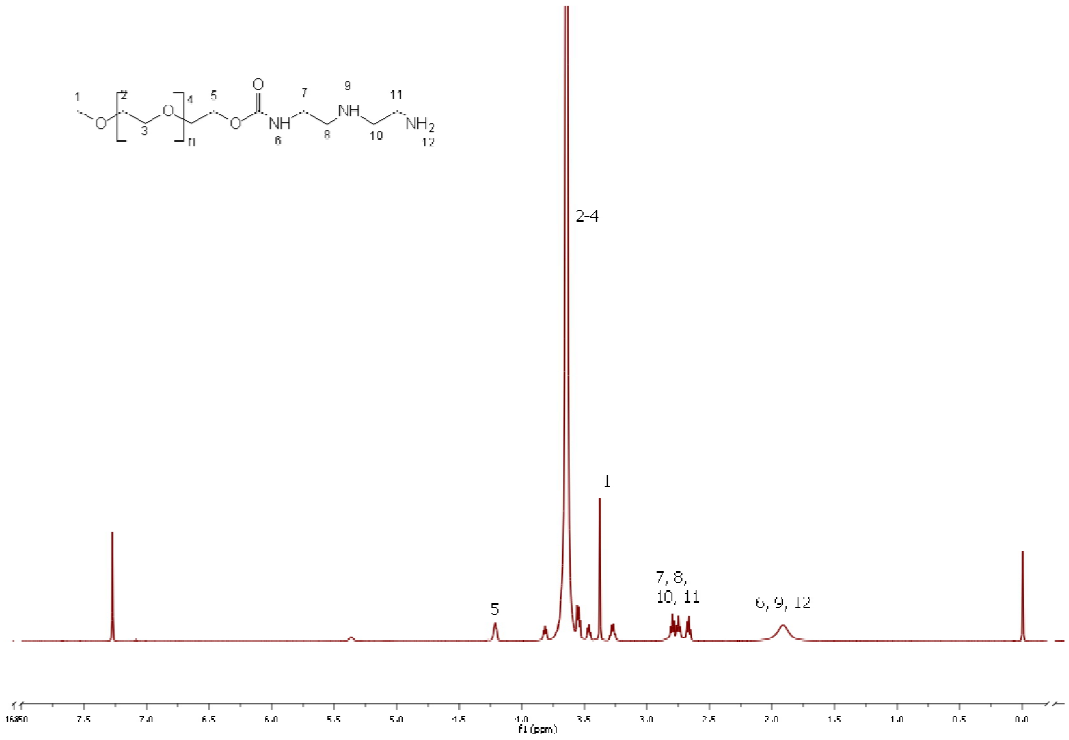

Figure 3.9 A ^{1}H-NMR spectrum of PEO-49-DETA obtained in $CDCl_3$.

It can be seen from the ^{1}H-NMR that the signals from the imidazole have disappeared and instead a multiplet at 2.67-2.80 ppm is observed. The multiplet arises from the protons of DETA, the ratio of the integral from the multiplet to the signal from PEO at 3.6 ppm can be used to calculate the number of amines to one PEO chain. This gives that each PEO chain is coupled to one DETA molecule.

In the MALDI spectrum a clear shift to a higher molecular mass is visible; MALDI of PEO-44 and PEO-44-DETA and PEO-44-PEHA is presented in figure 3.10. The shift to a higher molecular mass is in good agreement with the molecular mass of the added amines.

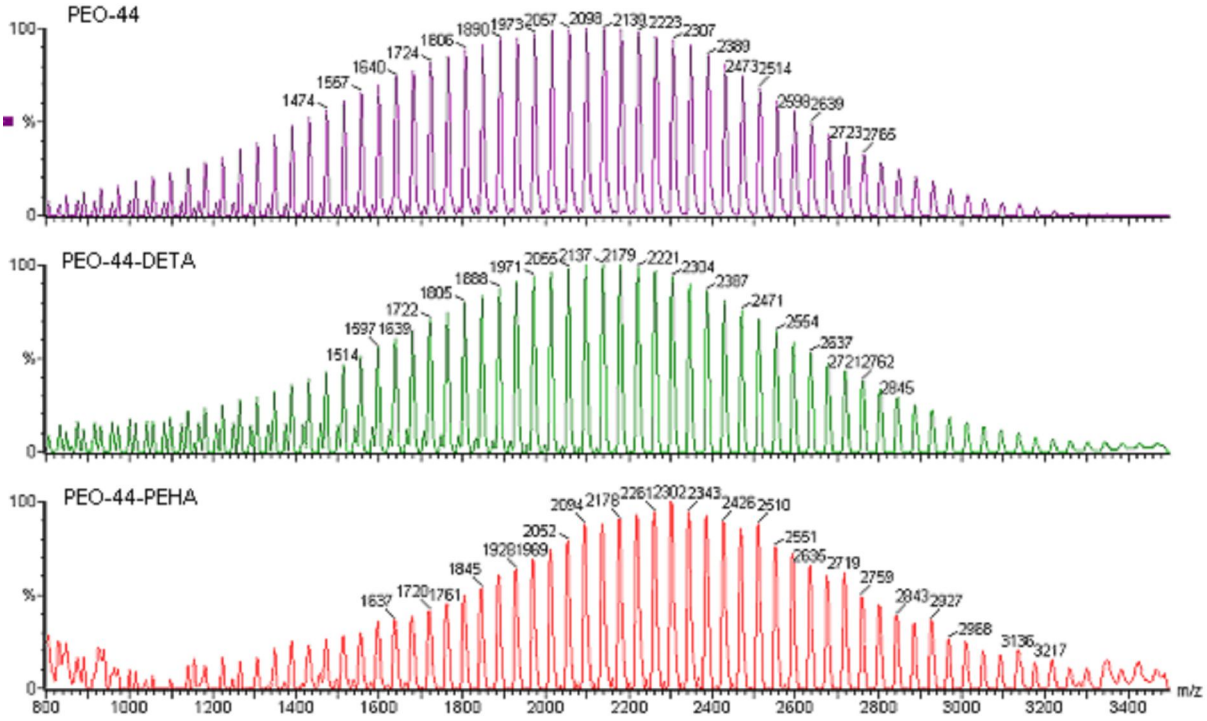

Figure 3.10 MALDI spectrums of PEO-44, PEO-44-DETA and PEO-44-PEHA.

The reaction with the branched PEI was also performed via the activation of PEO with CDI, but no excess of amine was used. The idea was instead to obtain two PEO molecules on each PEI molecule. The ^{1}H-NMR spectrum of PEO-49-PEI is illustrated in figure 3.11.

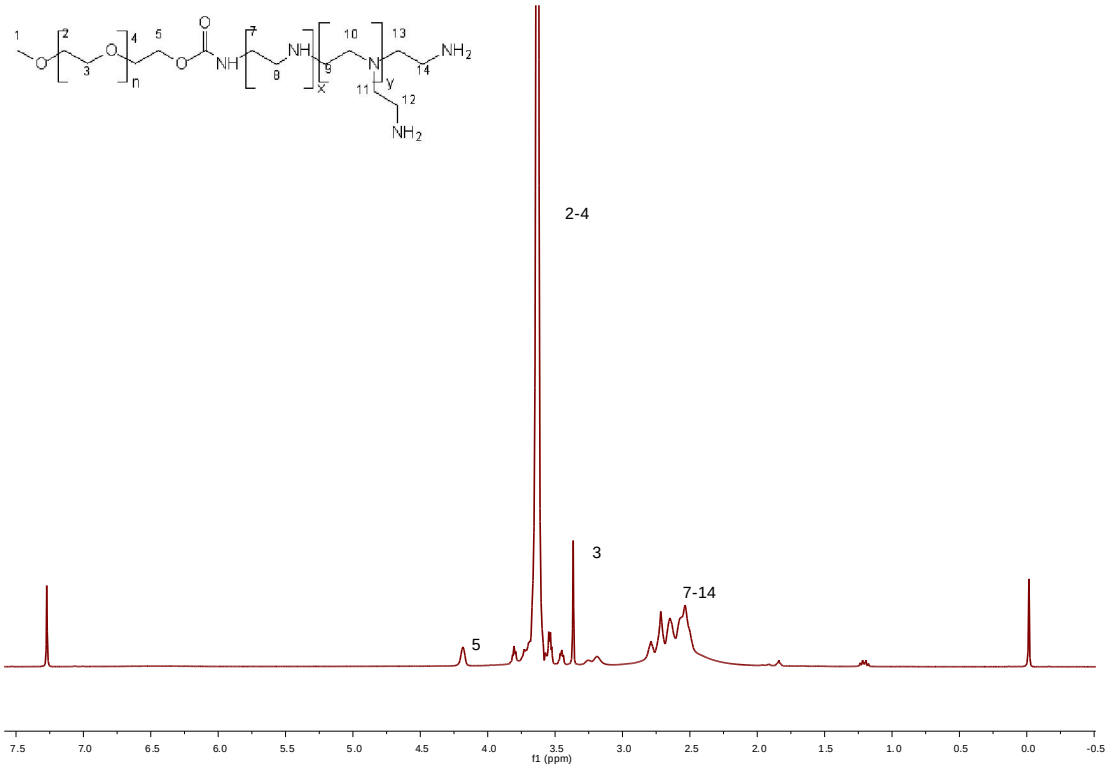

Figure 3.11 ^{1}H-NMR spectrum of PEO-49-PEI obtained in $CDCl_3$.

The GPC spectra of PEO-44-PEI can be seen in figure 3.12, and a tendency to two peaks that cannot be completely separated is visible. The first shows a molecular mass of a PEI with one PEO, and the second is one PEI coupled to two PEO chains. The mixture of these was directly used in the ligand exchange without further purification.

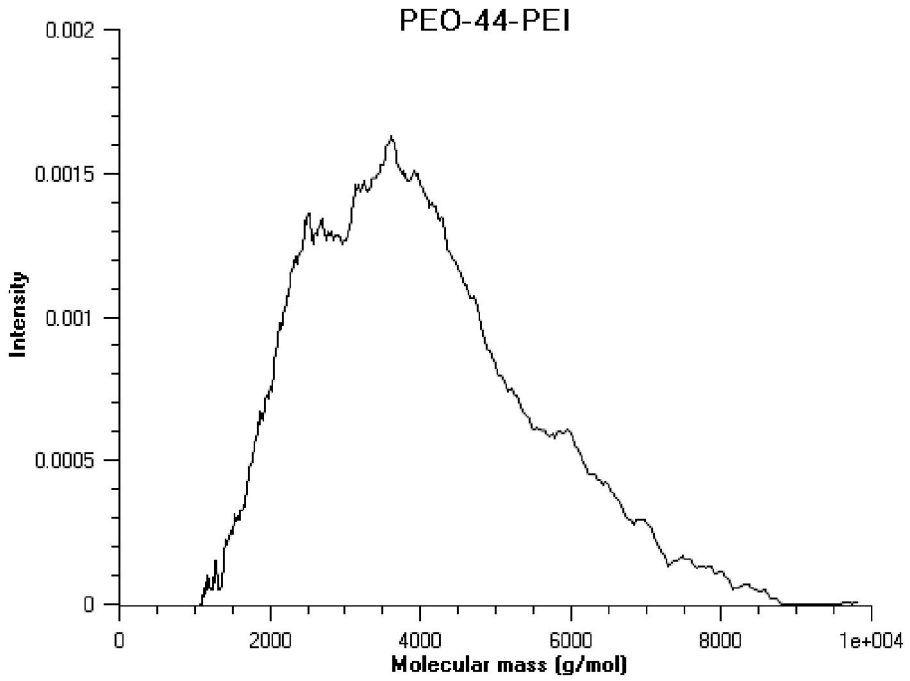

Figure 3.12 A GPC-spectrum of PEO-44-PEI obtained in DMF at 70°C. A mixture of PEI with one respectively two PEO chains is observed.

3.2.2 Thiol

A PEO with a mercapto group was synthesized to compare its stability on the NC with that of the amino functionalized PEOs. Cysteine was chosen to introduce a mercapto group to the PEO. Cysteine is an amino acid, which means that it is biocompatible, and hence interesting as a ligand within the field of drug delivery.

The introduction of cysteine on the polymer was performed with the same activation procedure as for the amines. PEO-imidazole can react with the amine group on the cysteine and form the required product.

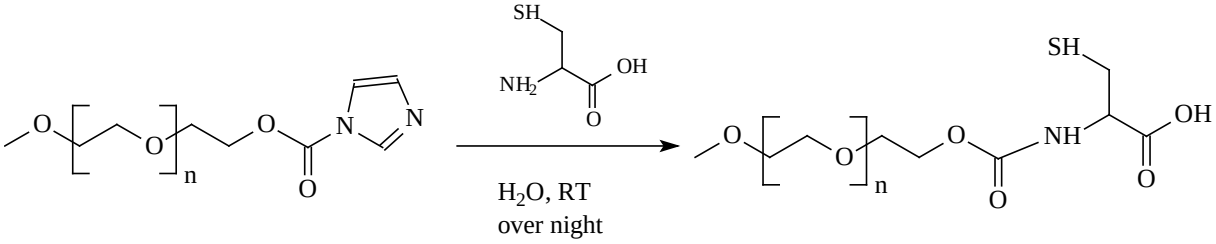

Scheme 3.12 The synthetic route of the coupling between activated PEO and cysteine.

In the MALDI spectrum (figure 3.13) a visible shift to a higher molecular mass is observed, which is in good agreement with the molecular mass of cysteine.

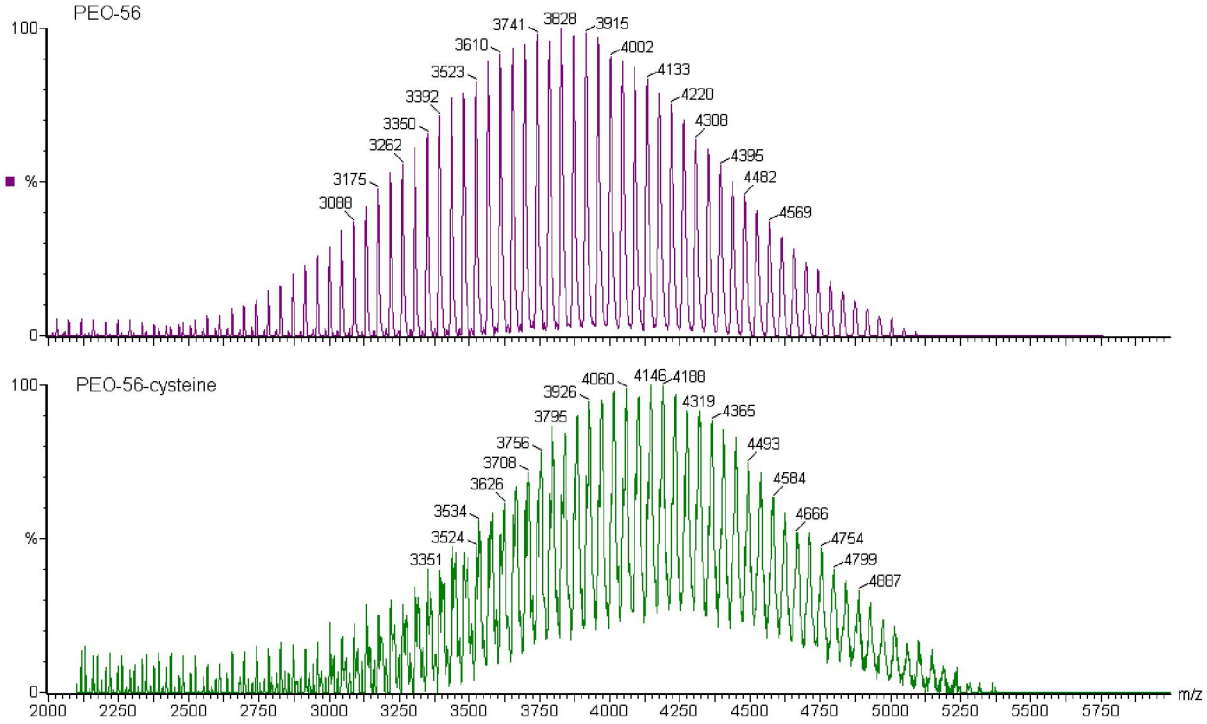

Figure 3.13 MALDI spectrums of PEO-56 and PEO-56-cystein.

3.2.3 Fluorescein

The carboxy capped PEO was used to stabilize magnetic NP. Magnetic particles have the disadvantage of being invisible in microscopic studies, thus flourescein (an organic dye) was coupled to the PEO.

It is known that amines and hydroxyl groups can be covalently linked to aldehyde groups, and this was used to obtain the required PEO-fluorescein. The reaction was performed in water at room temperature for 24 h. To remove the excess fluorescein, dialysis was performed for approximately 3 days. The reaction route can be seen in scheme 3.13.

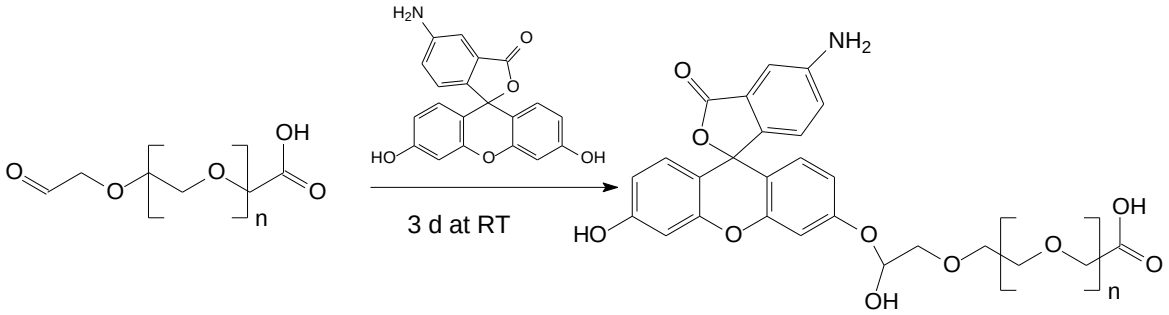

Scheme 3.13 The synthetic route of PEO-fluorescein.

MALDI spectrum of the PEO-54-fluorescein showed, in comparison to PEO-54, a shift to a higher molecular mass. This shift is in good agreement with the molecular mass of fluorescein (figure 3.14).

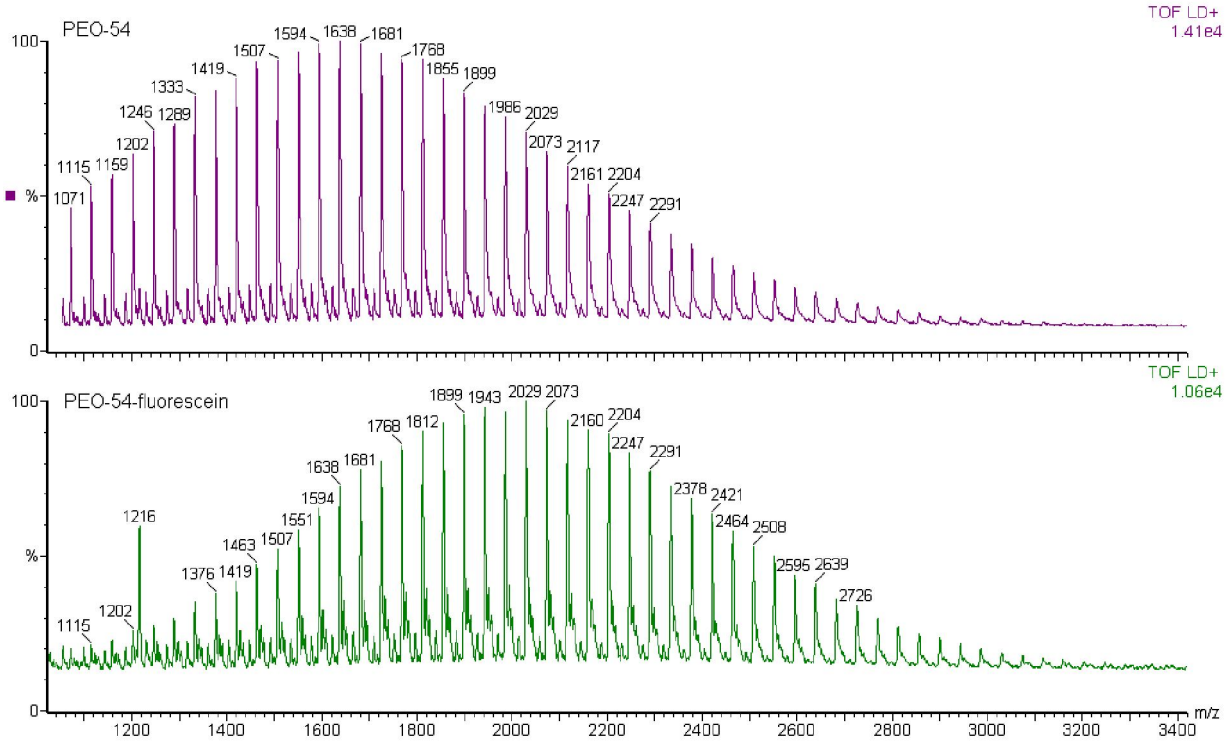

Figure 3.14 MALDI spectrums of PEO-54 and PEO-54-fluorescein.

4 Polymer-nanoparticle-conjugates

To be able to use NPs within the field of biomedicine it is necessary to make them water soluble. Most of the reported syntheses of NPs lead to a coating of hydrophobic molecules[64, 65]. Two main strategies exist for converting hydrophobic NPs into hydrophilic particles. The first approach is based on the inclusion of hydrophobic NPs into amphiphilic micelles leading to an interdigitated bilayer[66, 67]. However, the supramolecular assembly is large (diameter >10 nm), and mainly maintained by local hydrophobic interactions. The second approach involves an exchange of the original hydrophobic layer with hydrophilic ligands. This strategy has successfully been applied using functional groups that strongly adhere to the NP surface, such as phophines, amines, thiols and carboxylic acids.

Most of the reported work with the latter strategy has been performed with small molecules that have one group that binds to the NP and another group that provides for the water solubility. In this thesis a longer chain, PEO, has been used to serve for the water solubility. The water solubility of PEO is very good due to the hydrogen bonding between the water molecules and the oxygen in the polymer backbone[68]. The inertness of PEO makes it suitable to use by surface treatment to provide for biocompatibility. However, the inertness also means that PEO has no groups that can adhere to the surface of the NPs. In order to use PEO for changing the solubility of the NPs, PEO must be properly functionalized. In this thesis, amines, a thiol and a carboxylic acid were used as functional groups that adhere to the NP surface.

4.1 CdSe/CdS Quantum dots

Amines are known to strongly interact with Cd sites on the QD surface, which makes them appropriate as ligands for CdSe/CdS QDs. When the nanoparticles are exposed to a large excess of a new ligand, ligand exchange occurs. In order to promote ligand exchange, all the samples were thoroughly washed before the ligand exchange procedure to remove as much of the old ligand as possible. To separate the old ligands from the new-capped nanoparticles, the new capped-nanoparticles were precipitated. Hexane and cyclohexane, which function as a non-solvent for the new ligands, and serve as a solvent for the old ligands (TOP/TOPO), were

used for these ligand exchanges. After centrifugation, the obtained pellet was soluble in solvents for the new capping group, such as water for PEO.

A control experiment was performed in which non-functionalized PEO was used. The addition of cyclohexane to a chloroform solution containing nanoparticles and polymer resulted in a precipitation of the polymer only, and the nanoparticles remained well dispersed in the chloroform/cyclohexane mixture. This control test showed that ligand exchange occurred only when an amine-functionalized PEO was used, excluding any possible agglomeration of the nanoparticles by the polymer itself. The visible changes on the nanoparticle after ligand exchange with different polymer/nanoparticle ratios are shown in table 4.1.

Table 4.1. Visible characteristics after ligand exchange on QDs.

Polymer/ QD ratio	250	500	1000	1500
PEO-49-DETA	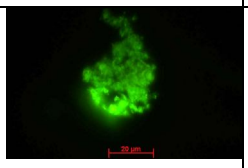	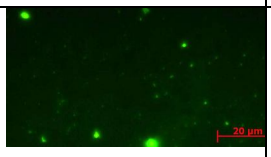	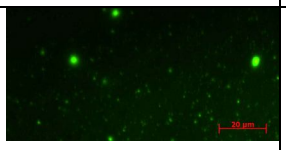	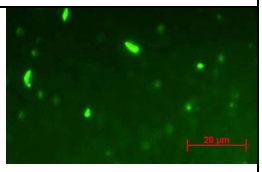
PEO-49-TETA	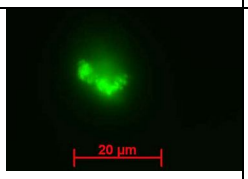	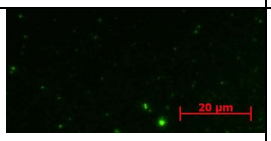	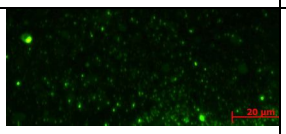	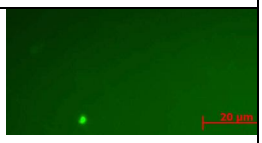
PEO-49-TEPA	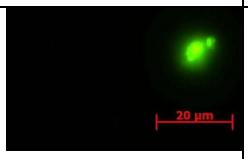	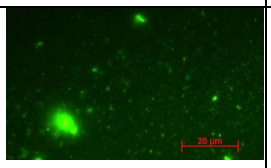	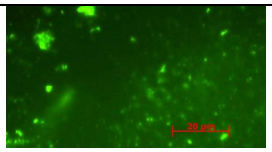	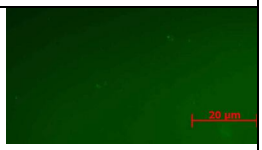
PEO-49-PEHA	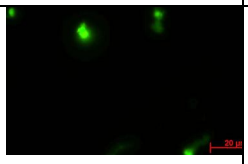	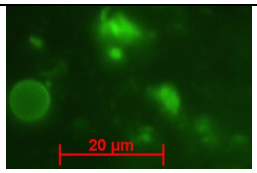	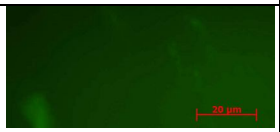	
PEO-49-PEI	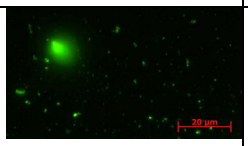	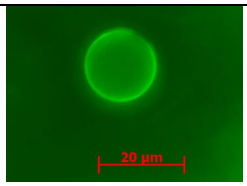	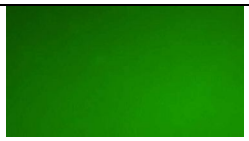	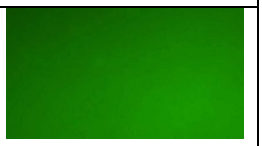

PEO-47-DETA	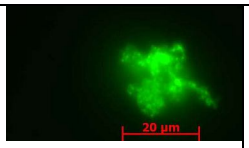	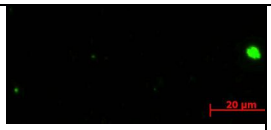	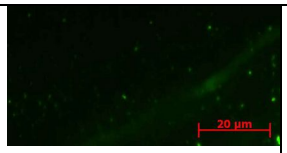	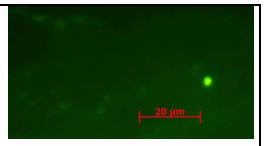
PEO-47-PEHA	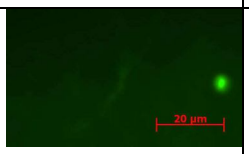		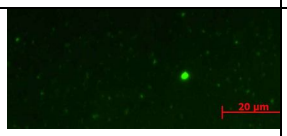	No luminescence
PEO-47-PEI	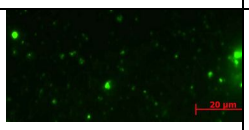	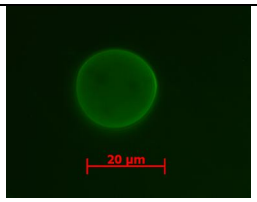		No luminescence
PEO-56-cystein	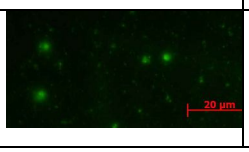	No luminescence	No luminescence	No luminescence

Fluorescence microscopy studies of the nanoparticles after ligand exchange (table 4.1) showed that the nanoparticles with PEO, functionalized with a shorter amine as a ligand, aggregate. This was observed for the molecular weight of 2000 g/mol (PEO-49) and 5000 g/mol (PEO-47), less aggregation was observed for the higher ratios of polymer to nanoparticles but a homogeneously even luminescent solution was not observed. Ligand exchanges with polymer/QD ratios up to 2500 were performed without any improvement in the stability. The QDs with the PEO ligands DETA, TETA and TEPA showed a visible precipitation for the higher ratios (>1000) after a couple of hours up to a couple of days. The lower polymer/QD ratios have poor water solubility and a visible precipitate was observed directly after ligand exchange. The QDs with PEO with PEHA on the other hand is stable in room temperature for a couple of weeks, while the PEO-PEI nanoparticles can be stored in water at room temperature for several months.

To exclude that the poor stability of the water-soluble QDs with short amines was due to an incomplete ligand exchange, different factors were changed during the exchange to see if the stability could be improved. If some of the old ligands, in this case TOP/TOPO, were still present after the ligand exchange they would make the water solution unstable. Therefore, two precipitations following the ligand exchange were performed to remove more of the old ligands. However, the resulting water-soluble QDs did not show any improved stability, instead a lower luminescence in comparison to the QDs made with only one precipitation was observed. Another strategy to improve the ligand exchange was to extend the incubation time

of the exchange procedure. The QDs were mixed with the new ligand and stirred for 1, 2 or 3 hours. None of the water soluble QDs from this exchange procedure showed any enhancement in stability or luminescence.

In table 4.1 it can also be seen for the amine ligands that the QDs with the shorter PEO chain (PEO-49) show a higher luminescence than the QDs with the longer PEO chain (PEO-47). This is probably due to the fact that the higher molecular weight ligands cannot be as tightly packed around the nanoparticle, hence are not able to passivate the surface as efficiently as the shorter PEOs.

The same ligand exchange procedure was applied for the thiol ligands. This gave more stable QDs in comparison to the shorter amine ligands but with a lower luminescence, which completely disappeared after 1-2 days. When using higher polymer/QD ratios (1000) the luminescence completely disappeared directly after the ligand exchange.

For the PEO-PEI ligand it was observed that a specific polymer to nanoparticle ratio gave a homogeneously even luminescent solution. For the lower ratios the nanoparticles started to aggregate, and self-assembly of the nanoparticles that looked like vesicles could be seen. The formation of vesicles is noteworthy. It is well known that amphiphilic molecules like surfactants, lipids and blockcopolymers spontaneously self-assemble into micelles or vesicles. Presently notice is given to the use of nanoparticles as inorganic building blocks[69, 70, 71]. An organized arrangement of the nanoparticles in a solution is usually achieved by attaching them to molecules that show spontaneous assembly such as DNA[72] , proteins[73] or amphiphilic polymers[74, 75]. Self-assembly by amphiphilicity could in principle be translated to nanoparticles with a hydrophilic ligand. This would enable spontaneous self-assembly into one-, two-, and three-dimensional structures similar to those of lipids and surfactants. As explained in chapter 2.4 the resulting structure of amphiphilic self-assembly can be described by the surfactant parameter $N_s = \frac{v}{la_0}$. For amphiphilic nanoparticles, l corresponds to the radius of the particle, R, and v correspond to the partial volume of the nanoparticle per polymer ligand and can be expressed as $v = \frac{V}{N}$, where N is the number of polymeric ligands per nanoparticle and V the nanoparticle volume. The surfactant parameter can then be described as follows

$$N_s = \frac{V}{NRa_0} = \frac{4\pi R^2}{Na_0} \qquad (4.1)$$

It was confirmed by microscopy that aminofunctionalized polymers have no tendency of organizing themselves in water in the absence of nanoparticles, as expected from their composition. A control experiment was also performed with a small amount of the old ligand (TOP/TOPO) present, however without any tendency of self-assembly. Hence, the observed structures are self-organizing systems obtained only through interaction between the nanoparticles and the polymeric ligands. The type of self-assembly observed for the nanoparticle-polymer conjugates, resembles those typical for tenside molecules.
In figure 4.1 PEO-49-PEHA with CdSe/CdS nanoparticles form vesicle-like structures. The contours of the rings are not solid as if the nanoparticles have aggregated together at a couple of places. These vesicles are not stable and can only be observed directly after the ligand exchange, and already after a couple of hours only undefined aggregates could be seen.

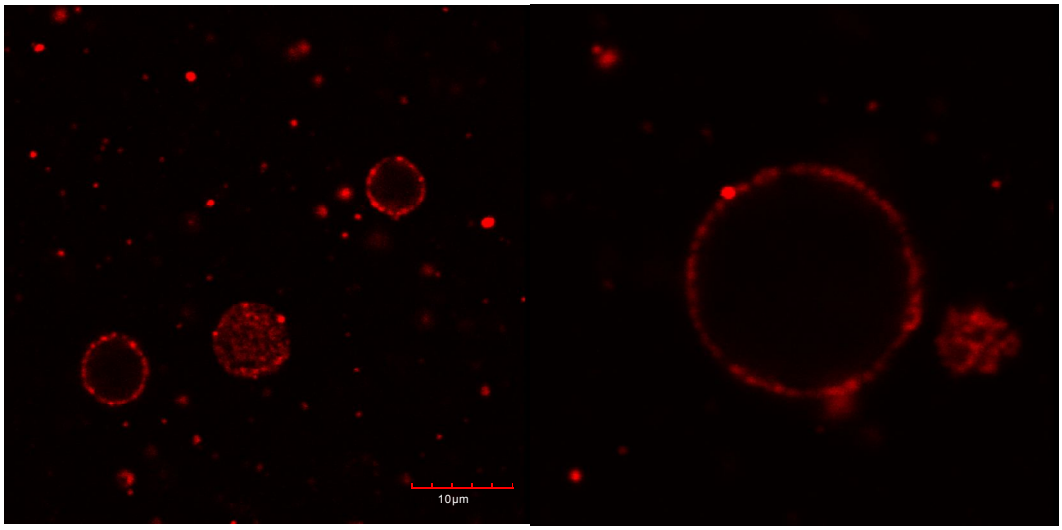

Figure 4.1 CLSM pictures of PEO-49-PEHA with CdSe/CdS (2.8 nm).

The contour of the vesicles formed with PEO-49-PEI and CdSe/CdS nanoparticles (figure 4.2) are slightly more defined and remain stable up to a couple of hours.

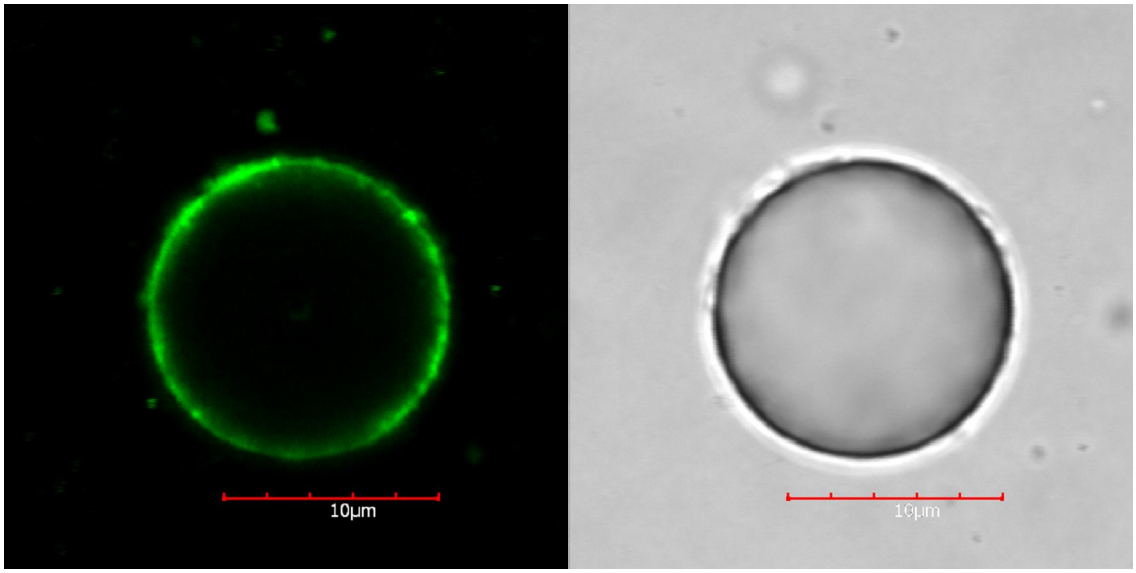

Figure 4.2 CLSM picture of PEO-49-PEI and CdSe/CdS (2.6 nm).

In figure 4.3 a vesicle of PEO-47-PEI with CdSe/CdS (3.1 nm) can be seen. The vesicles formed with this polymer were stable for 1 day and a definite ring could be observed. These vesicles were more stable than the vesicles formed with a shorter PEO, making it possible to obtain three-dimensional pictures in the CLSM (figure 4.4).

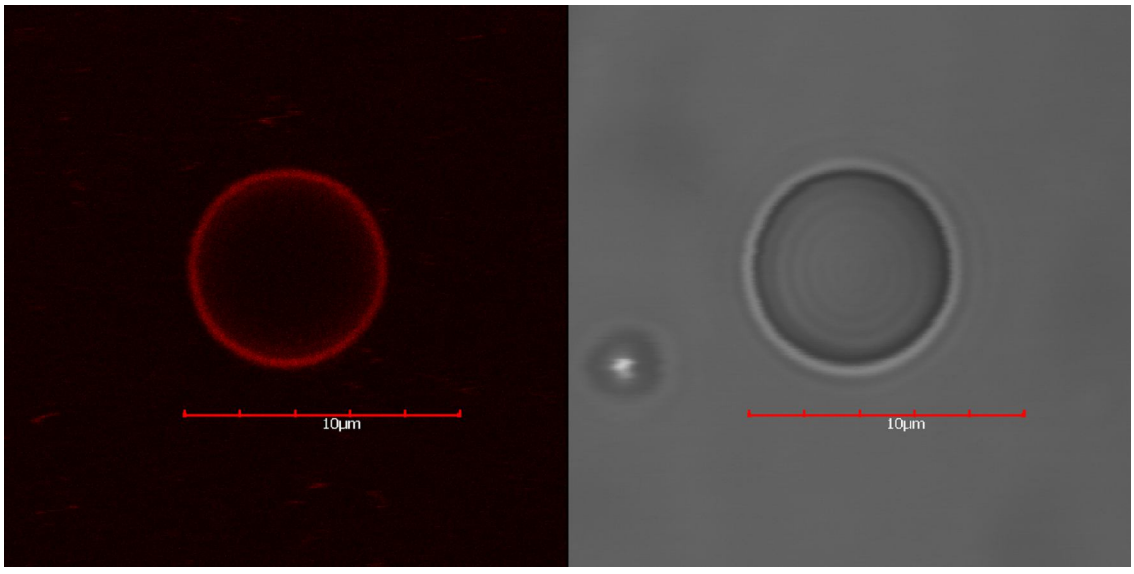

Figure 4.3 Image of CdSe/CdS QD 3.1 nm with PEO-47-PEI as ligand.

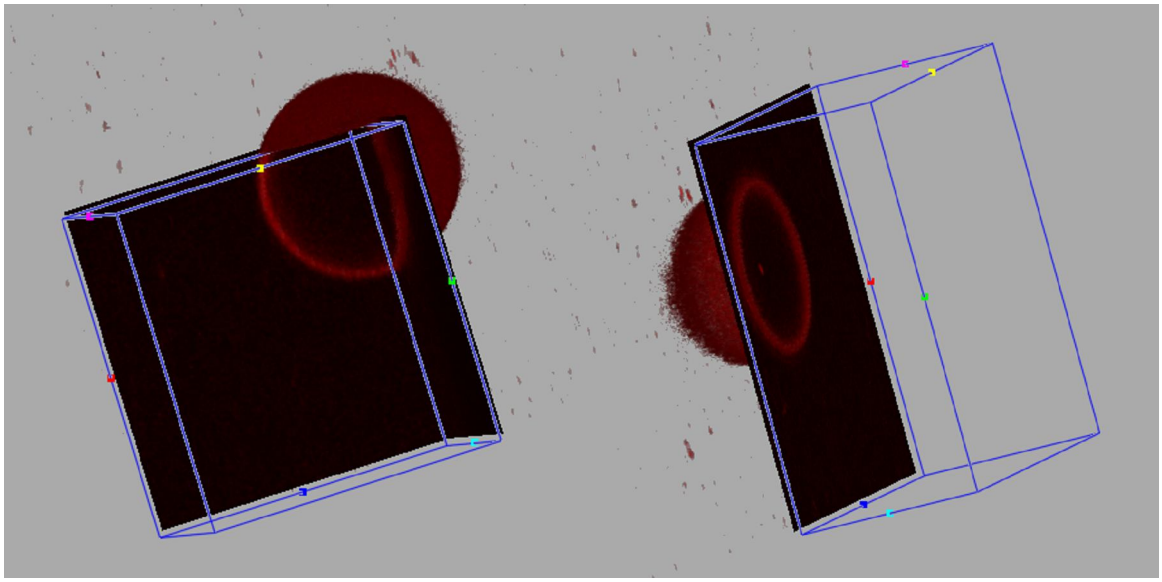

Figure 4.4 3D image of a vesicle formed of PEO-47-PEI and CdSe/CdS 3.1 nm.

4.1.1 QD with bifunctional PEOs

To synthesize water soluble QDs with a functional group, ligand exchange with a bifunctional PEO is necessary. Ligand exchange with an α-acetal-ω-PEI-PEO in a polymer/QD ratio that promotes QDs with good water solubility was executed. To transform the acetal into an aldehyde the water-soluble nanoparticles were exposed to pH 2 for 2 hours and thereafter the pH was adjusted to neutral again. This procedure gave water soluble QDs with aldehyde groups. To ensure that the acetal was transformed into an aldehyde, a drop of the solution was placed on a glass plate. After 15 minutes the plate was thoroughly rinsed with water, which removed all solution that was not covalently attached to the hydroxy groups on the glass plate. When the plate was analyzed in a fluorescent microscope an even fluorescent film could be seen (figure 4.5). A control test with the water soluble QDs, before transformation of the acetals to aldehydes, was performed. After rinsing the glass plate with water no fluorescence could be observed. The fact that fluorescence is only detected for the aldehyde QDs and not for the acetal QDs, indicates that the aldehydes form acetals with the hydroxy groups on the glass plate.

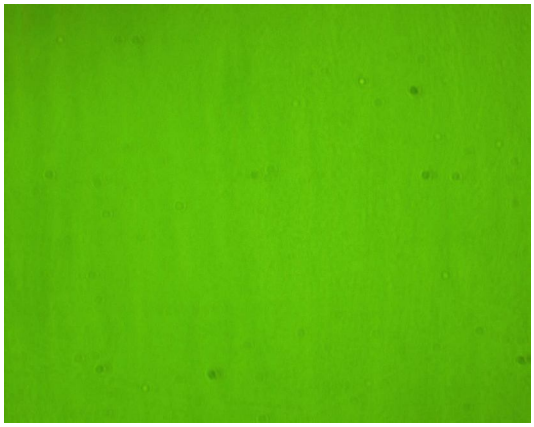

Figure 4.5 Glass plate with covalently bonded water soluble nanoparticles.

The aldehyde nanoparticles were added to a solution of poly(isoprene-*b*-ethylene oxide) (PI-PEO) vesicles with hydroxy groups on the outside. The mixture was left to stir over night and the resulting solution was studied in microscope. Fluorescent rings were observed meaning that the aldehyde on the nanoparticles had reacted with the hydroxy groups of the vesicles (figure 4.6, left panel). The vesicles were to some extent coupled to each other, probably via the nanoparticles since one nanoparticle can bind to several hydroxy groups (figure 4.6, right panel).

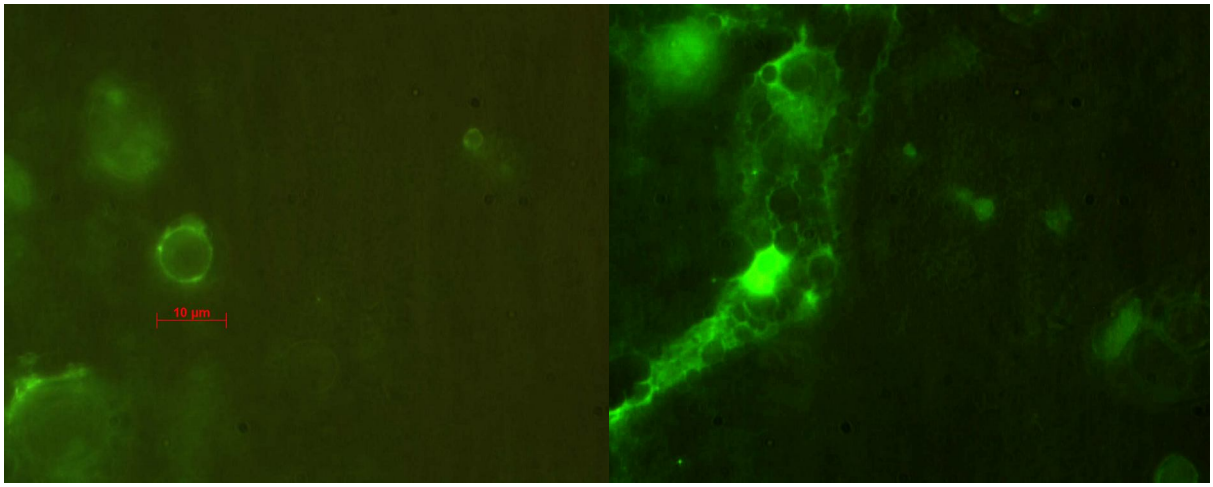

Figure 4.6 Watersoluble QDs with aldehyde coupled to PI-PEO vesicles.

4.1.2 Titration microcalorimetric measurements

To measure the binding strength between the nanoparticles and the ligands titration microcalorimetric measurements were performed. PEO-amines were titrated in a solution of nanoparticles in chloroform and the concentrations were calculated so that at the end of an experiment a 500-time molar excess of PEO-amine was in the solution. QDs from the same batch were used in all experiments presented in figures 4.7, 4.8 and 4.9. The heat contribution from the dilution was also measured and subtracted from the results.

In figure 4.7 the heat flow for PEO-PEI titrated in a QD solution can be seen. The peaks arise as a result from the addition of ligand. The peaks are showing a negative heat flow, which indicates that the ligand exchange is endothermic. The peaks tend to get smaller with each addition but they do not completely vanish, which would be the case if no more ligand exchange takes place. To verify this trend, an experiment with up to 1000 fold molar excess of ligand was performed. The result thereof gave slightly weaker signals but did not completely disappear (data not shown). This small heat flow contribution probably depends on the fact that the ligand exchange is an equilibrium reaction and the addition of more ligand slightly disturbs the equilibrium.

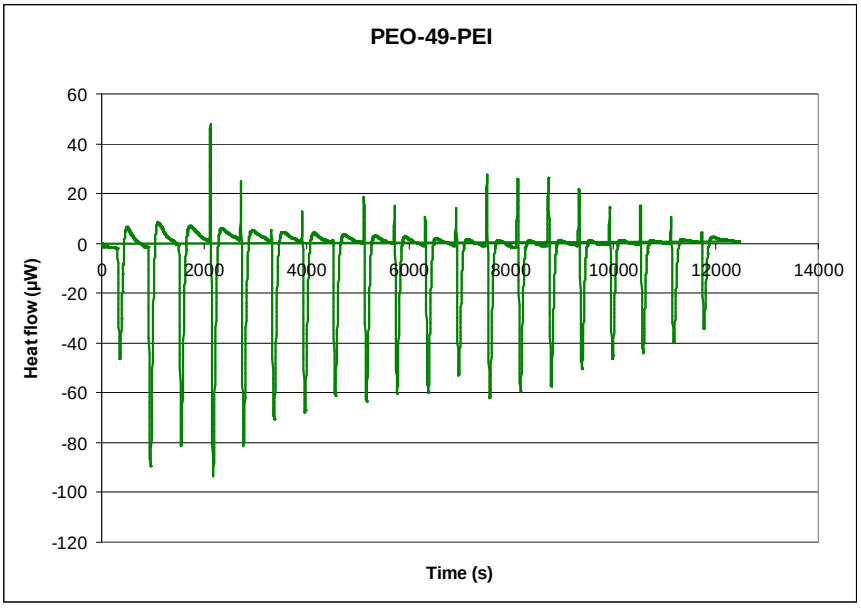

Figure 4.7 Microcalorimetric measurements of PEO-PEI to QDs.

In figure 4.8 the result from the titration in PEO-TEPA to a solution of QDs can be seen. The result differs from the titration of PEO-PEI and a positive heat flow is observed which means that the ligand exchange for this ligand is exothermic. When more ligand is added, a small increase of the heat flow is seen.

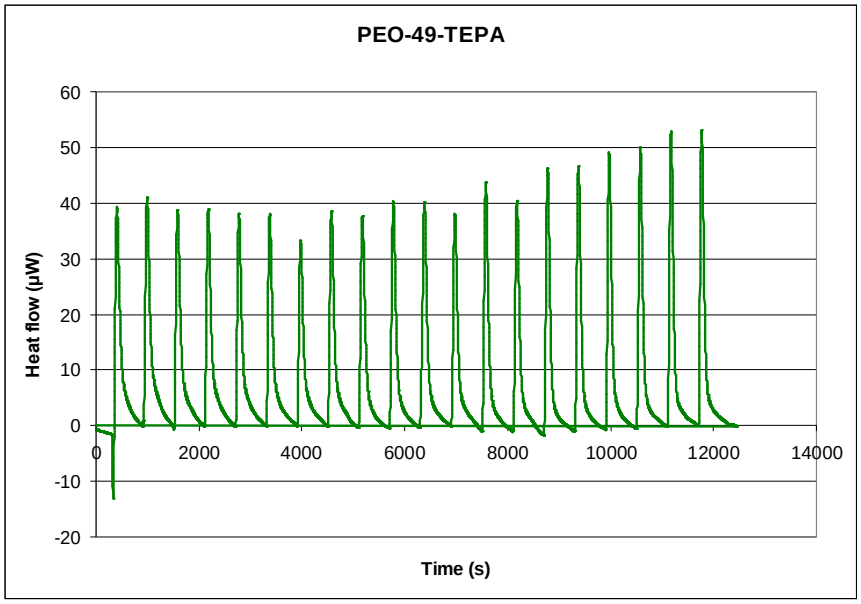

Figure 4.8 Microcalorimetric measurements of PEO-TEPA to QDs.

In figure 4.9 the titration of PEO-DETA to QDs can be observed. This ligand exchange is also exothermic, although only a very small heat flow contribution can be seen when ligand is added.

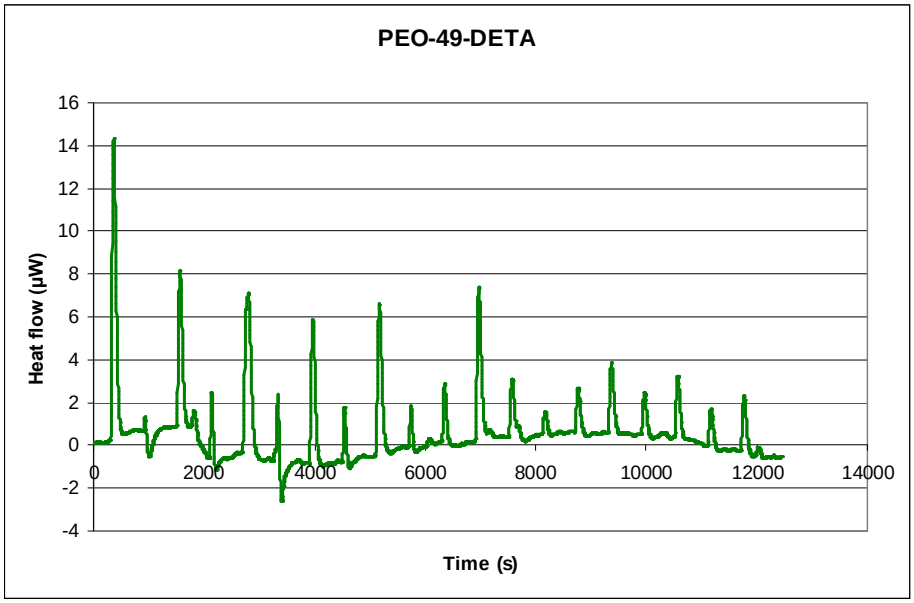

Figure 4.9 Microcalorimetric measurements of PEO-DETA to QDs.

From these measurements using the different ligands it is obvious that the shorter amine ligands work differently in comparison to the PEO-PEI ligand. The curve for PEO-TEPA shows a larger heat contribution than the curve for PEO-DETA, which hardly show any heat flow at all. This is probably due to a higher affinity of the longer amine of PEO-TEPA to the QDs. The PEO-PEI ligand on the other hand contains more amines than PEO-TEPA and still gives an endothermic curve. However, the PEI ligand also contains many primary amines whereas the PEO-TEPA ligand contains more secondary amines than primary. The secondary amines are more basic and therefore probably better coordinators to the QDs. The fact that the QDs with PEO-PEI ligands show a higher stability depends on a higher entropy contribution. Since the PEO-PEI is a large ligand and occupies a lot of space on the QD surface, several TOP/TOPO ligands have to leave the QD surface and go into the solution. The results obtained from these microcalorimetric measurements are very interesting although additional measurements are needed to further elucidate how the ligands and QDs interact with each other.

4.2 Magnetite

The magnetic NPs were made water soluble with carboxy-capped PEOs as ligands. To achieve stable water soluble nanoparticles, different ligand/NP ratios and precipitation methods were tested and a ligand/NP ratio of 500 was shown to be necessary to obtain a stable solution. An increase of ligand did not show any alteration in the stability, leading to the assumption that the NP is completely covered with polymers at this ratio. The ligand exchange procedure was also tested to find the optimal procedure. The ligand exchange was performed in the same manner as for the QDs. The different variables that were changed were the number of precipitations and the incubation time for the exchange. Experiments were performed with 1, 2 and 3 precipitations and with different time frames for the ligand exchange (0, 1, 2 and 3 hours). The optimal results were obtained by two precipitations and 1-hour incubation time.

The size distribution for the magnetic nanoparticles before and after ligand exchange can be seen in figure 4.10. The magnetic NPs before ligand exchange were stabilized with trioctylamine and it can be seen that the NPs with polymers as ligands show a slightly larger hydrodynamic radius. This was expected considering that the PEOs have a molecular mass of 2000 g/mol and the trioctylamine only has 353 g/mol.

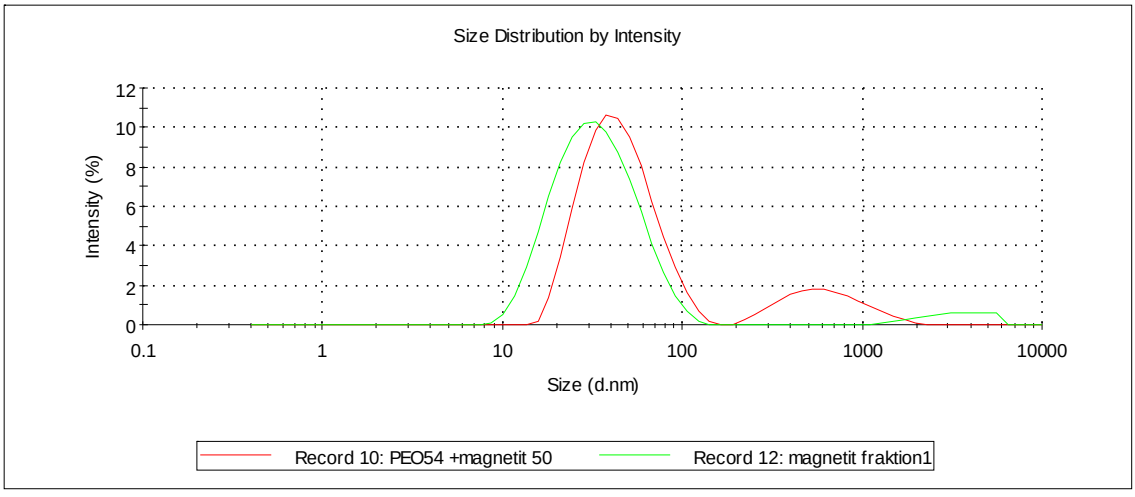

Figure 4.10 Size distribution of magnetic nanoparticles before ligand exchange (green line) and after (red line).

For the polymer-stabilized NPs a small peak at a higher hydrodynamic radius can be observed, which is probably due to aggregated NPs. After one day a new measurement was

performed showing that no further aggregation took place (not shown here). The polymer-stabilized NPs were filtered through a 0.45 µm syringe filter before used in any further experiments.

In order to observe the magnetic NPs in microscope, PEO with flourescein was used as ligand. This gave luminescent magnetic NPs making them visible in microscope. The ligand exchange was performed in the same manner and ratio, which was proven to be ideal before. A mixture of PEO-54 and PEO-54-flourescein (1:1) was used for the ligand exchange.

5 Vesicle encapsulation

Vesicles consist of a double layer of membrane forming molecules that form a hollow room in the center. The hollow room in the center makes the vesicles suitable as carriers, for example within the field of drug delivery. Since vesicles are not directly recognized by the immune system as intruders, active substances can be transported with a reduced risk of the immune system to interfere.

The amphiphilic block copolymers used in this thesis to form vesicles was poly(isoprene)-poly(ethylene oxide) (PI-PEO) and poly(butadiene)-poly(ethylene oxide) (PB-PEO). These block copolymers were delivered by courtesy of Volkan Filiz and Franziska Krause. There are several different methods to form vesicles from amphiphlic block copolymers; the reverse-phase evaporation method, the film hydration method, the syringe method and the Hewlett Packard printer method.

5.1 Vesicle encapsulation of CdSe/CdS

In the reverse-phase evaporation method 10 mg of block copolymer was solved in chloroform and covered with a layer of water. The chloroform slowly evaporated during stirring in an open vessel and the polymer entered the water phase forming vesicles. To encapsulate QDs in the vesicles, the chloroform solution with the block copolymers was covered with water containing QDs. However, this resulted in a transfer of the QDs to the chloroform phase and as the chloroform evaporated the QDs precipitated and stayed on the bottom of the vessel.

In the second method, the film hydration method, 8-10 mg of block copolymers was dissolved in chloroform in a small round bottom flask. The chloroform was subsequently evaporated on a rotation evaporator leaving a thin film of polymer with a large area on the glass wall. Water was added to the polymer film resulting in the swelling of the polymer to form vesicles. The swelling process for PB-PEO vesicles to form takes approximately 10 hours and for the PI-PEO vesicles approximately 48 hours. To encapsulate the QDs, these were dissolved in water and added to the polymer film. The vesicles that were formed were both surrounded by and filled with QDs.

To separate vesicles from organic dyes, filtration with a sephadex column is normally used. However, for the separation of the QD-filled vesicles from the surrounding QDs this method did not work. The QDs adhered to the filling in the sephadex column thereby blocking it, with the result that most of the vesicles got trapped on the top of the column. In an alternative approach the solution was filtered through a syringe filter. After one filtration no visible difference was observed, but the vesicles survived the procedure and more filtration steps with different filter sizes were tested. The best result was obtained with the following filtration procedure; twice through a 0.45 µm filter and once through a 0.2 µm filter. This resulted in the fluorescent vesicles showed in figure 5.1.

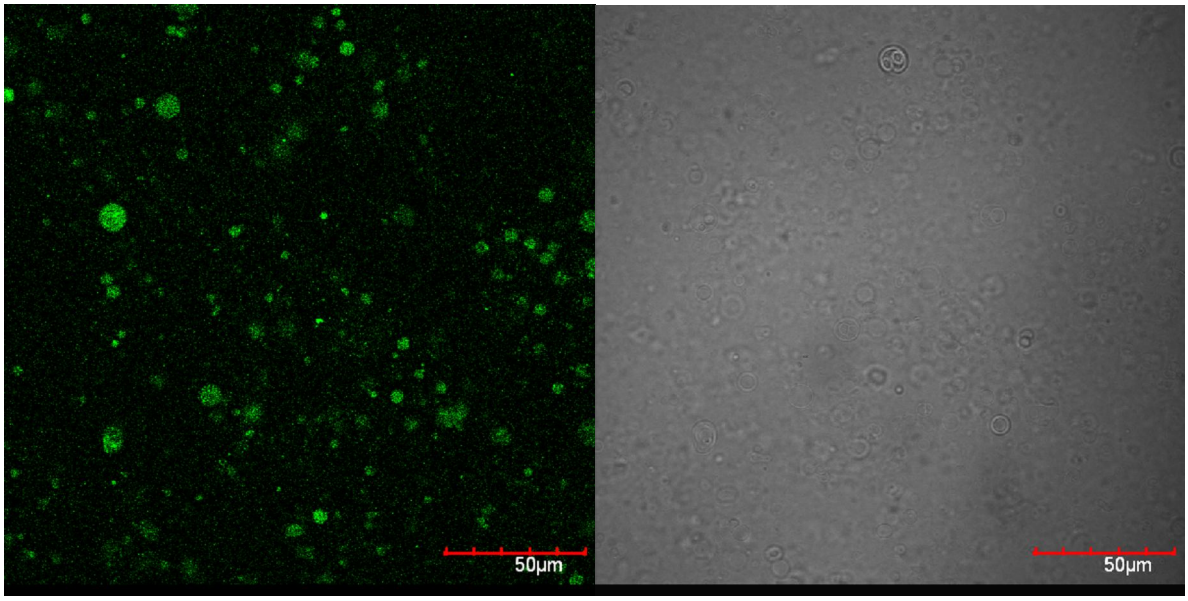

Figure 5.1 PB-PEO vesicles with CdSe/CdS nanoparticles coated with PEO-49-PEI

The disadvantage of the film hydration method is that the photo luminescence is very weak and high laser intensity is required to observe the vesicles in the CLSM. The luminescence was completely quenched after a couple of days.

One way of achieving a longer period of luminescence and more stable photoluminescence is to shorten the preparation time. The vesicle preparation is easiest step to shorten and instead of the film rehydration method the syringe and the printer method were employed.

The printer method, developed by Hauschild in the Förster group[76], is used to obtain vesicles of the same size. To form vesicles with this method the amphiphilic blockcopolymer was dissolved in a solvent miscible with water. The solution was filled in an ink cartridge situated in a modified ink printer. The command “to print”, prints small droplets of the block

copolymer solution into a beaker with water which is stirring vigorously (figure 5.2). This means that small droplets of the polymer solution enter the water phase, become diluted and form vesicles. These droplets are approximately of the same size, hence containing the same amount of polymers forming vesicles of the same size. The disadvantage is that the vesicles normally are too small to be observed in a light microscope.

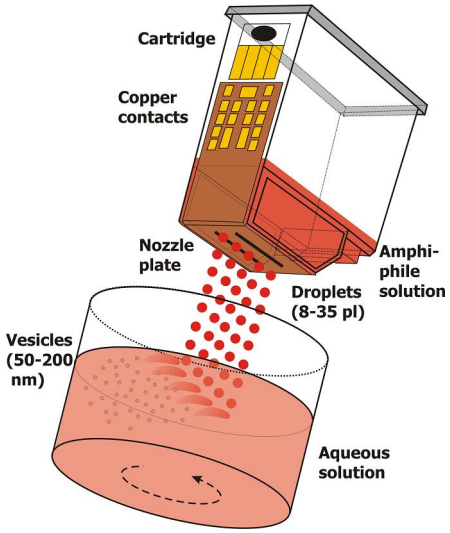

Figure 5.2 A schematic picture of the printer method.

The syringe method is another fast method to form vesicles from block copolymers. The principle of this method is basically the same as for the printer method, with the difference that a syringe is used instead of a printer. The block copolymer is dissolved in a solvent miscible with water, filled in a syringe and subsequently sprayed in a defined amount of water under stirring. As the solvent becomes diluted in the water the polymer forms vesicles. The first tryouts with this method were not optimal, possibly caused by the solvent which is not as finely dispersed as for the printer method when entering the water and consequently the solvent disturbed the process of forming vesicles. To avoid this disturbance, the temperature was altered and the experiment was performed at 60°C and 80°C. This gave better results and the polymer solution was sprayed with a syringe in a water solution with QDs. After separation of the vesicles from the surrounding QDs, luminescent vesicles with varying size but large enough to see in the microscope were seen.

It was decided to continue with the syringe method and the obtained fluorescent vesicles were studied in the CLSM. In figure 5.3, PB-PEO vesicles with PEO-49-PEI stabilized QD can be seen.

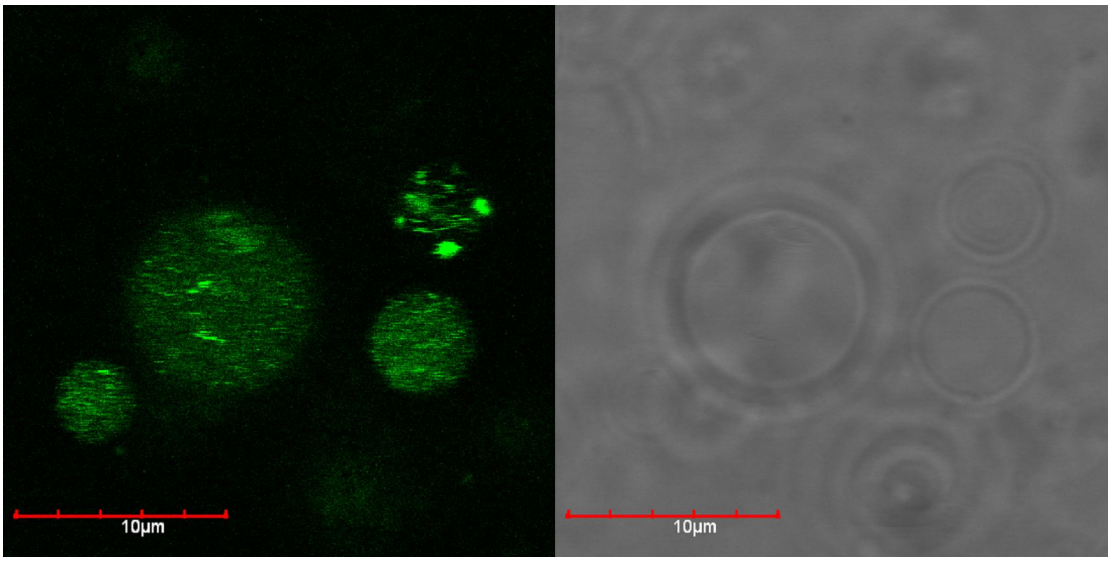

Figure 5.3 CdSe/CdS nanoparticles coated with PEO-49-PEI in PB-PEO vesicles

Encapsulation experiments with QDs stabilized with PEO-47-PEI were also performed. However, addition of block copolymer to the solution caused the QDs to precipitate. Few vesicles could be found in this solution and none of them contained QDs.

In contrast, vesicles with PEO-49-PEI stabilized QDs were observed in the CLSM. Figure 5.3 shows a couple of vesicles with QDs after one scan. In one of the small vesicles to the right in the image larger dots can be seen indicating that the QDs have started to aggregate. Figure 5.4 shows the same vesicles after a couple of seconds. When exposed to the laser beam the QDs aggregates completely. A possible explanation to this phenomenon could be that the sulphur on the QD surface starts to oxidate and transforms into sulphate. This leads to aggregation of the QDs since the ligands are removed, which destabilizes the QDs. Due to this phenomenon it was impossible to make 3D images of the vesicles. Experiments with different laser intensities were performed to see if the precipitation could be delayed, however these were unsuccessful. Even with the lowest laser intensity possible, a direct precipitation inside the vesicles was observed.

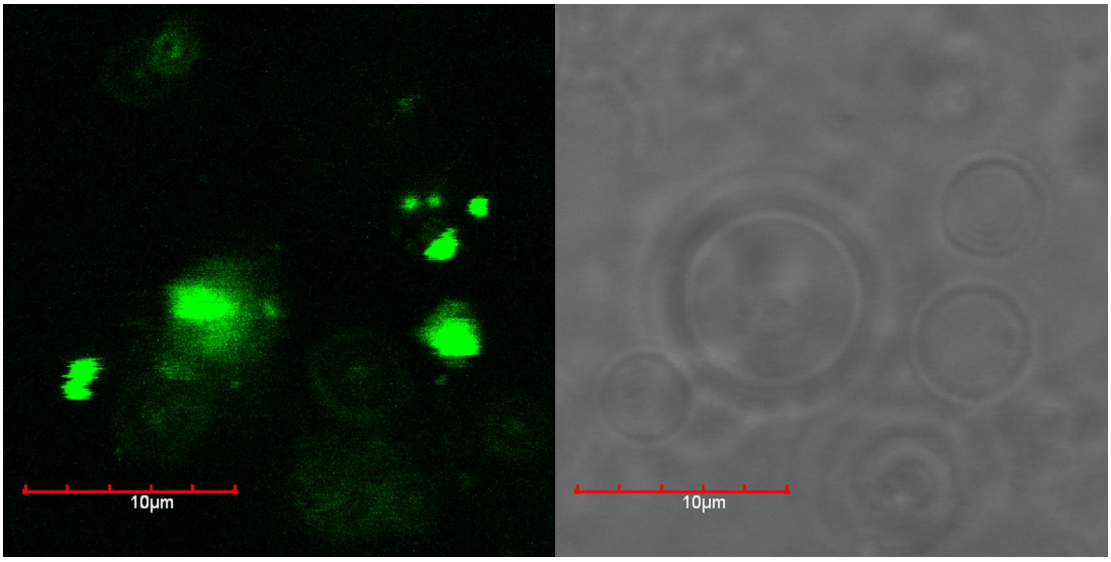

Figure 5.4 The same vesicles as in figure 5.3 after a couple of seconds. The QDs have formed aggregates within the vesicles.

Encapsulations of QDs in PI-PEO vesicles were also performed with the same result as for the PB-PEO. An immediate aggregation of the QDs, stabilized with PEO-47-PEI, following addition of the block copolymer PI-PEO was observed and no encapsulation of these QDs were possible. An image of a PI-PEO vesicle with PEO-49-PEI stabilized QDs can be seen in figure 5.5. It can also be seen that there is a tendency to aggregation even at the first scan. During a second scan of the same vesicle the same phenomena appears as for the PB-PEO vesicles, and the QDs precipitate within the vesicle (figure 5.6).

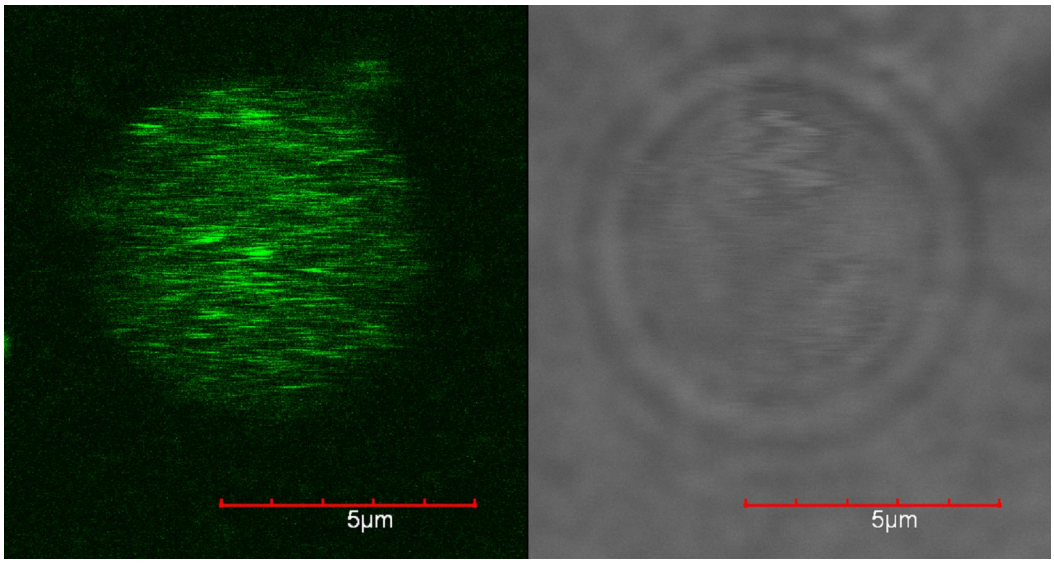

Figure 5.5 CdSe/CdS nanoparticles coated with PEO-49-PEI in PI-PEO vesicles.

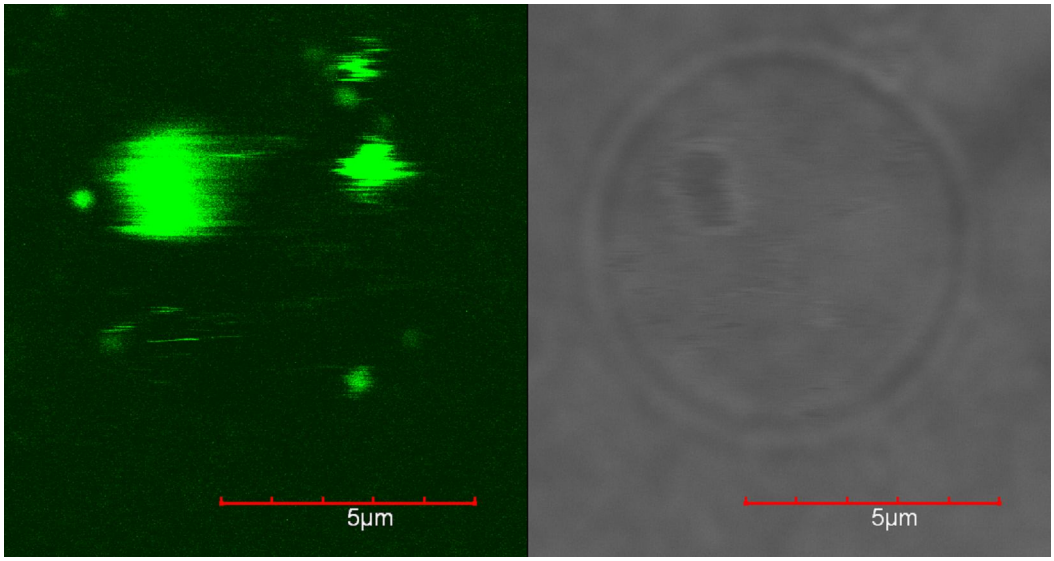

Figure 5.6 The same vesicle as in figure 5.5 after a couple of seconds. The QDs have formed aggregates within the vesicle.

It was discovered that the exposure of QDs with a laser beam induced an immediate precipitation of the nanoparticles. If the reason is as previously stated, that an oxidation on the QD surface takes place, this should also happen when exposed to light, although slower. A sample of PEO-49-PEI stabilized QDs encapsulated in PI-PEO vesicles was exposed to light for a week and then examined with CLSM (figure 5.7). The QDs had precipitated and moved towards the wall of the vesicle. From this experiment it can not be deduced if the QDs actually go inside the wall to the hydrophobic core or if they just go to the vicinity of the wall.

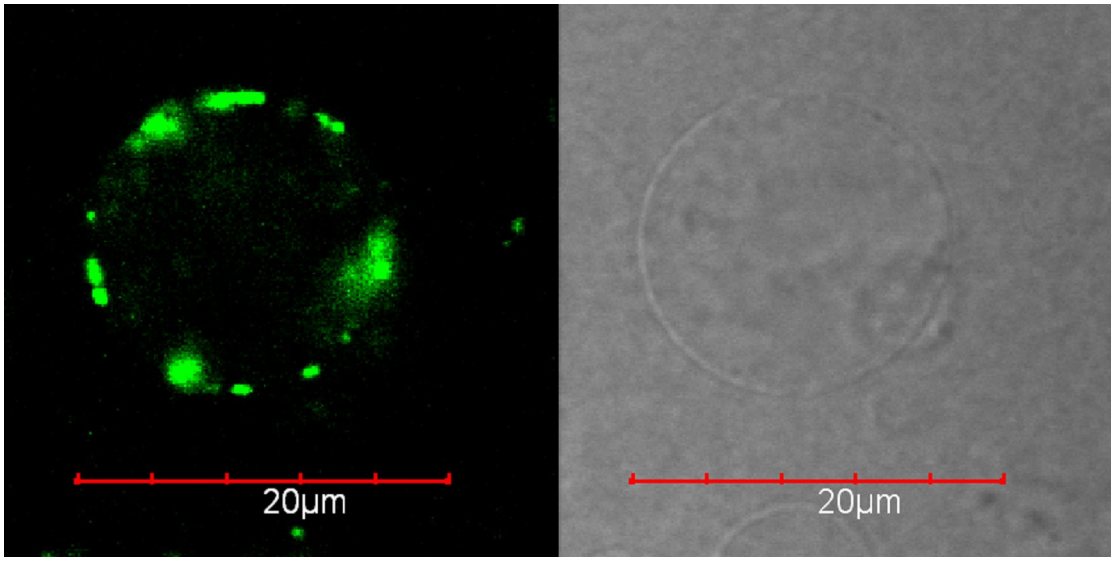

Figure 5.7 CdSe/CdS nanoparticles coated with PEO-49-PEI in PI-PEO vesicles after a week of exposure to light.

5.2 Vesicle encapsulation of magnetic nanoparticles

A series of encapsulation experiments with different ratios of water-soluble magnetic NPs and block copolymers were performed. The result from these experiments showed that a high concentration of NPs (5 mg NP/mg block copolymer) disturbed the formation of vesicles, resulting in none or very few vesicles, whereas with a lower NP concentration vesicles were formed. All the vesicle formation strategies that have already been described were also tested with the magnetic NPs, and these gave similar results as for the QDs. All the methods resulted in vesicle formation up to a certain NP concentration, however the syringe method was chosen because it is the most rapid method for forming large vesicles.

Unfortunately the magnetic NPs could not be seen in a microscope and it was not possible to determine whether the NPs were inside the vesicles or not. A cryo-TEM measurement was performed (figure 5.8) where it was seen that the NPs are both inside and around the vesicles. Before the cryo-TEM measurement, the sample was filtered once through a 0.45 µm syringe filter and after the cryo-TEM measurement it was obvious that it is not enough with one filtration to remove all NPs outside of the vesicles.

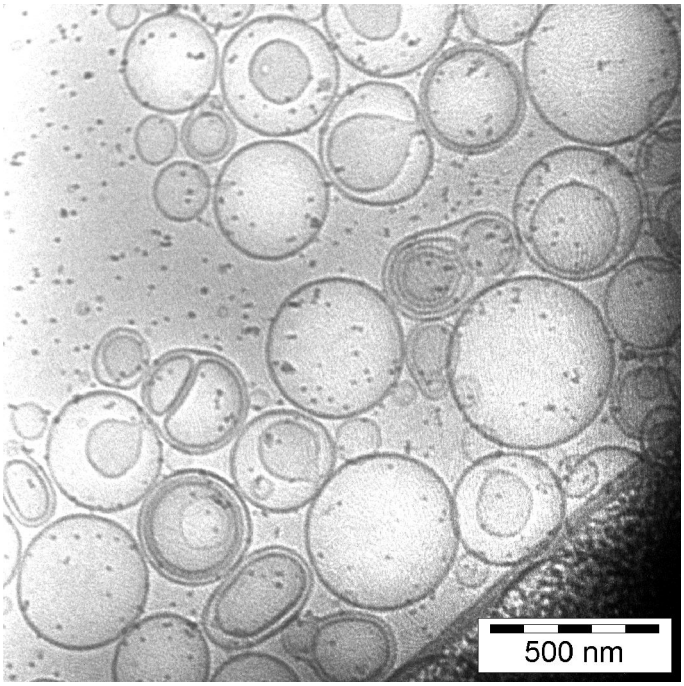

Figure 5.8 A cryo-TEM image of a vesicle solution with magnetic nanoparticles.

To obtain NPs visible in the microscope, PEO coupled to the dye, fluorescein, was used as ligand. This resulted in fluorescent magnetic NPs, which could be observed in the microscope as a fluorescent film. By adding block copolymer to the fluorescent NP solution vesicles were formed and a homogeneous fluorescent solution could be seen in the fluorescent microscope. The solution was filtered through syringe filters, first once through a 0.45 µm filter and subsequently twice through a 0.22 µm filter. In the resulting solution fluorescent vesicles were detectable (figure 5.9).

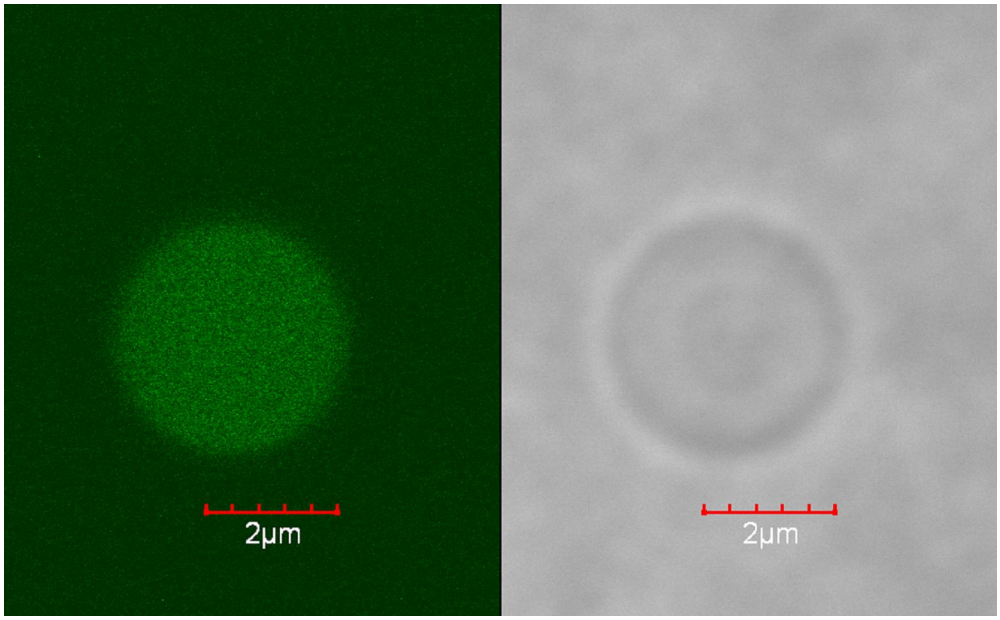

Figure 5.9 A CLSM image of a PI-PEO vesicle with magnetic fluorescent nanoparticles.

Vesicles are, as mentioned earlier, possible carriers for drug delivery. A biologically active substance may be encapsulated inside the vesicle and transported to the intended place without detection of the organism. Once there, the challenge is to find a controlled method for release of the substance. A possible approach is to place magnetic NPs in the vesicle and expose them to a varying magnetic field with the aim to heat the NPs and thereby destroy the vesicles.

Experiments were performed using the approach above. First the hydrophobic NPs were placed in an induction coil and the solution was heated to 40 °C after 10 minutes using a power of 40%. The water-soluble NPs were also heated with 40% power, needing 30 minutes to reach 40 °C. The solution with water-soluble NPs has a lower concentration, explaining the longer heating time. For experiments with encapsulated NPs no temperature rise could be detected, which is probably due to the low concentration of the NPs in the vesicles. To achieve a higher concentration within the vesicles, probably a more gentle method for separation of the vesicles from the surrounding NPs is required. The drawback with the used filtration method is that some of the vesicles break during the filtration, particularly the larger ones. The larger vesicles probably contain a larger number of NPs leading to a high loss of NPs during the filtration. Another alternative could be to separate by centrifugation and then only use the larger vesicles for the induction experiments.

6 Conclusion

The main focus of this thesis is the synthesis of bifunctional poly(ethylene oxides) (PEOs) that can be used as stabilizing ligands for nanoparticles (NPs). The PEOs were synthesized from ethylene oxide via anionic polymerization. Different initiators and quenching agents were used to obtain bifunctionality. In this thesis amino, mercapto and carboxylic acid functionalities were used as binding groups of the PEO to enable binding to the NPs.

For the generation of an amino functionality, the polymerization was quenched with acetic acid which results in a hydroxy group on one end of the PEO. To transform the hydroxy group into an amine, it first has to be activated for further reaction. Several different activation groups were tested: N-hydroxysuccinimide (NHS), 4-nitrophenyl chloroformate (NPCF), triflouroethanesulphonyl chloride (TRES), N, N'-disuccinimidyl carbonate (DSC) and carbonyldiimidazole (CDI). The best suited group for activation of PEO was CDI. Many of the activation reagents caused problems with double coupling of the PEOs, but this could be avoided by using an excess of CDI. The activated PEO was reacted with different amines: diethylenetriamine (DETA), triethylenetetramine (TETA), tetraethylenepentamine (TEPA) and pentaethylenehexamine (PEHA), which all create linear polymers. A branched ligand was synthesized by coupling two PEOs to a small molecular weight poly(ethylene amine) PEI. For the synthesis of thiol functionalized PEOs, the same reaction route was used as for the amino functionality, and a cysteine molecule was coupled to PEO via CDI activation. To synthesize a PEO with a carboxyl group the polymerization was quenched with ethyl bromoacetate and the obtained ester was hydrolyzed to give a carboxylic acid.

Different initiators were used to obtain various groups on the other end of PEO. The initiators used in this thesis were: methoxyethanol (methoxy group), diphenylmethyl (diphenyl group) 2-hydroxy acrylate (acrylate) and diethoxy propanol (acetal). All the synthesized PEOs were characterized by GPC, MALDI-TOF and ^{1}H-NMR.

Ligand exchange was achieved by exposure of the NPs to a large excess of amino-functionalized PEO-based ligands. The subsequent addition of a non-solvent for the PEO ligands enabled the NPs covered with PEO to be separated from the original ligands. The PEO-covered NPs were readily soluble in water. After ligand exchange a general loss of luminescence was observed for the quantum dots (QDs) in water. It was also observed that the luminescence for QDs with a longer PEO chain was weaker than for QDs with shorter PEO ligands. The stability of the QDs in water was higher for ligands with many amine groups,

and the most stable QDs were obtained with the branched PEO-PEI. The ratio of amino-functionalized PEO/QD employed during the ligand exchange dictates the number of attached polymers to each QD. For lower ratios self-assembly of the conjugate was observed. The formed structures observed by confocal microscopy resembled those of vesicles formed with amphiphilic blockcopolymers. These structures were seen for lower ratios with the longer amino ligands (PEO-PEI and PEO-PEHA) whereas for the shorter amines aggregation without any organized structure was observed.

The same method for ligand exchange was applied in the case of the mercapto-functionalized PEO ligand. The mercapto-functionalized PEOs contained only one thiol group and the stabilized QDs were thereby compared to the QDs stabilized with the shortest amine-PEO (PEO-DETA). The QDs with mercapto-PEO were shown to be more stable than its amino-functionalized counterpart. However, the luminescence was considerably weaker than for the QDs with mono-amino ligands and the luminescence had completely disappeared after 1-2 days.

A bifunctional PEO was synthesized with 3,3-diethoxy-1-propanol as initiator and functionalized with PEI. The QDs, stabilized with the obtained α-acetal-ω-PEI-PEO, were hydrolyzed to give QDs with aldehydes. When observed in a fluorescent microscope the QDs showed the formation of a homogeneous film on the glass substrate. This was seen even after rinsing the glass plate thoroughly with water, indicating that the hydroxy groups on the plate formed acetals with the aldehyde on the QDs. The QDs were also mixed with PI-PEO vesicles with hydroxy groups, giving vesicles with a fluorescent ring.

For stabilization of the magnetic nanoparticles, PEOs with a carboxylic group were used. The ligand exchange was basically performed in the same manner as for the QDs. However, experiments showed that two precipitations and an incubation time of 1 hour were optimal for a successful ligand exchange. Since the magnetic NPs cannot be observed in a light microscope, a dye (fluorescein) was coupled to the PEO ligands. A bifunctional PEO was used and the fluorescein was coupled to an aldehyde group, leaving a free carboxyl group on the other end of the PEO which was thereafter attached to the NP.

Both the magnetic NPs and the QDs were encapsulated into vesicles formed with the amphiphilic blockcopolymers PI-PEO and PB-PEO. Different methods were tested for the vesicle preparation and the syringe method was found to be the most suitable. This method gave large vesicles of different sizes. To separate the vesicles from the surrounding NPs a syringe with a filter was used. For the vesicles filled with QDs a precipitation of the QDs

inside the vesicle was observed. This precipitation accelerated when the vesicle was observed in the confocal laser scanning microscope, which led to the conclusion that the QDs release their ligands due to an oxidation of the surface.

In order to observe the magnetic NPs in a light microscope, ligands with fluorescein were used. The separation of the surrounding NPs from the vesicles was then possible to observe, and fluorescent vesicles could be seen in the microscope. In order to disrupt the vesicles filled with magnetic NPs an magnetic induction experiment was performed. It was possible to heat solutions with hydrophobic NPs and hydrophilic NPs, respectively. However, for NPs encapsulated in vesicles no temperature alteration was detected, indicating that a higher concentration of the NPs inside the vesicles is necessary to be able to release the content of the vesicle. To achieve this, a different approach for the separation of the surrounding NPs from the vesicles should be developed.

7 Zusammenfassung

Der Schwerpunkt dieser Arbeit ist die Synthese von bifunktionellen Polyethylenoxiden (PEOs), die als stabilisierende Liganden für Nanopartikel verwendet werden können. Die PEOs wurden aus Etylenoxid durch anionische Polymerisation synthetisiert. Verschiedene Initiatoren und Abbruchreagenzien wurden benutzt, um die Bifunktionalität zu erhalten. In dieser Arbeit wurden Amino-, Mercapto- und Carboxylsäure-gruppen verwendet, um eine Anbindung des PEOs an die NPs zu ermöglichen.

Für die Darstellung der Aminofunktionalität wurde die Polymerisation von PEO mit Essigsäure abgebrochen, was in einer Hydroxygruppe am Ende des PEO resultierte. Der erste Schritt um eine Aminogruppe zu erhalten, war die Aktivierung der Hydroxygruppe. Verschiedene Aktivierungsgruppen wurden dabei untersucht; N-Hydroxysuccinimid (NHS), 4-Nitrophenylchloroformat (NPCF), Trifluoroethanesulfonylchlorid (TRES), N,N´-Disuccinimidylcarbonat (DSC) und Carbonyldiimidazol (CDI). Das beste Ergebnis für die Aktivierung an PEO lieferte das Aktivierungsreagenz CDI. Viele der verschiedenen Aktivierungsreagenzien führten zu Problemen mit Doppelkopplung der PEOs. Im Falle des CDIs konnte eine Doppelkopplung durch den Einsatz eines Überschusses von CDI vermieden werden. Das aktivierte PEO wurde danach mit verschiedenen Aminogruppen funktionalisiert: Diethylentriamin (DETA), Triethylentetraamin (TETA), Tetraethylenpentaamin (TEPA) und Pentaethylenehexaamin (PEHA), die alle lineare Polymere bilden. Weiterhin wurde ein verzweigter Ligand synthetisiert, indem zwei PEO Moleküle an ein niedermolekulares PEI gekoppelt wurden. Für die Synthese von thiolfunktionalisierten PEOs wurde derselbe Reaktionsweg wie für die Aminofunktionalisierung benutzt. Dabei wurde ein Cysteinmolekül an das CDI aktivierte PEO gekuppelt. Um eine Carbonsäurefunktion einzuführen wurde die Polymerisation des PEOs mit Ethylbromoacetat abgebrochen. Der erhaltene Ester wurde hydrolysiert um eine Carboxylsäure herzustellen.

Unterschiedliche Initiatoren wurde eingesetzt, um verschieden Gruppen am anderen Ende des PEO zu erhalten. Die Initiatoren, die in dieser Arbeit eingesetzt wurden, sind: Methoxyethanol, Diphenylmethyl, 2-Hydroxyacrylat und Diethoxypropanol. Die synthetisierten PEOs wurden mittels GPC, MALDI-TOF-MS und ^{1}H-NMR charakterisiert.

Der Ligandenaustausch an den Nanopartikeln wurde mit einem hohen Überschuss von aminofunktionalisierten PEO-Liganden durchgeführt. Die anschließende Zugabe eines Lösungsmittels, in welchem PEO nicht löslich ist, ermöglichte die Separation von PEO

umhüllten NPs vom ursprünglichen Liganden. Die PEO umhüllten NPs konnten anschließend in Wasser gelöst werden. Nach dem Ligandenaustausch wurde ein genereller Lumineszensverlust für die QDs in Wasser beobachtet. Weiterhin wurde beobachtet, dass die Lumineszens für QDs mit längeren PEO Ketten schwächer war als für die QDs mit kürzeren PEO Ketten. Die Stabilität der QDs in Wasser war höher für die Liganden mit vielen Aminogruppen und die stabilsten QDs waren die mit verzweigten PEO-PEI Liganden. Der Anteil von aminofunktionalisierten PEO/QD, die für den Ligandenaustausch eingesetzt wurden, bestimmt wie viele Polymere an jeden QD binden. Für einen niedrigeren Anteil von PEO wurde Selbstorganisation der PEO-QD-Konjugate beobachtet. Die gebildeten Strukturen wurden im konfokalen Laserrastermikroskop beobachtet. Die Strukturen ähnelten denen, die von Vesikeln aus amphiphilen Blockkopolymeren gebildet werden. Diese Strukturen wurden nur für Konjugate mit niedrigeren Anteilen an längeren Aminoliganden (PEO-PEI und PEO-PEHA) beobachtet. Für Konjugate mit kürzeren Aminoliganden wurde lediglich eine Aggregation ohne übergeordnete Strukturen beobachtet.

Für die mercaptofunktionalisierten PEO-Liganden wurde dieselbe Methode für den Ligandenaustausch benutzt. Die mercaptofunktionalisierten PEOs enthalten nur eine Thiolgruppe. Daher wurden die so stabilisierten QDs mit den QDs verglichen, die mit dem kürzesten Amino-PEO (PEO-DETA) stabilisiert wurden. Die QDs mit mercapto-PEOs stellten sich als stabiler als die entsprechende aminofunktionalisierten QDs heraus. Allerdings stellte sich die Lumineszens als beträchtlich schwächer als für die Monoamino-Liganden heraus. Nach 1-2 Tagen war die Luminiszens ganz erloschen.

Ein bifunktionelles PEO wurde mit 3,3-diethoxy-1-propanol als Initiator synthetisiert und dann mit PEI funktionalisiert. Die QDs wurden mit dem hergestellten α-acetal-ω-PEI-PEO stabilisiert und die Acetalfunktion anschließend hydrolisiert, um QDs mit einer Aldehydgruppe zu erhalten. Die QDs waren als homogener Film auf dem Glassubstrat im Fluoreszensmikroskop zu beobachten. Der Film konnte sogar nach sorgfältigem Spülen mit Wasser noch beobachtet werden, was darauf hinweist das die Hydroxygruppen des Glases mit den Aldehydgruppen der QDs eine acetalbindung gebildet hatten. Außerdem wurden QDs mit PI-PEO Vesikeln mit Hydroxygruppen gemischt. Im Fluoreszensmikroskop konnten diese Vesikel anschliessend als fluoreszierende Ringe erkannt werden.

PEO mit einer Carboxylgruppe wurde für die Stabilisation von magnetischen NPs benutzt. Der Ligandenaustausch wurde prinzipiell auf die gleiche Weise wie bei den QDs ausgeführt. Dabei stellten sich zwei Fällungen und eine Inkubationszeit von einer Stunde als optimal für

einen erfolgreichen Ligandenaustausch heraus. Da es nicht möglich ist, die magnetische NPs im Lichtmikroskop zu beobachten, wurde ein Farbstoff (Fluoreszein) an die PEO-Liganden gekuppelt. Ein bifunktionelles PEO wurde eingesetzt und das Fluoreszein an die Aldehydgruppe gekuppelt, während das andere Ende des PEO mit seiner freien Carboxylsäure an einen NP gekuppelt wurde.

Sowohl die magnetische NPs als auch die QDs wurde anschließend in Vesikel aus den amphiphilen Blockcopolymeren PI-PEO und PB-PEO eingekapselt. Unterschiedliche Methoden für die Vesikelpräparation wurden ausprobiert und die Spritzenmethode wurde als die effektivste Methode ausgewählt. Mit dieser Methode bildeten sich relativ große Vesikel. Um die Vesikel von den umliegenden NPs zu separieren, wurde eine Spritze mit einem Filter benutzt. Für die mit QDs gefüllten Vesikel wurde eine Ausfällung der QDs im Inneren der Vesikel beobachtet. Diese Fällung wurde durch die Untersuchung der Vesikel im Konfokalen Laserraster-Mikroskop beschleunigt. Dies führte zu der Schlussfolgerung, dass die QDs aufgrund der Oxidation auf ihrer Oberfläche ihre Liganden abstoßen.

Für die magnetischen NPs wurden Liganden mit Floureszein eingesetzt, was die Beobachtung am Lichtmikroskop ermöglichte. Die Separation der Vesikel von den umgebenden NPs konnte somit verfolgt werden und nach der Abtrennung waren fluoreszierende Vesikel im Mikroskop sichtbar. Um die Vesikel über die Erhitzung von magnetischen NPs aufzubrechen, wurden magnetische Induktionsexperimente durchgeführt. Es war möglich sowohl die Lösung mit hydrophoben NPs als auch die Lösung mit hydrophilen NPs zu erwärmen. Für die eingekapselten NPs wurde allerdings keine Temperaturänderung festgestellt, was darauf hinweist, dass für eine freisetzung des Inhalts der Vesikel eine größere Konzentration von NPs in den Vesikeln notwendig ist. Um eine höhere Konzentration an NPs in den Vesikeln zu erreichen muss eine verbesserte Methode für die Separation der freien NPs von den Vesikeln entwickelt werden.

8 Experimental Part

All chemicals were, if not otherwise stated, used without further purification. The block copolymers used for the encapsulation experiments were synthesized and kindly provided by Volkan Filiz (PI-PEO) and Franziska Krause (PB-PEO). The quantum dots were synthezised and kindly provided by Marija Nicolic and Andrea Salcher.

8.1 Anionic synthesis

All anionic synthesis procedures were performed under an inert nitrogen atmosphere using the Schlenk technique.

8.1.1 Synthesis of initiators

Diphenymethylpotassium:
4.23 g (128 g/mol, 33 mmol) naphthalene was dissolved in 40 ml THF and 1.17 g (39 g/mol, 29.9 mmol) potassium was added and stirred at room temperature over night. To the resulting deep green solution 5.54 g (168 g/mol, 33 mmol) diphenylmethane was added and left to stir at room temperature for three days, resulting in a solution with dark red color.
Methoxyethanylpotassium:

4.23 g (128 g/mol, 33 mmol) naphthalene was dissolved in 40 ml THF and 1.17 g (39 g/mol, 29.9 mmol) potassium was added and stirred at room temperature over night. To the resulting deep green solution 2.65 ml (776 g/mol, 33 mmol) methoxyethanol was added and left to stir at room temperature for three days, resulting in a solution with deep blue color.
3,3-diethoxypropanylpotassium

0.77 g (128 g/mol, 6 mmol) naphthalene was dissolved in 40 ml THF and 0.22 g (39 g/mol, 5.6 mmol) potassium was added and stirred at room temperature over night. To the resulting deep green solution 0.95 ml (148 g/mol, 6 mmol) 3,3-diethoxypropanol was added and left to stir at room temperature for three days, resulting in a solution with slightly yellow color.

8.1.2 Synthesis of poly(ethylene oxide)

The purification of ethylene oxide (EO) was performed in three steps. Firstly, the ethylene oxide was condensed to a 100 ml round bottom flask containing a couple of spatula tips of calcium hydride. In the two following steps the EO was stirred with first a sodium mirror and then with n-BuLi, for 20 minutes at approximately –50°C respectively. Thereafter the EO was condensed to an ampulla with a measuring scaleand then to the reaction flask with about 0.5 l dry THF to which the initiator was quickly added. The reaction mixture was left to stir at 40°C for three days.

Hydroxy-PEO:

After completion of the polymerization the reaction was quenched with acetic acid to obtain a hydroxyl group. The solution was concentrated under reduced pressure and purified by precipitation in cold diethyl ether, resulting in the product as a white powder.

Carboxylic acid-PEO:

After completion of the polymerization the reaction was quenched with bromoethyl acetate to obtain an ester group. The solution was concentrated under reduced pressure and dissolved in 1 M NaOH and left to stir for 2 h at room temperature. Thereafter HCl was added to the solution to reach pH 2. The product was extracted with $CHCl_3$ and washed with water.

8.2 Functionalization of poly(ethylene oxide)

8.2.1 Activation of poly(ethylene oxide)

with N-hydroxysuccinimide (NHS)

2.5 g of freeze dried carboxy-capped PEO (3030 g/mol, 0.825 mmol) and 0.47 g NHS (4.13 mmol) were dissolved in 25 ml dichloromethane and placed in a flask with a magnetic stirring bar. The flask was cooled in an ice-water bath, and 0.185 g DCC (0.9 mmol) was added. The reaction was performed under a nitrogen atmosphere and stirred for 1 h in the water-ice bath and thereafter at room temperature for 24 h. The precipitated 1,3-dicyclohexylurea was removed by filtration and the filtrate was precipitated in diethyl ether and recovered by filtration under vacuum. The white powdery solid was dried under vacuum at 40°C to give 0.32 g (12%) of the product.

with 4-nitrophenyl chloroformate (NPCF)

In the first approach for activation of PEO with NPCF, 1.7 g of freeze dried PEO (1700 g/mol, 1 mmol) was placed in an ice-water bath and dissolved in 5 ml dichloromethane. 0.403 g NPCF (201.6 g/mol, 2 mmol) and 0.28 ml TEA (101 g/mol, 2mmol) was added under stirring. The ice bath was removed and the pH was monitored and brought to 8 with TEA. The mixture was allowed to react at room temperature for 16 h. The product was precipitated in cold diethyl ether and recovered by filtration under vacuum. The resulting yellow powder was analysed in the GPC (elution solvent DMF at 70˚C with toluol as an internal standard).

In the second approach 1.7 g of freeze dried PEO (1700 g/mol, 1 mmol) was dissolved in 200 ml anhydrous THF and 0.576 g NPCF (3 mmol) and 0.37 g DMAP (122 g/mol, 6 mmol) was added. The reaction mixture was stirred for 2 h at room temperature. However, purification of the product was not possible.

with trifluoroethanesulfonyl chloride (TRES)

1.7 g of freeze dried PEO (1700 g/mol, 1 mmol) was dissolved in 35 ml dry THF and 400 µl TEA (101 g/mol, 3 mmol) was added. The mixture was cooled to 0°C and 213 µl TRES (182.6 g/mol, 2 mmol) was slowly added. The reaction was performed under a nitrogen atmosphere and stirred for 4 h at room temperature. The precipitated triethyl-ammoniumchloride was removed by filtration and the product was precipitated in diethyl ether. The white powdery solid was dried under vacuum at room temperature to give 0.47 g (25%) of the product.

with N, N'-disuccinimidyl carbonate (DSC)

1.7 g of freeze dried PEO (1700 g/mol, 1 mmol) was dissolved in 20 ml dry (molecular sieve) dioxane and 1.5 g DSC (256 g/mol, 6 mmol) dispersed in dry acetone, was added. 0.73 g DMAP (122 g/mol, 6 mmol) dissolved in 10 ml of dry acetone was added slowly under stirring. The reaction mixture was stirred for 6 h at room temperature. The product was precipitated in cold diethyl ether. However, no product could be detected in NMR. Other solvents for DSC such as THF, $CHCl_3$ and $CHCl_2$ were tested without success. The reaction was also performed at 40°C but no product could be detected.

with N, N'-carbonyldiimidazole (CDI)

1.1 g of freeze dried PEO (2200 g/mol, 0.5 mmol) was dissolved in 20 ml chloroform. The chloroform had previously been washed with water and dried over anhydrous sodium sulphate to remove traces of water. To this chloroform solution, 1.65 g CDI (162 g/mol, 10 mmol) was added and the reaction mixture was stirred for 4 h in room temperature. After concentration of

the solution, the obtained PEO-CDI was washed with 20 ml water, dried over anhydrous sodium sulphate and precipitated twice in cold diethyl ether. The resulting PEO-CDI was dried under vacuum at 40°C to give 0.87 g (76 %).

8.2.2 Coupling of poly(ethylene oxide) with diethylenetriamine, PEO-DETA .

The obtained PEO-CDI was further reacted with diethylenetriamine. 1 g of PEO-CDI (2294 g/mol, 0.44 mmol) was dissolved in 30 ml chloroform and a solution of 0.91 g diethylenetriamine (103 g/mol, 8.8 mmol) dissolved in 20 ml chloroform was slowly added during stirring. After stirring for 3 h in room temperature the obtained PEO-DETA was precipitated 3 times into a 20-fold excess of cold diethyl ether (8-10°C) to remove the unreacted DETA. The resulting PEO-DETA was characterized by GPC (elution solvent DMF at 70˚C with toluol as an internal standard), MALDI and ^{1}H-NMR.

8.2.3 Coupling of poly(ethylene oxide) with triethylenetetramine, PEO-TETA.

The obtained PEO-CDI was further reacted with triethylenetetramine. 1 g of PEO-CDI (2294 g/mol, 0.44 mmol) was dissolved in 30 ml chloroform and a solution of 1.28 g triethylenetetramine (146 g/mol, 8.8 mmol) dissolved in 30 ml chloroform was slowly added during stirring. After stirring for 3 h in room temperature the obtained PEO-TETA was precipitated 3 times into a 20-fold excess of cold diethyl ether (8-10°C) to remove the unreacted TETA. The resulting PEO-TETA was characterized by GPC (elution solvent DMF at 70˚C with toluol as an internal standard), MALDI and ^{1}H-NMR.

8.2.4 Coupling of poly(ethylene oxide) with tetraethylenepentamine, PEO-TEPA.

The obtained PEO-CDI was further reacted with tetraethylenepentamine. 1 g of PEO-CDI (2294 g/mol, 0.44 mmol) was dissolved in 30 ml chloroform and a solution of 1.66 g tetraethylenepentamine (189 g/mol, 8.8 mmol) dissolved in 30 ml chloroform was slowly added during stirring. After stirring over night in room temperature the obtained PEO-TEPA was precipitated 3 times into a 20-fold excess of cold diethyl ether (8-10°C) to remove the

unreacted TEPA. The resulting PEO-TEPA was characterized by GPC (elution solvent DMF at 70˚C with toluol as an internal standard), MALDI and ^{1}H-NMR.

8.2.5 Coupling of poly(ethylene oxide) with pentaethylenehexamine, PEO-PEHA

The obtained PEO-CDI was further reacted with tetraethylenepentamine. 1 g of PEO-CDI (2294 g/mol, 0.44 mmol) was dissolved in 30 ml chloroform and a solution of 2.04 g tetraethylenepentamine (232 g/mol, 8.8 mmol) dissolved in 30 ml chloroform was slowly added during stirring. After stirring over night in room temperature the obtained PEO-PEHA was precipitated 3 times into a 20-fold excess of cold diethyl ether (8-10°C) to remove the unreacted PEHA. The resulting PEO-PEHA was characterized by GPC (elution solvent DMF at 70˚C with toluol as an internal standard), MALDI and ^{1}H-NMR.

8.2.6 Coupling of poly(ethylene oxide) with branched poly(ethylene imine), PEO-PEI .

In a two-necked round bottom flask equipped with a reflux condenser, 0.18 g PEI (800 g/mol, 0.22 mmol) was dissolved in 20 ml chloroform. To this solution, 1.0 g of PEO-CDI (2294 g/mol, 0.44 mmol) in 20 ml chloroform was added dropwise. The ratio of PEO to PEI was chosen to produce a polymer with two PEO branches on each PEI core. The reaction mixture was stirred over night at 40°C. PEO-PEI was precipitated from chloroform into cold diethyl ether (8-10°C) twice.

8.2.7 Coupling with fluorescein

1.0 g PEO-54 (1781 g/mol, 0.56 mmol) was dissolved in water and brought to pH 2 with HCl. The reaction mixture was stirred for 2 h at room temperature and then the pH was adjusted to neutral again. The mixture was freeze dried to give α-aldehyde-ω-carboxy-PEO as a white solid powder. This was dissolved in 20 ml water and 22 mg 6-aminofluorescein (347 g/mol, 0.063 mmol) was added. The reaction mixture was stirred over night at room temperature. After completion of the reaction, the PEO-fluorescein was dialyzed for 4 days and subsequently freeze dried to give a yellow powdery solid.

8.2.8 Coupling of imidazole activated poly(ethylene oxide) with cysteine

1 g of PEO-CDI (2294 g/mol, 0.44 mmol) was dissolved in 20 ml water and 2.66 g cysteine (121 g/mol, 22 mmol) dissolved in water was added. The reaction mixture was stirred over night at room temperature. When the reaction was completed the mixture was freeze dried. To remove the unreacted cysteines the obtained powder was dissolved in chloroform and the free cysteines were removed by filtration. The solution was freeze dried and characterized by GPC (elution solvent DMF at 70˚C with toluol as an internal standard), MALDI and ^{1}H-NMR.

8.3 Synthesis of magnetic nanoparticles

10.8 g of iron chloride ($FeCl_3 \cdot 6\ H_2O$, 270 g/mol, 40 mmol) and 36.5 g of sodium oleate (304 g/mol, 120 mmol) was dissolved in a mixture solvent composed of 80 ml ethanol, 60 ml distilled water and 140 ml hexane. The resulting solution was heated to 70°C and kept at this temperature for 4 h. After the completion of the reaction, the upper organic layer containing the iron-oleate complex was washed three times with 30 ml distilled water. After the washing, hexane was evaporated off resulting in an iron-oleate complex in a waxy solid form. 36 g of the iron-oleat complex (40 mmol) and 5.7 g of oleic acid (285 g/mol, 20 mmol) were dissolved in 200 g of trioctylamine at room temperature. The reaction mixture was heated to 360°C with a constant heating rate of 3.3 °C/min, and then kept at that temperature for 30 minutes. The resulting solution containing the nanoparticles was then cooled to room temperature, and precipitated with ethanol. The nanoparticles were separated by centrifugation.

8.4 Ligand exchange procedures

8.4.1 Ligand exchange on QDs

QDs dissolved in chloroform were mixed with the desired amount of the new ligand which was also dissolved in chloroform. After a short mixing a non-solvent, such as hexane or cyclohexane, for the new capping groups, the PEO based ligands, was added. The QDs covered with the polymer are insoluble in the aliphatic solvents, agglomerated and could

easily be separated by centrifugation. Most of the original TOP/TOPO ligands remained dispersed in the supernatant.

8.4.2 Ligand exchange on magnetic nanoparticles

NPs dissolved in toluol were mixed with a toluol solution containing the desired amount of the new ligand. After 2 h mixing, a non-solvent, such as hexane or cyclohexane, for the new capping groups, the PEO based ligands, was added. The NPs covered with polymers are insoluble in the aliphatic solvents, agglomerated and could easily be separated by centrifugation. Most of the original trioctylamine ligands remained dispersed in the supernatant. The precipitation procedure was repeated once to remove more of the old ligands.

8.5 Coupling of aldehyde QDs to hydroxy groups

Transformation of an acetal to an aldehyde group on the QDs

After ligand exchange with α-acetal-ω-poly(ethylene imine)-PEO the obtained QDs were dissolved in water and brought to pH 2 with HCl. The mixture was stirred for 2 h where after the pH was adjusted to neutral again.

Coupling to a glass plate

20 µl of the QDs (42 µmol/l in water) with aldehyde groups obtained in the first step was placed on a glass plate. The glass plate was thoroughly rinsed after 20 minutes to remove the QDs which were not covalently attached to the glass plate.

Coupling to vesicles

100 µl of the QDs (42 µmol/l in water) with aldehyde groups obtained in the first step was mixed with a water solution containing PI-PEO vesicles with a hydroxyl group pointing in the water solution. The mixture was allowed to react over night.

8.6 Microcalorimetry

In a typical procedure 700 µl of a QD solution (52 µmol/l) in chloroform was placed in a 1 ml vessel in the microcalorimeter. A solution with a PEO ligand solved in chloroform was placed in a 250 µl syringe. The PEO solution was titrated to the QD solution so that a total of 200 µl was added. Every 10 minutes 10 µl was added while stirring. The concentration of the PEO solution was chosen to give a 500 molar excess of PEO in the solution after the last titration. In order to obtain the heat flow, the heat flow originating from the dilution must be subtracted from the total heat flow and hence a dilution experiment was performed. To 700 µl of a QD solution in chloroform 10 µl of chloroform was added every 10 minutes to a total of 200 µl chloroform.

8.7 Characterization

8.7.1 Nuclear Magnetic Resonance Spectroscopy (NMR)

^{1}H-NMR and ^{13}C-NMR spectra were recorded in $CDCl_3$ using tetramethylsilane as the internal standard. An AMX400 Bruker spectrometer (400 MHz) was used. The spectra were evaluated using the MestRe Nova program from Mestrelab.

8.7.2 Size Exclusion Chromatography (SEC)

Molecular weights (M_w and M_n) and molecular weight distribution (polydispersity index, *PI*) of all of the polymers were determined by SEC. Four columns (300*8 mm, Sdplus, 5 µm) (10^5, 10^3, 500, 100 Å) from the company MZ, thermostated at 70°C, were used. The pump was from Thermo Separation Product (P100) and the degasser from Uniflows (DG1210). The polymers were detected using an UV detector (Spectra Series UV1000) and an RI detector (Shodex 71). The eluent was dimethylformamide at a flow rate of 1 ml/min. The polymer concentrations were in the range of 2-6 g/l and 20 µl were injected for each run. The calibration was performed with PEO standards from the company PSS. For the evaluation of M_w, M_n and *PI*, the software HSNTeqGPC, version 6.2.13 was used.

8.7.3 Matrix Assisted Laser Desorption and Ionization – Time Of Flight (MALDI-TOF)

The MALDI-TOF-mass spectroscopy spectra were obtained with a M@LDI L, a linear instrument from Micromass Ltd, equipped with a nitrogen laser (λ = 337 nm). The pulse voltage was varied between 1700 V and 2000 V and the source voltage was kept constant at 15000 V. The spectra were evaluated using MassLynx^{TM} 4.0.

8.7.4 Dynamic light scattering (DLS)

Dynamic light scattering analysis was performed on a Malvern Zetasizer Nano ZS system equipped with a single angle 173° backscatter system, using He-Ne laser illumination at 633 nm. For each measurement, the autocorrelation function was the average of three runs of 30 s each, and for each sample three measurements were performed. The hydrodynamic radii were obtained using Dispersion Technology Software (DTS) Version 4.00 (Malvern Instruments)

8.7.5 Cryo-TEM

Cryo-TEM was carried out on a TEM LEO912 (Zeiss) electron microscope at the Pharmaceutical Institute, Albert-Ludwigs-University Freiburg.

8.7.6 Light microscope

A light microscope Axiovert S100 (Zeiss) with 100-times power objective lenses was used with immersion oil. The microscope was also equipped with a fluorescence device and the images were taken with the digital camera AxioCamHRc (Zeiss).

8.7.7 Confocal laser scanning microscope

The CLSM images were obtained with a Fluoview FV 1000 FV10-ASW (Olympus). A 60-times objective lens with immersion oil was used. The evaluation of the 2D and 3D images was performed with the software Fluoview version 1.6a.

8.7.8 Microcalorimeter

For the calorimetric measurements an isothermal titration calorimeter TAMIII from Thermometric AB (now TA instruments) was used. The TAMIII system consists of a 1 ml removable titration ampoule with stirring facilities and a precision syringe pump for efficient titrant delivery. The evaluation was performed with the lab assistant software version 0.9.1012.43 (TAM assistant).

8.7.9 Magnetic induction

For the induction experiments a high frequency generator HFG-15 from Linn High Term GmbH was used. It consists of a water-cooled three-turn coil and can reach a frequency of approximately 250 kHz. It has a maximum capacity of 10 kW which can be adjusted between 0 and 100%.

9 Appendix

9.1 Abbreviations and symbols

a_0 = effective area of the head group

AO = atomic orbitals

B = magnetic density flux

CDI = Carbonyldiimidazole

d = thickness of a particle

D = diffusion coefficient

d_0 = distance for sharpest vision

DCC = Dicyclohexylcarbodiimide

DCM = Dichloromethane

DETA = Diethylenetriamine

Dithranol = 1,8,9-trihydroxyanthracen

DLS = dynamic light scattering

DMAP = 4-(Dimethylamino)pyridine

DMF = Dimethylformamide

DSC = N,N'-disuccinimidyl carbonate

E_g = band gap

f_{oc} = focal distance of the ocular

g = correlation

G = angular magnification

GPC = gel permeation chromatography

h = hight of the object

h = Planks constant

H = enthalpy

H = field strength

H = mean curvature

h' = hight of enlarged object

H_c = coercivity field strength

I = initiator

ITC = isothermal titration calorimetry

K = gaussian curvature

k_0 = incident light

K_b = binding constant

K_B = Boltzmann's constant

k_s = scattered light

l = length of the hydrocarbon chain

L = free ligand

L_1 = objective

L_2 = ocular

LCAO = linear combination of atomic orbitals

m = mass of an electron

M = monomer

M_n = number-averaged molecular weight

M_w = weight-averaged molecular weight

MALDI-TOF = matrix assisted laser desorption and ionisation – time of flight

MO = molecular orbitals

MS = mass spectroscopy

N_p = degree of polymerisation

N_s = surfactant parameter

n, n_p, n_m = refractive index (particle, medium)

NA = numerical aperture

n-BuLi = n-Butyllithium

NC = nanocrystals

NHS = N-hydroxysuccinimide

NL = nanoparticle-ligand-complex

NPCF = 4-nitrophenyl chloroformate

PD = polydispersity

PEG = poly (ethylene glycol)

PEHA = Pentaethylenehexamine

PEI = Poly (ethyleneimine)

PEO = poly (ethylene oxide)

q = magnitude of the scattering wave vector

q = heat

QD = quantum dot

R = gas constant

R_1 / R_2 = Radii of curvatures

R_h = hydrodynamic radius

S = entropy

t = time

T = temperature

T = tube length

TEA = Triethanolamine

TEM = transmission electron microscope

TEPA = Tetraethylenepentamine

TETA = Triethylenetetramine

THF = tetrahydrofuran

TOP = trioctylphosphine

TOPO = tri-*n*-octylphosphine oxide

TRES = triflouroethanesulphonyl chloride

v = volume of the hydrophobic portion of an amphiphilic molecule

Y = yield

α = angle of vision

β = angle of vision with an optical instrument

Γ = decay rate

ΔG° = standard reaction Gibbs energy

Δx = resolution

η = viscosity

θ = scattering angle

θ_1 = incident angle

θ_2 = refraction angle

λ = wave length

υ = velocity

9.2 Safety precaution information of the used chemicals

Substance	R-phrases	S-phrases	Hazard signs
Acetic acid	10-35	23-26-45	C
Acetone	11-36-66-67	9-16-26	F, Xi
6-aminofluorescein	36/37/38	26-36	Xi
Bromoethyl acetate	36/37/38	26	Xi
n-Butyllithium	11-14-19-22-38-51/53-65-66-67	61-62	F, Xi, N
Cadmium selenide	21-23/25-33-50/53	53-22-36/37-45	T, N
Calcium hydride	15	24/25-43-7/8	F
N, N'-carbonyldiimidazole	22-34	26-36/37/39-45	C
Chloroform	22-38-40-48/20/22	36/37	Xn
Cyclohexane	11-38-50/53-65-67	9-16-25-33-60-61-62	F, Xn, N
Cysteine	-	-	-
Dichloromethane	40	23-24/25-36/37	Xn
Dicyclohexylcarbodiimide	22-24-41-43	24-26-37/39-45	T
1,3-dicyclohexylurea	21-51/53	61	Xn
3,3-Diethoxypropanol			
Diethylenetriamine	21/22-34-43	26-36/37/39-45	C
Diethyl ether	12-19-22-66-67	9-16-29-33	F+, Xn
4-(Dimethylamino)pyridine	25-27-36/37/38	16-18-36/37/39-45	T+
Dimethylformamide	67-20/21-36	53-45	T
Dioxane	11-19-36/37-40-66	9-16-36/37-46	F, Xn
Diphenylmethane	50/53	24-61	N
N, N'-disuccinimidyl carbonate	22-36/37/38	26-37/39	Xn
Ethanol	11	7-16	F
Ethylene oxide	45-46-23-12-36/37/38	53-45	T, F+
Hexane	11-38-48/20-51/53-62-65-67	9-16-29-33-36/37-61-62	F, Xn, N
Hydrochloric acid 4%	36/37/39	26	Xi
N-hydroxysuccinimide	-	22-24/25	-
Iron chloride	22-38-41	26-39	Xn
Methoxyethanol	60-61-10-20/21/22	53-45	T
Naphthalene	22-40-50/53	36/37-46-60-61	Xn, N
4-nitrophenyl chloroformate	34-36/37	26-36/37/39-45	C
Oleic acid	38		Xi
Pentaethylenehexamine	34-43-50/53	26-36/37/39-45-60-61	C, N
Poly (ethylene imine)	-	-	-

Poly(ethylene oxide)	-	-	-
Potassium	14/15-34	8-43-45	F, C
Sodium	14/15-34	8-43-45	F, C
Sodium hydroxide	35	26-37/39-45	C
Sodium oleate	-	22-24/25	-
Sodium sulphate	-	-	-
Tetraethylenepentamine	21/22-34-43-51/53	26-36/37/39-45-61	C, N
Tetrahydrofuran	11-19-36/37	16-29-33	F, Xi
Toluol	11-38-48/20-63-65-67	36/37-46-62	F, Xn
Triethanolamine	36/37/38	26	Xi
Triethylenetetramine	21-34-43-52/53	26-36/37/39-45-61	C
Trifluoroethanesulfonyl chloride	34	26-36/37/39-45	C
Trioctylamine	36/37/38	26	Xi
Trioctylphosphine	34	26-36/37/39-45	C
trioctylphosphine oxide	34-50/53	26-36/37/39-45-60-61	C, Xi

Risk (R-) and safety precaution (S-) phrases used in the classification, packaging, labelling and provision of information on dangerous substances

Risk phrases (R-Phrases)

R1: Explosive when dry
R2: Risk of explosion by shock, friction fire or other sources of ignition
R3: Extreme risk of explosion by shock friction, fire or other sources of ignition
R4: Forms very sensitive explosive metallic compounds
R5: Heating may cause an explosion
R6: Explosive with or without contact with air
R7: May cause fire
R8: Contact with combustible material may cause fire
R9: Explosive when mixed with combustible material
R10: Flammable
R11: Highly flammable
R12: Extremely flammable
R13: Extremely flammable liquefied gas
R14: Reacts violently with water
R15: Contact with water liberates highly flammable gases
R16: Explosive when mixed with oxidising substances
R17: Spontaneously flammable in air
R18: In use, may form flammable/explosive vapour-air mixture
R19: May form explosive peroxides
R20: Harmful by inhalation
R21: Harmful in contact with skin
R22: Harmful if swallowed
R23: Toxic by inhalation
R24: Toxic in contact with skin

R25:	Toxic if swallowed
R26:	Very toxic by inhalation
R27:	Very toxic in contact with skin
R28:	Very toxic if swallowed
R29:	Contact with water liberates toxic gas
R30:	Can become highly flammable in use
R31:	Contact with acids liberates toxic gas
R32:	Contact with acids liberates very toxic gas
R33:	Danger of cumulative effects
R34:	Causes burns
R35:	Causes severe burns
R36:	Irritating to eyes
R37:	Irritating to respiratory system
R38:	Irritating to skin
R39:	Danger of very serious irreversible effects
R40:	Possible risk of irreversible effects
R41:	Risk of serious damage to eyes
R42:	May cause sensitisation by inhalation
R43:	May cause sensitisation by skin contact
R44:	Risk of explosion if heated under confinement
R45:	May cause cancer
R46:	May cause heritable genetic damage
R47:	May cause birth defects
R48:	Danger of serious damage to health by prolonged exposure
R49:	May cause cancer by inhalation
R50:	Very toxic to aquatic organisms
R51:	Toxic to aquatic organisms
R52:	Harmful to aquatic organisms
R53:	May cause long-term adverse effects in the aquatic environment
R54:	Toxic to flora
R55:	Toxic to fauna
R56:	Toxic to soil organisms
R57:	Toxic to bees
R58:	May cause long-term adverse effects in the environment
R59:	Dangerous to the ozone layer
R60:	May impair fertility
R61:	May cause harm to the unborn child
R62:	Possible risk of impaired fertility
R63:	Possible risk of harm to the unborn child
R64:	May cause harm to breastfed babies

Combination of risks

R14/15:	Reacts violently with water, liberating highly flammable gases
R15/29:	Contact with water liberates toxic, highly flammable gas
R20/21:	Harmful by inhalation and in contact with skin
R20/21/22:	Harmful by inhalation, in contact with skin and if swallowed
R20/22:	Harmful by inhalation and if swallowed
R21/22:	Harmful in contact with skin and if swallowed
R23/24:	Toxic by inhalation and in contact with skin

R23/24/25:	Toxic by inhalation, in contact with skin and if swallowed
R23/25:	Toxic by inhalation and if swallowed
R24/25:	Toxic in contact with skin and if swallowed
R26/27:	Very toxic by inhalation and in contact with skin
R26/27/28:	Very toxic by inhalation, in contact with skin and if swallowed
R26/28:	Very toxic by inhalation and if swallowed
R27/28:	Very toxic in contact with skin and if swallowed
R36/37:	Irritating to eyes and respiratory system
R36/37138:	Irritating to eyes, respiratory system and skin
R36/38:	Irritating to eyes and skin
R37/38:	Irritating to respiratory system and skin
R42/43:	May cause sensitization by inhalation and skin contact
R48/20:	Harmful: danger of serious damage to health by prolonged exposure
R48/20/21:	Harmful: danger of serious damage to health by prolonged exposure through inhalation and in contact with the skin
R48/20/21/22:	Harmful: danger of serious damage to health by prolonged exposure through inhalation, in contact with skin and if swallowed
R48/20/22:	Harmful: danger of serious damage to health by prolonged exposure through inhalation, and if swallowed
R48/21:	Harmful: danger of serious damage to health by prolonged exposure in contact with skin
R48/21/22:	Harmful: danger of serious damage to health by prolonged exposure in contact with skin and if swallowed
R48/22:	Harmful: danger of serious damage to health by prolonged exposure if swallowed
R48/23:	Toxic: danger of serious damage to health by prolonged exposure through inhalation
R48/23/24:	Toxic: danger of serious damage to health by prolonged exposure through inhalation and in contact with skin
R48/23/24/25:	Toxic: danger of serious damage to health by prolonged exposure through inhalation, in contact with skin and if swallowed
R48/23/25:	Toxic: danger of serious damage to health by prolonged exposure through inhalation and if swallowed
R48/24:	Toxic: danger of serious damage to health by prolonged exposure in contact with skin
R48/24/25:	Toxic: danger of serious damage to health by prolonged exposure in contact with skin and if swallowed
R48/25:	Toxic: danger of serious damage to health by prolonged exposure if swallowed
R50/53:	Very toxic to aquatic organisms, may cause long term adverse effects in the aquatic environment
R51/53:	Toxic to aquatic organisms, may cause long term adverse effects in the aquatic environment
R52/53:	Harmful to aquatic organisms, may cause long-term adverse effects in the aquatic environment

Safety precaution phrases (S-Phrases)

S1:	Keep locked up
S2:	Keep out of reach of children

S3:	Keep in a cool place
S4:	Keep away from living quarters
S5:	Keep contents under … (appropriate liquid to be specified by the manufacturer)
S6:	Keep under … (inert gas to be specified by the manufacturer)
S7:	Keep container tightly closed
S8:	Keep container dry
S9:	Keep container in a well ventilated place
S12:	Do not keep the container sealed
S13:	Keep away from food, drink and animal feeding stuffs
S14:	Keep away from …(incompatible materials to be indicated by the manufacturer)
S15:	Keep away from heat
S16:	Keep away from sources of ignition-No Smoking
S17:	Keep away from combustible material
S18:	Handle and open container with care
S20:	When using do not eat or drink
S21:	When using, do not smoke
S22:	Do not breathe dust
S23:	Do not breathe gas/fumes/vapour/spray (appropriate wording to be specified by manufacturer)
S24:	Avoid contact with skin
S25:	Avoid contact with eyes
S26:	In case of contact with eyes, rinse immediately with plenty of water and seek medical advice
S27:	Take off immediately all contaminated clothing
S28:	After contact with skin, wash immediately with plenty of …(to be specified by the manufacturer)
S29:	Do not empty into drains
S30:	Never add water to this product
S33:	Take precautionary measures against static discharges
S34:	Avoid shock and friction
S35:	This material and its container must be disposed of in a safe way
S36:	Wear suitable protective clothing
S37:	Wear suitable gloves
S38:	In case of insufficient ventilation, wear suitable respiratory equipment
S39:	Wear eye/face protection
S40:	To clean the floor and all objects contaminated by this material use (to be specified by the manufacturer)
S41:	In case of fire and/or explosion do not breath fumes
S42:	During fumigation/spraying wear suitable respiratory equipment (appropriate wording to be specified by the manufacturer)
S43:	In case of fire, use ... (indicate in the space the precise type of fire fighting equipment. If water increases the risk, add "never use water")
S44:	If you feel unwell, seek medical advice (show the label where possible)
S45:	In case of accident or if you feel unwell, seek medical advice immediately (show the label where possible)
S46:	If swallowed, seek medical advice immediately and show the container or label

S47:	Keep at temperature not exceeding ... °C (to be specified by the manufacturer)
S48:	Keep wetted with ... (appropriate material to be specified by the manufacturer)
S49:	Keep only in the original container
S50:	Do not mix with ... (to be specified by the manufacturer)
S51:	Use only in well-ventilated areas
S52:	Not recommended for interior use on large surface areas
S53:	Avoid exposure - obtain special instructions before use
S54:	Obtain the consent of pollution control authorities before discharging to waste-water treatment plants
S55:	Treat using the best available techniques before discharge into drains or the aquatic environment
S56:	Do not discharge into drains or the environment, dispose to an authorised waste collection point
S57:	Use appropriate containment to avoid environmental contamination
S58:	To be disposed of as hazardous waste
S59:	Refer to manufacturer/supplier for information on recovery/recycling
S60:	This material and/or its container must be disposed of as hazardous waste
S61:	Avoid release to the environment. Refer to special instructions / safety data sheet
S62:	If swallowed, do not induce vomiting: seek medical advice immediately and show the container label

Combined safety phrases

S1/2:	Keep locked up and out of reach of children
S3/9:	Keep in a cool, well ventilated place
S3/7/9:	Keep container tightly closed in a cool, well ventilated place
S3/14:	Keep in a cool place away from ... (incompatible materials to be indicated by the manufacturer)
S3/9/14:	Keep in a cool, well-ventilated place away from ... (incompatible materials to be indicated by the manufacturer)
S3/9/49:	Keep only in the original container in a cool, well ventilated place
S3/9/14/49:	Keep only in the original container in a cool, well-ventilated place away from (incompatible materials to be indicated by the manufacturer)
S3/9/49:	Keep only in the original container in a cool, well ventilated place
S3/14:	Keep in a cool place away from … (incompatible materials to be indicated by the manufacturer)
S7/8:	Keep container tightly closed and dry
S7/9:	Keep container tightly closed and in a well ventilated place
S7/47:	Keep container tightly closed and at a temperature not exceeding...°C (to be specified by manufacturer
S20/21:	When using do not eat, drink or smoke
S24/25:	Avoid contact with skin and eyes
S29/56:	Do not empty into drains, dispose of this material and its container to hazardous or special waste collection point
S36/37:	Wear suitable protective clothing and gloves
S36/37/39:	Wear suitable protective clothing, gloves and eye/face protection
S36/39:	Wear suitable protective clothing, and eye/face protection
S37/39:	Wear suitable gloves and eye/face protection

S47/49: Keep only in the original container at temperature not exceeding ...°C (to be specified by the manufacturer)

10 Literature

[1] D. E. Owens, III, and N. A. Peppas *Int. J. Pharm.* **2006**, 307, 93-102

[2] H. Weller *Angew. Chem. Int. Ed. Engl.* **1993**, 32. 41-53

[3] J. Lee, V.C. Sundar, J. R. Heine, M.G. Bawendi, K. F. Jensen *Advanced materials* **2000** 12, 1102-1105

[4] W. U. Huynh, J.J. Dittmer, A. P. Alivisatos *Science* **2002**, 295, 2425-2427

[5] J. Liu, T. Tanaka, K. Sivula, A. P. Alivisatos, J. M. J. Fréchet *J. Am. Chem. Soc* **2004**, 126, 6550-6551

[6] W. A. Hild, M. Brewing, A. Goepferich *Eur J pharmaceutics and bioparmaceutics* **2008**, 68, 153-168

[7] W. Cay, A. R. Hsu, Z. Li, X. Chen, *Nanoscale Res Lett* **2007**, 2m 265-81

[8] L. Brus, *J. Phys. Chem.* **1986**, 90, 2555-2560

[9] J. K. Jaiwal, H. Mattoussi, J. M. Mauro, S. M. Simon, *Nature biotechnology* **2003**, 21, 47-51

[10] M. Bruchez Jr., M. Moronne, P. Gin, S. Weiss, A. P. Alivisatos *Science* **1998**, 281, 2013-2016

[11] *Nationalencyklopedin* tolfte bandet **1993**

[12] K. J. Klabunde *Nanoscale Materials in Chemistry*, John Wiley and Sons, Inc., New York, **2001**.

[13]http://www.britannica.com/eb/art-6024/Magnetic-hysteresis-loop

[14] M. Szwarc, Nature, 1956, 178, 1168

[15]P. J. Flory, *Journal of the American chemical society* **1940**;62:1561-5

[16] M.J Roberts, M.D Bentley, J.M. Harrris *Adv. Drug Delivery Reviews* **2002**, 54, 459-476

[17] R. B. Greenwald, Y. H. Choe, J. McGuire, C. D. Conover, *adv. Drug Delivery rev.* **2003**, 55, 217-250

[18] J. Li, W. J. Kao, *Biomacromolecules*, **2003**, 4, 1055-1067

[19] J. Li, C. F. Crasto, J. S Weinberg, M. Amiji, D. Shenoy, S. Sridhar, G. J. Bubley, G. B. Jones, *Bioorg. Med. Chem. Lett.* **2005**, 15, 5558-5561

[20] Y. Akiyama, H. Otsuka, Y. Nagasaki, M. Kato, K. Kataoka, *Bioconjugate Chem.* **2000**, 11, 947-950

[21] F. Zeng. C. Allen, *Macromolecules*, **2006**, 39, 6391-6398

[22] M. S. Thompson, T. P. Vadala, M. L. Vadala, Y. Lin, J. S. Riffle, *Polymer*, **2008**, 49, 345-373

[23] K. J. Widder, A. E. enyei, D. G. Scarpelli, *Proc. Soc. Exp. Biol. Med* **1978,** 58, 141

[24] A. K. Gupta, M. Gupta *Biomaterials* **2005**, 26, 3995

[25] C. C. Berry, A. S. G. Curtis, *J. Phys. D* **2003**, 36, R198

[26] S. Mornet, S. Vasseur, F. Grasset, E. Duguet, *J. Mater. Chem.* **2004**, 14, 2116

[27] S. Mornet, S. Vasseur, F. Grasset, P. Verveka, G. Goglio, A. Demourgues, J. Portier, E. Pollert, E. Duguet, *Prog. solid state Chem.* **2006**, 34, 237

[28] R. Hiergeist, W. Andrä, N. Buske, R. Hergt, I. Hilger, U. Richter, W. Kaiser, *J. Magn. Magn. Mater.* **1999**, 201, 420

[29] Kulzer F *et al Nature* **1997**, 387, 688-91

[30] R. M. Et al *Nature* **1997**, 388, 355-358

[31] M. S. Nikolic, M. Krack, V. Aleksandrovic, A. Kornowski, S. Förster, H. Weller,

[32] S. N. Sharma, Z. S. Pillai, P. V. Kamat, *J. Phys. Chem. B*, **2003**, 107, 10088-10093

[33] Y. Liu, M. Kim, Y. Wang, Y. A. Wang, X. Peng, *Langmuir*, **2006**, 22, 6341-6345

[34] G. P. Mitchell, C. A. Mirkin, R. L. Letsinger, *J. Am. Chem. Soc.*, **1999**, 121, 8122

[35] T. Uyeda, I. L. Medintz, J. K. Jaiswal, S. M. Simon, H. Mattoussi, *J. Am. Chem. Soc.* **2005**, 127, 3870

[36] S. Kim, M. G. Bawendi, *J. Am. Chem. Soc.*, **2003**, 125, 14652

[37] S.-W. Kim, S. Kim, J. B. Tracy, A. Jasanoff, M. Bawendi, *J. Am. Chem. Soc.* **2005**, 127, 4556-4557

[38] W. C. W. Chan, S. Nie *Science*, **1998**, 281, 2016-2018

[39] W. J. Parak, D. Gerion, T. Pellegrino, D. Zanchet, C. Micheel, S. C. Williams, R. Boudreau, M. A Le Gros, C. A. Larabell, A. P. Alivisatos, *Nanotechn.* **2003**, 14, R15-R27

[40] M. J. Parak et. al. *Chem. Mater.* **2002**, 14, 2113-2119

[41] C. Bullen, P. Mulvaney, *Langmuir*, **2006**, 22,3007-3013

[42] S. Förster, T. Plantenberg, *Angew. Chem.*, **1988**, 114, 712

[43] http://openlearn.open.ac.uk/mod/resource/view.php?id=297093

[44] D. F. Evans, H, Wennerström *The colloidal domain where Physics, Chemistr, Biology and Technology meet* second edition Wiley-VCH **1999**

[45] M. Karas, F Hillenkamp, *Anal. Chem.* **1988**, 60, 2301-2303

[46] K. Tanaka et al. *Rapid communications in mass spectrometry*, **1988**, 2, 8, 1511-153

[47]http://dbs.umt.edu/courses/fall2006/bioc380/lectures/009/images/maldi-tof.jpg

[48] Malvern Instruments Ltd., *Zetasizer Nano User Manual* (Issue 2.2), **2005**.

[49] B. J. Frisken, *Appl. opt.***2001**, 40, 4087-4091

[50] G. Jönsson *Våglära och optik* second edition **1994**

[51] http://www.microscopyu.com/articles/formulas/formulasindex.html

[52] http://www.mikroskopie.de

[53] U. Borchert, *dissertation*, Hamburg **2006**

[54] http://www.olympusfluoview.com.

[55] F. M. Veronese, B. Saccà, P. Polverino de Laureto, M. Sergi, P. Caliceti, O. Schiavon, P. Orsolini, *Bioconjugate chem.* **2001**, 12, 62-70

[56] S. Zalipsky, *Bioconjugate chem.* **1995**, 6, 150-165

[57]X. Shuai, T. Merdan, F. Unger, M. Wittmar, T. Kissel, *Macromolecules*, **2003**, 36, 57551-5759

[58] M. Ballico, S. Drioli, G. M. Bonora, *Eur. J. Org. Chem.*, **2005**, 2064-2073

[59] R. B. Greenwald, H. Zhao, J. Xia, D. Wu, S. Nervi, S. F. Stinson, E. Majerova, C. Bramhall, D. W. Zaharevitz, *Bioconjugate chem.*. **2004**, 15, 1076-1083

[60] C. Delgado, J. N. Patel, G. E. Francis, D. Fisher, *Biotechnol. Appl. Biochem.* **1990**, 12, 119-128

[61] T. Miron, M. Wilchek, *Bioconjugate Chem.* **1993**, 4, 568-569

[62] P. Ferruti, E. Ranucci, *Synth. Comm.* **1990**, 20, 2951-2957

[63] U. Lipprandt, *dissertation*, Hamburg **2004**

[64] D. V. Talapin, A. L. Rogach, A. Kornowski, M. Haase, H. Weller, *Nano Lett.* **2001**, 1, 207-211

[65] C. B. Murray, D. J. Norris, M. G. Bawendi, *J. Am. Chem. Soc.* **1993**, 115, 8706-8715

[66] B. Dubertret, P. Skourides, D. J. Norris, V. Noireaux, A. H. Brivanlou, A. Libchaber, *Science*, **2002**, 298, 1759-1762

[67] T. Pellegrino, L. Manna, S. Kudera, T. Liedl, D. Koktysh, A. L. Rogach, S. Keller, J. Rädler, G. Natile, W. J. Parak, *Nano Lett.* **2004**, 4, 703-707

[68] J. Lal, I. F. Hakem *Eur. Phys. J. E*, **2004**, 15, 217-223

[69] C. P. Collier, T. Vossmeyer, J. R. Heath, *Annu. Rev. Phys. Chem.* **1998**, 49, 371-404

[70] N. R. Jana, *Angew. Chem. Int. Ed.* **2004**, 43, 1536-1540

[71] C. Pacholski, A. Kornowski, H. Weller, *Angew. Chem. Int. Ed.* **2002**, 41, 1188-1191

[72] J. Richter, R. Seidel, R. Kirsch, M. Mertig, W. Pompe, J. Plaschke, H. K. Schackert, *Adv. Mater.* **2000**, 12, 507-510

[73] Y. Wang, Z. Tang, S. Tan, N. A. Kotov, *Nano. Lett.* **2005**, 5, 243-248

[74] N. Duxin, F. Liu, H. Vali, A. Eisenberg, *J. Am. Chem. Soc.* **2005**, 127, 10063-10069

[75] M. Zhang, M. Drechsler, A. H. E. Muller, *Chem. Mater.* **2004**, 16, 537-543

[76] S. Hauschild, U. Lipprandt, A. Rumplecker, U. Borchert, A. Rank, R. Schubert,S. Förster, *Small*, **2005**, 1, 12, 1177-1180.

Acknowledgements

First of all, I would like to thank Prof. Dr. Stephan Förster for giving me the opportunity to work with this interesting theme and for all his help, support and positive attitude. I would also like to thank Prof. Dr. Horst Weller for acting as a referee of this work.

I would like to thank the Graduate School GK611 for the financial support and their members for a great exchange of knowledge.

Special thanks go to Sigrid “Sigi” Zeckert and Rosemarie Pakula for their patience and willingness to help, with bureaucratic matters during my stay in Hamburg.
Many thanks go to the people from the NMR service at TMC. For the cryo-TEM pictures, I am very grateful to Sabine Barnert in Freiburg.

Thanks a to my roommates;
Michael Stolzenburg; for the warm welcome to “AK” and for showing me the best sides of Hamburg. I would never have enjoyed living in Hamburg as much without you as a guide!
Volkan Filiz; I really enjoyed working with you. It was allways rewarding and I would never have gotten through the last months of work without your company.
Jasmin Nitsche; for great company and interesting talks. I will really miss the flying of the “plastic bottles“.

I would also like to thank Carsten Schellbach, for all help with the student protocols, which at times were quite hard to interpret, and of course for the interesting “Mitarbeiterbesprechungen”.
Martin Kehden for his willingness to help and take over when I found something dangerous and he thought it was fun.
A special thank you to Ulf König for all help with the large “radio”, I would never been able to perform any induction test without you.
Thanks to Nina Schober for the amusing times during all the troubles with the GPC.
Thank you to the whole AK Förster for a great atmosphere throughout my stay in Hamburg, during working hours and after.

Special thanks to Madeleine Dahlbäck for thorough proofreading of my thesis.

I want to thank my parents, my sister and brother who are always there for me. Without their constant support and encouragement, I might not be here writing this thesis.

Not only for the proofreading of this work, but for all his support, patience and love, I want to thank my Olov.

Erklärung

Hiermit versichere ich an Eides statt, die vorliegende Arbeit selbstständig und ohne fremde Hilfe sowie nur mit den angegebenen Hilfsmitteln und Quellen erstellt zu haben. Die benutzten wörtlich oder inhaltlich entnommenen Stellen habe ich als solche kenntlich gemacht.
Außerdem erkläre ich, dass ich noch keinen Promotionsversuch an einer anderen Einrichtung unternommen habe.

Malmö, 26. Mai 2009

Charlotta Olsson